KfK 4477
Juni 1989

The WECHSL-Mod 2 Code: A Computer Program for the Interaction of a Core Melt with Concrete including the Long Term Behavior

Model Description and User's Manual

M. Reimann, S. Stiefel
Institut für Reaktorbauelemente
Projektgruppe LWR-Sicherheit

Kernforschungszentrum Karlsruhe

KERNFORSCHUNGSZENTRUM KARLSRUHE

Institut für Reaktorbauelemente
Projektgruppe LWR-Sicherheit

KfK 4477

The WECHSL-Mod2 Code: A Computer Program for the Interaction of a Core Melt with Concrete including the Long Term Behavior

Model Description and User's Manual

M. Reimann
S. Stiefel

Kernforschungszentrum Karlsruhe GmbH, Karlsruhe

Kernforschungszentrum Karlsruhe GmbH
Postfach 3640, 7500 Karlsruhe 1

ISSN 0303-4003

Abstract

The WECHSL-Mod2 code is a mechanistic computer code developed for the analysis of the thermal and chemical interaction of initially molten LWR reactor materials with concrete in a two-dimensional, axisymmetrical concrete cavity. The code performs calculations from the time of initial contact of a hot molten pool over start of solidification processes until long term basemat erosion over several days with the possibility of basemat penetration.

The code assumes that the metallic phases of the melt pool form a layer at the bottom overlayed by the oxide melt atop. Heat generation in the melt is by decay heat and chemical reactions from metal oxidation. Energy is lost to the melting concrete and to the upper containment by radiation or evaporation of sumpwater possibly flooding the surface of the melt.

Thermodynamic and transport properties as well as criteria for heat transfer and solidification processes are internally calculated for each time step. Heat transfer is modelled taking into account the high gas flux from the decomposing concrete and the heat conduction in the crusts possibly forming in the long term at the melt/concrete interface.

The WECHSL code in its present version was validated by the BETA experiments. The test samples include a typical BETA post test calculation and a WECHSL application to a reactor accident.

Der WECHSL-Mod2 Code: Ein Rechenprogramm für die Wechselwirkung einer Kernschmelze mit Beton mit Einschluß des Langzeit-Verhaltens

Zusammenfassung

Der WECHSL-Mod2 Computer Code ist ein mechanistisches Rechenprogramm, das zur Analyse der thermischen und chemischen Wechselwirkung einer zu Beginn flüssigen LWR-Kernschmelze mit Beton in zweidimensionaler, achsensymmetrischer Betonkaverne entwickelt wurde. Das Programm kann Rechnungen ausführen vom Beginn des Kontaktes eines heißen flüssigen Schmelzbades über das Einsetzen von Erstarrungsvorgängen bis zur langzeitigen Erosion des Fundaments über mehrere Tage mit der Möglichkeit der Fundamentdurchdringung.

Das Programm nimmt an, daß der Metallanteil der Schmelze eine Schicht am Boden der Kaverne bildet und von der Oxidschmelze überdeckt ist. Die Wärmeerzeugung in der Schmelze erfolgt durch die nukleare Nachwärme sowie durch chemische Energie infolge Oxidation der Metalle. Die Energie wird abgeführt an den aufschmelzenden Beton und in den oberen Sicherheitsbehälter. Für letzteres sind die thermische Strahlung oder das Verdampfen von Sumpfwasser, das die Schmelzenoberfläche möglicherweise fluten kann, von Bedeutung.

Die thermodynamischen und die Transport-Größen sowie die Kriterien für Wärmetransport und Erstarrung werden für jeden Zeitpunkt berechnet. Die Wärmeübergangsmodellierung berücksichtigt die hohe Gasfreisetzung aus der Betonzerstörung und die Wärmeleitung in Krusten, die sich möglicherweise langzeitig an der Grenzfläche der Schmelze zum Beton ausbilden.

Das WECHSL-Programm in seiner derzeitigen Form wurde durch die BETA-Experimente verifiziert. Die Beispielrechnungen beinhalten die Nachrechnung eines typischen BETA-Experiments und eine Anwendung auf einen Reaktorunfall.

Contents

Appendix A: Test Sample 1: BETA Test

Appendix B: Test Sample 2: Reactor Calculation

Nomenclature

a	Laplace constant
A	area
A_i, a_i	constants
Ar	Archimedes number
b	exponent
B_i, b_i	constants
Bi	Biot number
c	specific heat
c	constant
c_o	Stefan-Boltzmann-constant
D	coefficient
Eö	Eötvös number
F	force
f	factors characterizing transition from gas film to discrete bubble heat transfer
f	correction factor
f_{TP}	friction factor
g	acceleration of gravity
Gr	Grashof number
h	heat transfer coefficient
h	specific enthalpy
h_d	latent heat of melting or decomposition
h_{fus}	latent heat of phase change
h_{wv}	latent heat of evaporation
H	enthalpy
k	thermal conductivity
K	equilibrium constant
L	characteristic length
M	molecular weight
$\dot{m}$	mass flux
$\dot{m}/A$	mass flux density
n	exponent
n	coordinate perpendicular to the wall
Nu	Nusselt number
P	pressure
$\bar{p}$	module in transient heat conduction

Pr	Prandtl number
Q	heat flux, volume flux
Q/A	heat flux density
r	radius, radial coordinate
r	reaction enthalpy
r_{eq}	equivalent bubble radius
$\mathbb{R}$	universal gas constant
Re	Reynolds number
s	coordinate in direction of the wall
s	exponent
Ste	Stefan (phase change) number
T	temperature
u_b	bubble rise velocity
v	wall shear velocity
v_g	artificial gas velocity
V_M	partial molar volume
w	flow velocity
We	Weber number
y^+	dimensionless distance

α	angle of inclination
β	coefficient of volumetric expansion
γ	heat transfer enhancement factor
γ	heat transfer ratio
δ	layer thickness (boundary layer, gas film)
δ_s	crust thickness
$\tilde{\delta}$	dimensionless layer thickness
δ^*	flow cell height
δx	mesh width
$\delta \xi$	dimensionless length between two nodes
$\delta \tau$	time step
ΔH_c	specific decomposition enthalpy
ΔH_{LS}	molar latent heat of freezing
$\Delta \rho$	density difference
ε	void fraction
ε	emissivity
θ	ratio of layer thicknesses
ζ	friction coefficient

$\dot{\zeta}$	melt front velocity
λ	Taylor wave length
μ	dynamic viscosity
ν	kinematic viscosity
ξ	dimensionless coordinate
π	3.14159
ρ	density
σ	surface tension
τ	time
τ_w	wall shear stress
ϕ_s	solid fraction
ϕ	boundary condition parameter
ϕ_g	porosity
χ	molar fraction
ψ	weight fraction

Subscripts

ax	axial
b	bulk
b	bubble
bb	nuclear boiling
bs	bubble swarm
c	concrete
c	turbulent core
chem	chemical
cond	conductive
conv	convective
d	decomposition
decay	nuclear decay
dO	melting surface
eff	effective
eq	equivalent
fb	film boiling
freez	freezing
g	gaseous
h	high
h	hydrodynamical

i	species i, mesh i
i	interphase
j	time index
l	low
l	liquid
L	liquidus
LS	between liquidus and solidus
m	mean
m	melting
m	metal
n	mesh index
o	oxide
rad	radiative
s	solid
sur	surface
surr	surroundings
S	solidus
t	thermal
tot	total
v	steam
w	liquid water
w	wall

LIST OF FIGURES

1. INTRODUCTION

Light water reactors are designed and constructed with great attention paid to safety. As a result, it is highly improbable that an accident leading to meltdown of the nuclear core will occur. However, in the unlikely event of the simultaneous failure of a number of safety systems, it is possible that cooling of the core could be completely lost. If this occurred, decay heat would cause the reactor core to melt. In the course of such a core meltdown accident, molten fuel together with cladding and structural materials would accumulate in the lower plenum of the reactor pressure vessel. This molten material would melt through the pressure vessel within 20-160 min. after initiation of the accident, depending on the type and the course of the accident. Following reactor pressure vessel meltthrough, the molten core would drop onto the concrete base structure of the reactor building. The interaction of the core melt with concrete would continue for a long period of time.

During this interaction, a number of phenomena have an important bearing on the subsequent course of the accident [40]. These include:

- concrete decomposition,
- release of steam and gases from the decomposing concrete,
- chemical reactions of these gases with metallic constituents of the melt and within the containment atmosphere,
- dilution of the molten fuel materials by molten concrete constituents and alteration of the freezing behavior of the molten pool.

The phenomena above have a decisive influence on the basic safety related questions, i.e.:

Can the containment fail by overpressurization?
Can the conrete basemat melt through?
Can building structures inside the containment collapse?

Even though a core melt accident is very unlikely, the potential health consequences on the public require that best-estimate answers are given to these questions. In the early risk studies [1, 2], conservative assumptions were formulated to estimate the source term. Better understanding of the physical background of the molten core/concrete interaction would provide a more realistic basis for an advanced risk study. Furthermore, good understanding of this part of the accident sequence could lead to design measures which would help reducing the risk of a core meltdown accident.

It is impossible to completely simulate the interaction in experiments because of the materials, masses, time scales, and dimensions involved. Recourse must be made to mathematical models or computer codes in order to extrapolate the limited tests which can be performed with the expected materials, masses, and dimensions involved in a meltdown accident. In this context, simulation experiments characteristic of the different situations occuring during the sequence of a core melt/concrete interaction are of special importance.

Therefore, the Nuclear Safety Project (PNS) in February 1977 suggested a multi-stage concept to simulate experiments allowing a number of experiments to be performed on the 100 kg scale, with variation of such characteristic parameters as the composition and the temperature of the molten pool, the heat flow, and the amount of decay heat to be simulated by inductive heating. The BETA test facility [3] was started up in early 1984 and the experimental program including a series of high power and low power experiments was executed within two years. Since February 1986, all experimental results have been available [4]. The visual observations as well as the measured data in the BETA tests were extremely helpful in acquiring a deeper understanding of separate effects and improving modeling in the WECHSL code. But, above all, the BETA tests served for integral verification of the WECHSL code.

The WECHSL code is a mechanistic code based on the current understanding of the phenomena occurring during the interaction of a molten pool with concrete. As far as possible, the code is capable of treating both the simulation experiments with non-radioactive materials and melt masses between 100 and 600 kg and, in addition, hypothetical core meltdown accidents with real, full scale reactor dimensions. The code was originally based on the INTER code [5] developed in 1977. However, in the meantime so many improvements and changes have been made that the WECHSL code now bears nearly no resemblance to the INTER code.

WECHSL served for dimensioning the BETA test facility and for precalculations of the BETA tests. The first documentation of the WECHSL code representing this early status was written in 1981 [6]. It is the basis for the documentation on the following pages.

WECHSL considers the separation of the molten pool into metal and oxide layers. Numerous experiments with simulant materials have shown that the metal and oxide layers rapidly segregate [7, 8]. Although some of the high power BETA tests show intermixing of the metal and oxide layers, driven by the high gas release at the early stage of interaction, the long term stable situation is the layered situation, with the heavier metal at the bottom. Further observations in these tests showed that vast amounts of combustible gases were produced that stirred the layers of the molten pool vigorously. These phenomena suggest a conceptual model as shown schematically in Figure 1.

Energy can be produced internally by decay heat or by exothermic reactions. Energy is lost to the conrete and to the overlying environment by a variety of mechanisms. Moreover, energy can be exchanged between the molten layers.

The thermal attack on concrete gives rise to a vigorous evolution of gases. Much of these gases pass through the melt. During their passage, the melt is thoroughly stirred, so that each layer is nearly isothermal. Water vapor and carbon dioxide are reduced as they pass through the metallic layer. Liquid concrete decomposition products dilute the oxide layer. Thus, composition and, consequently, the material properties of the layers are continuously changing.

From the top of the melt heat is transferred to the upper containment by thermal radiation or - if the melt pool is flooded by sump water - by evaporation.

Because of the high rate of heat extracted from the melt pool, the temperatures of the melt layers drop continuously. Crust formation sets in, if the temperature of the relevant melt surface drops below the freezing temperature. Figure 2 shows schematically the possibilities of crust formation as handled in the WECHSL code. On the metal layer surfaces crusts start to be formed in the bottom region and at the side walls. If the melt bulk temperature is higher than that of the oxide, metal crust growth at the interface between the metal and the oxide melt layers is possible, too. In the oxide layer crust growth may occur at the top of the layer and in the side wall region. If the oxide bulk temperature is higher than that of the metal bulk, an oxide crust may build up at the oxide/metal interface.

Crust formation reduces considerably the heat extraction from the bulk of the melt. Consequently, the long term behavior of a core melt in the basemat of a

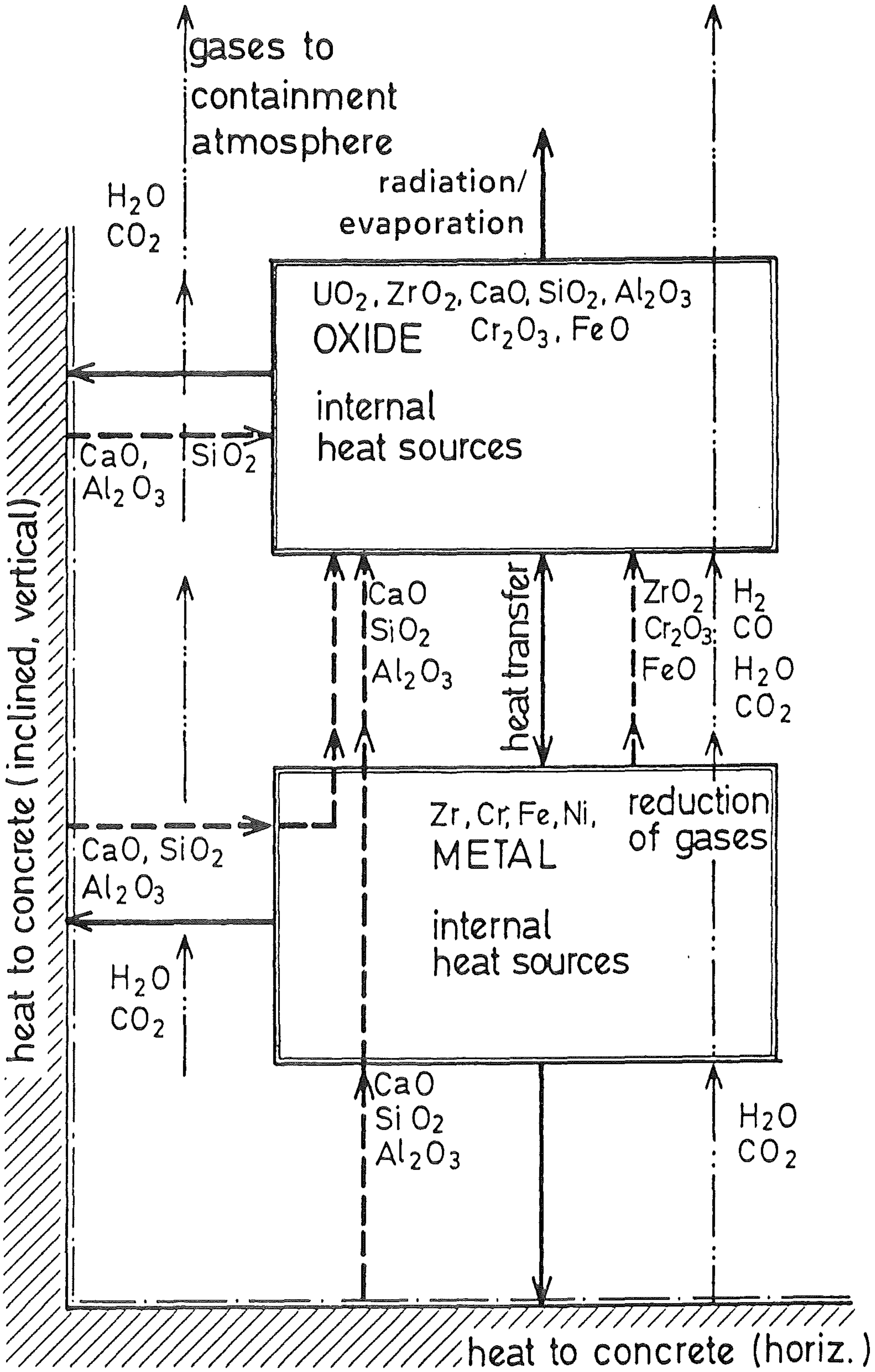

Figure 1: Flows of energy and material in WECHSL.

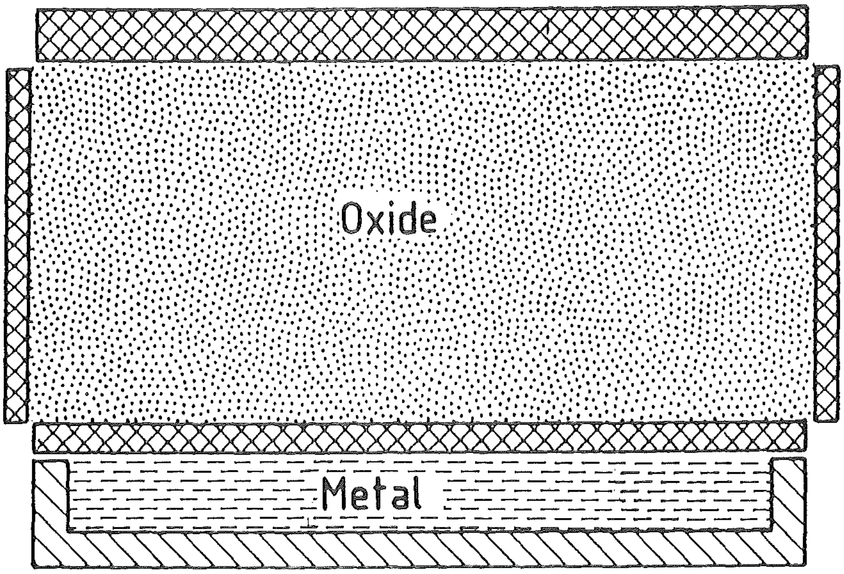

Figure 2: Schematic representation of the crust formation in WECHSL.

reactor building will be governed by encrusted melt layers, with the decay heat released inside the layers balanced by the heat transmission through crusts to the concrete and to the upper structures and the atmosphere of the containment building.

In the late phase of a core melt accident, the temperature of the metal bulk may drop below the solidification temperature. Then, a block of frozen metal will attack the conrete basemat. This situation is also considered in WECHSL.

Liquid decomposition products of the conrete dilute the oxide layer. This changes continuously the properties of the oxide bulk. Above all, the solidification temperature is reduced. In the late phase of a core melt accident, the freezing temperature of the oxide bulk may drop to values near or even below the ablation temperature of the concrete. This is due to the formation of eutectic mixtures with solidification temperatures as low as 1200 °C [9]. Because the decay heat can only be removed by concrete ablation or via the top of the melt, while the heat conduction in the basemat is not effective in heat removal for many days after attack on the conrete starts, it is not possible that the whole oxide bulk solidifies. Therefore, only a completely liquid or encrusted oxide bulk with increasing viscosity must be considered in WECHSL. To estimate the final dimension of the melt cavity which is formed after many weeks of erosion and which, indeed, is dominated by heat conduction in the concrete, additional calculations with heat conduction analysis codes are useful [10].

In the first German Risk Study [2], and also in the updated version, Phase B, of this study presently under preparation, core melt accident sequences in a German standard pressurized water reactor of the Biblis B type are analyzed. In such a reactor, the building structure around the reactor pressure vessel is an enclosed cylindrical concrete cavity with an inner diameter of about 6 m. If the molten core slumps into this cavity, the height of the pool without void will be of the order of one meter. The WECHSL code as well as the BETA experimental program were developed to cope with that situation. Therefore, WECHSL is directly applicable only to deep melt pools similar to those existing in enclosed cavities. For shallow layers, as may occur, e.g., in a German boiling water reactor with a wide reactor cavity, where the core melt could spread over a large area at the concrete basemat, additional considerations are necessary before the WECHSL code can be used. With the ongoing discussion about severe accidents, especially after the Chernobyl accident in 1986, special interest was devoted to BWR accident scenarios. The higher zirconium content in that type of reactor and the boron carbide (B_4C) control blade material may change considerably the composition of the melt and its freezing behavior, so that the WECHSL code is not fully applicable. Moreover, prototypical experiments in this area, from which supplementary information could be extracted are presently lacking.

2. Physical Modeling in the WECHSL Code

2.1 General Remarks

The analysis of the core melt/concrete interaction traces the following rationale:

- Identification of the physical phenomena by small scale benchmark experiments with simulant materials.
- Establishing of physical separate effect models.
- Linkage of the separate effect models in the WECHSL code.
- Verification of the WECHSL code by integral experiments with hot, non-radioactive melts with simulation of the decay heat (BETA tests).
- Upgrading to full reactor dimensions by computations with the validated computer code.

Consequently, each of the phenomena modeled in the code has been included in such a way as to permit experimental verification. In some models, empirical constants have been fixed to represent adequately the sufficient representation of the BETA test results.

Each of the important models contained in the code will be described in detail in the following sections. Also the sources from which the submodels have been built will be given.

2.2 Melt/Concrete Interface

2.2.1 Concrete Decomposition

The decomposition of concrete is a highly complex process. Differential thermal analyses of conrete with different aggregates [11] yield the consecutive steps of dehydration, $CaCO_3$ decomposition, and the range of melting with increasing temperature. Each of these decomposition steps takes place in a certain temperature range. Furthermore, as indicated by Powers [12], chemical kinetics can alter each range of effective decomposition temperature. The released gases flow through the residual porous concrete matrix and are transporting energy. Moreover, energy is transferred in this matrix of changing porosity by transient heat conduction.

In the WECHSL code a strongly simplified model is applied. It is assumed that under the impact of a high heat flux the decomposition process of concrete can be treated as one-dimensional heat conduction in a semi-infinite body. At the melting surface, the molten material is continuously being removed. The gas release and other chemical reactions are assumed to occur at definite temperatures during the process of concrete heatup. The higher the heat flux density is, the smaller is the zone in the conrete where the temperature drops from the melting point of the silicates to the ambient temperature. This means that a quasi-stationary temperature profile will be established in the concrete shortly after the surface is exposed to a high temperature melt.

The model for the decomposition process is formulated for n different layers [13]. In the layer i, the porosity of the concrete is ϕ_{gi} and the weight percentage of the released gases escaping through this layer is ψ_{gi}. By assuming perfect temperature exchange between the solid and the gases, coupling of the two relevant energy equations by source and sink terms results in a quasi-stationary energy equation for the whole system. Between the layers of the concrete, heat is absorbed by chemical or physical reactions. One set of boundary conditions is given by the melting temperature at the surface and the decomposition temperatures between the layers. Another set of boundary conditions can be established by energy balances at the boundaries between the layers.

The quasi-stationary energy equation can be described by an exponential temperature distribution. Applying the boundary conditions to this solution, we obtain the decomposition velocity, $\dot{\zeta}$, according to [14] as

$$\dot{\zeta} = \frac{(Q/A)}{\rho_c \Delta H_c} . \qquad (2.2.1\text{-}1)$$

This equation indicates that the rate of quasi-stationary decomposition depends only on the heat flux imposed . The enthalpy of concrete decomposition

$$\Delta H_c = (1 - \psi_{g0}) h_{d0} + \left((\rho c)_{eff\,0} / \rho_c \right) (T_{d0} - T_{00}) \qquad (2.2.1\text{-}2)$$

is a material property. The effective volumetric heat capacity, ρc, and the effective thermal conductivity, k, are given by

$$(\rho c)_{eff\,i} = \rho_{gi} c_{p\,gi} \, \phi_{gi} \left(1 + \frac{\psi_{gi} \, \rho_c}{\phi_{gi} \rho_{gi}} \right) + (1 - \phi_{gi}) \rho_{si} \, c_{si} , \qquad (2.2.1\text{-}3)$$

and

$$k_{eff\,i} = \phi_{gi} k_{gi} + (1 - \phi_{gi}) k_{si} \,. \qquad (2.2.1\text{-}4)$$

Equations (2.2.1-3 and 4) can be evaluated by applying averaged solid (subscript s) and gaseous (subscript g) properties of the relevant concrete components. The unknown temperature difference (T_{d0}-T_{00}) in Eq. (2.2.1-2) is determined by regression from

$$T_{d\,i-1} - T_{d0\,i-1} = T_{d\,i-1} - T_{d\,i} + \frac{\psi_i \rho_c h_{d\,i} + (T_{d\,i} - T_{0i})(\rho c)_{eff\,i}}{(\rho c)_{eff\,i-1}} \,. \qquad (2.2.1\text{-}5)$$

The decomposition reactions as considered in the model are given in Table 1. The exothermal formation of wollastonite ($CaSiO_3$) can be optionally included. A comparison between calculated and measured values for the decomposition enthalpies of different types of concrete is made in [11] and [15].

Decomposition Temperature (K)	Decomposition Reaction	Heat of Decomposition (kJ/mole)
1573	$SiO_{2s} \rightarrow SiO_{2l}$	-8.53
	$CaO + SiO_2 \rightarrow CaSiO_3$	+88.5
	$CaSiO_{3s} \rightarrow CaSiO_{3l}$	-46.5
1167	$CaCO_3 \rightarrow CaO + CO_{2g}$	-165.5
796	$Ca(OH)_2 \rightarrow CaO + H_2O_g$	-99.5
400	$H_2O_l \rightarrow H_2O_g$	-39.4

Table 1: Characteristics of the concrete decomposition.

By applying this model in the WECHSL-code, the decomposition process is characterized by a surface temperature T_{d0} and by a unique concrete property, the volumetric decomposition enthalpy $\rho_c \Delta H_c$.

The assumption of a quasi-stationary decomposition velocity as given in Eq. (2.2.1-1) introduces two principal errors; the first results from the time dependence of the heat flux imposed on the surface, and, consequently, the transient nature of the heat conduction process, and the second from chemical kinetics. Although these two components are actually coupled, an idea of their magnitude can be obtained by considering them separately.

The transient problem of heat conduction with simultaneous melting in a homogeneous solid has been solved by Landau [14]. Although concrete is certainly far from being homogeneous, it is instructive to apply the method of Landau to get a feeling of the magnitude of the error involved.

At time $\tau = 0$, the semi-infinite homogeneous concrete layer is at ambient temperature T_∞ and a constant heat flux density Q/A is imposed at the surface. The transient temperature distribution can be found analytically. From the time-dependent temperature profile, the time at which the surface reaches the melting temperature is evaluated as

$$\tau_m = \frac{\pi (T_m - T_\infty)^2}{4(Q/A)^2} k \rho c \qquad (2.2.1\text{-}6)$$

or, after introducing the parameter

$$\theta = \frac{\pi^{1/2}}{2} \frac{c(T_m - T_\infty)}{h_{d0}} ; \qquad (2.2.1\text{-}7)$$

$$\tau_m = \left(\rho \frac{h_{d0}}{(Q/A)} \frac{k}{\rho c} \theta \right)^2 . \qquad (2.2.1\text{-}8)$$

After the surface has reached the melting temperature, the melt front starts moving. The subsequent heatup process with simultaneous melting was treated numerically in [14]. In Figure 3, the ratio of the actual melt front velocity to the quasi-stationary melt front velocity resulting from Eq. (2.2.1-1) is plotted over the dimensionless time τ/τ_m with the material property θ as the parameter. For a typical siliceous concrete, this property yields $\theta = 16.9$. By integration of the relevant curve in Figure 3, it follows that for this type of concrete the acceleration phase of the melt front can be substituted by a displacement of the time ordinate as

$$\tau_{q,st} = 1.26\,\tau_m . \qquad (2.2.1\text{-}9)$$

By evaluating Eqs. (2.2.1-8, 9) the results given in Table 2 are obtained:

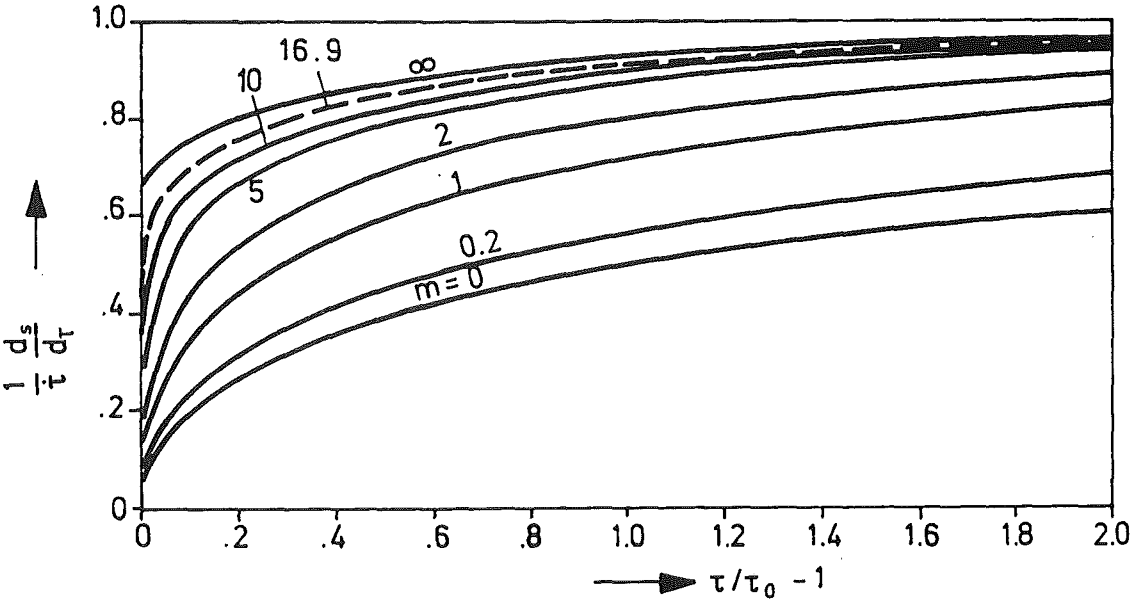

Figure 3: Melt front accellaration phase.

$\tau_{q,st}$ s	Q/A 10^4 W/m^2
1	377.2
10	119.3
100	37.7

Table 2: Time ordinate displacement substituting the initial heatup process

The error due to chemical reactions is not as easily assessed. An approximate magnitude of the error can be obtained by assuming that the concrete is heated at a constant rate from room temperature to the decomposition temperature for each decomposition step in the time $\tau_{q,st}$. When the resulting temperature rate is substituted into the kinetic decomposition model proposed by Powers [12], it is found that the time required to decompose 90 % of the concrete constituents is of the order of the required displacement of the time axis, but generally shorter.

As mentioned above, the quasi-stationary concrete ablation model is characterized by two parameters:

- the surface ablation temperature of the concrete T_{do}, and
- the volumetric decomposition enthalpy $\rho_c \Delta H_c$.

Consequently, the properties T_{do} in K, ρ_c in kg/m^3 and ΔH_c in J/kg, must be specified as input to the WECHSL code. For the computation of the specific decomposition enthalpy ΔH_c, a separate computer program BEZENT based on equations (2.2.1-2) to (2.2.1-5) is available.

The applicability of the quasi-stationary concrete ablation model could always be derived from the BETA tests in which thermocouples had been embedded at different locations in the concrete crucible. Due to the poor thermal conductivity of the concrete, the penetration depth of the temperature front into the concrete structure is low, on the order of some centimeters only, as long as melting of the concrete surface proceeds. It is the lower, the higher the heat flux density (Q/A) imposed at the concrete surface is. Consequently, thermocouples in the concrete in front of the melting surface generally give the ambient temperature. Only upon direct arrival of the melt front, there is a sharp increase in the temperature reading and, finally, the thermocouple fails. This behavior is an indication of the limited range of temperature penetration. A long-range temperature distribution in the concrete crucible was only established after switching off inductive heating simulating the decay heat, when the interface temperature between the frozen slug and the concrete had dropped below the ablation temperature of the concrete and thus the melt front stopped propagating.

It should be noted that the quasi-steady-state concept holds even in the case of very low heat flux densities acting for a sufficiently long period of time on the concrete structure. In experiments carried out at Sandia Labs [16], solid blocks of metal or oxide were heated with very low power density. In these tests, the transient phase in which the relevant quasi-stationary temperature profile established took a comparatively long time on the order of several ten minutes, but, finally, the block started to move downwards attaining a slow, but constant velocity of propagation.

In a core melt accident as well as in the BETA experiments the melt is poured onto the conrete surface at high temperatures which results in very high initial heat flux densities so that the period of establishing the quasi-stationary temperature profile in the concrete may be neglected. However, the heat flux density is not constant so that the temperature profile in the concrete changes with time. By applying always the quasi steady-state concept, the transient storage of heat in the concrete structure is neglected and, consequently, the concrete ablation will be slightly overpredicted. Only in such tests whose duration - i.e. the time needed to solidify the melt - is less than several minutes and the transferred heat fluxes are mainly transient, the experimental results may deviate from the calculations. However, in the BETA tests with sustained induction heating and, with better justification, in a core melt accident, the period of interaction and concrete ablation is long enough to justify the application of the quasi-steady-state concept.

2.2.2 General Features of Heat Transfer From the Melt Bulk to the Concrete

The heat transfer from the melt bulk to the concrete is characterized by processes forming boundary layers at the melt pool surface facing the concrete. The most important process is the release of large volume fluxes of gases from the concrete, which govern the heat transfer phenomena.

Due to the heat flux density (Q/A), the concrete is decomposed into gaseous weight fraction ψ_g and into liquid (weight fraction $1-\psi_g$) decomposition products. From the quasi-stationary heat transport model discussed above, the mass flux density of the released gases is given by

$$(\frac{\dot{m}}{A}) = \frac{\Psi_g}{\Delta H_c} (\frac{Q}{A})_{tot} . \tag{2.2.2-1}$$

In Figure 4, the possible combinations at the core melt/concrete interface are shown schematically. When the melt layer is completely liquid, the concrete surface is passed by a large volume gasflow (H_2O, CO_2) exceeding the volume flows of liquid decomposition products (SiO_2, CaO, Al_2O_3) by some orders of magnitude. If the superficial velocity of the gases being released from the concrete is sufficiently high, a stable gas film is formed between the melt and concrete (Fig.4a). If the superficial gas velocity drops below a limiting value, the heat transfer will be governed by a nucleate boling type of discrete bubble gas release (Figure 4b). Due to cooldown of the melt, the temperature in the melt boundary layer facing the concrete may drop below the freezing temperature, which characterizes the onset of crust formation. The crusts are intially thin skins, which follow the movements of the meltpool interface. With crust growth stabilization can be observed to increase. Finally, the crust has reached a thickness which is sufficient to form a stable layer. There is an adequate number of holes in the stable crust which allow passage of the gases released from the

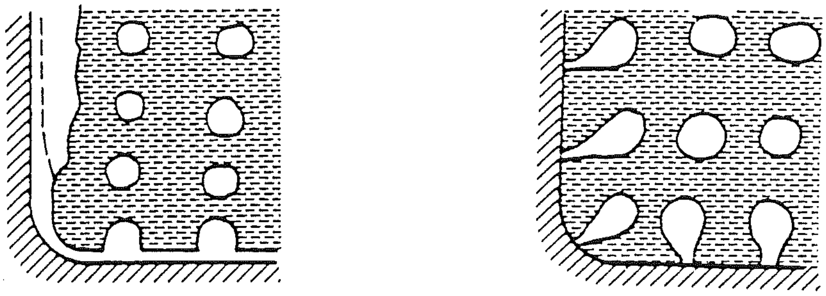

a) Gas film with adjacent boundary layer in the melt

b) Discrete bubble model

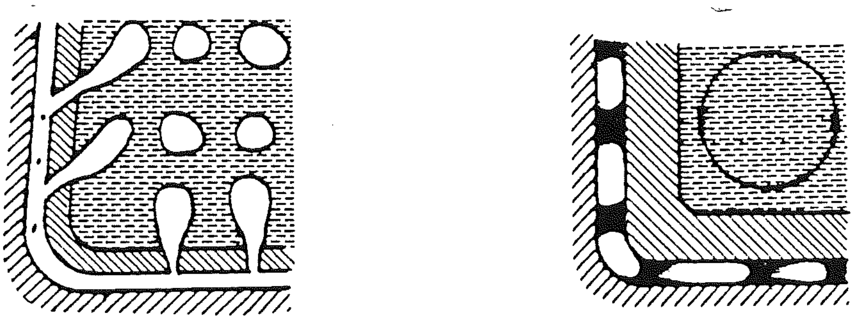

c) Transient growing gas permeable crust with film (outside) and discrete bubble model (inside)

d) Gas tight crust with two-phase (outside) and natural convection heat transfer (inside)

Figure 4: Schematic representation of the possible combinations of heat transfer models.

concrete (Figure 4c). Between the crust and the concrete a gas film exists. The heat transfer between the melt bulk and the inside of the crust is determined by a discrete bubble type heat transfer mechanism, with the driving temperature difference determined by the bulk temperature and the freezing temperature of the melt layer at the crust interface.

Crusts or even solidified metal reguli have always been observed to be completely gas permeable in the BETA tests. Consequently, the convection processes inside the encrusted melt slug are always gas driven. Single-phase natural convection inside the melt slug, as shown in Figure 4d, has not to be considered.

In the following sections, the relevant physical heat transfer models are given in detail.

2.2.3 Gas Film Model

The ratio of the released gas volume to the volume of liquid decomposition products from the concrete is on the order of 1000:1. Because of the dominance of the gaseous phase at very high heat flux densities, a gas film of thickness δ is likely to be present between the core melt and the concrete. Through this gas film, heat will be transferred by conduction and radiation. So, the total heat flux density is

$$(Q/A)_{tot} = (Q/A)_{cond} + (Q/A)_{rad} \tag{2.2.3-1}$$

with

$$(Q/A)_{cond} = \frac{A_{eff}}{A_{tot}} \frac{k_g (T_i - T_{d0})}{\delta} \tag{2.2.3-2}$$

and

$$(Q/A)_{rad} = \varepsilon_{id} c_0 (T_i^4 - T_{d0}^4) \tag{2.2.3-3}$$

where

$$\varepsilon_{id} = \frac{1}{1/\varepsilon_i + 1/\varepsilon_d - 1} \, . \tag{2.2.3-4}$$

As the heat is transferred from a molten pool to a gas liberating wall, the process can be considered as inverse film boiling. Consequently, the derivation of the heat transfer correlations follows closely the ideas of Berenson [17], Bromley [18], and Hsu, Westwater [19] with the heat transfer by radiation taken into account in addition.

Model experiments with dry ice slabs in a water pool are helpful to study the principles of an inverse film boiling process. As shown in [13], the carbon dioxide gas film which covers a horizontal sublimating dry ice slab gives rise to the formation of a square grid of bubble release sites. Similar experiments were carried out by Dhir et al. [20] who also proposed the Berenson model for this process. By passing over to strongly inclined or vertical walls, bubbles do not break away any longer and a continuous laminar gas layer streaming upwards separates the pool from the sublimating surface. Having reached a critical film thickness, the flow becomes increasingly turbulent. The different flow regimes as shown in Figure 5 and a model experiment showing the sublimation of a dry ice corner under water have been given in [21].

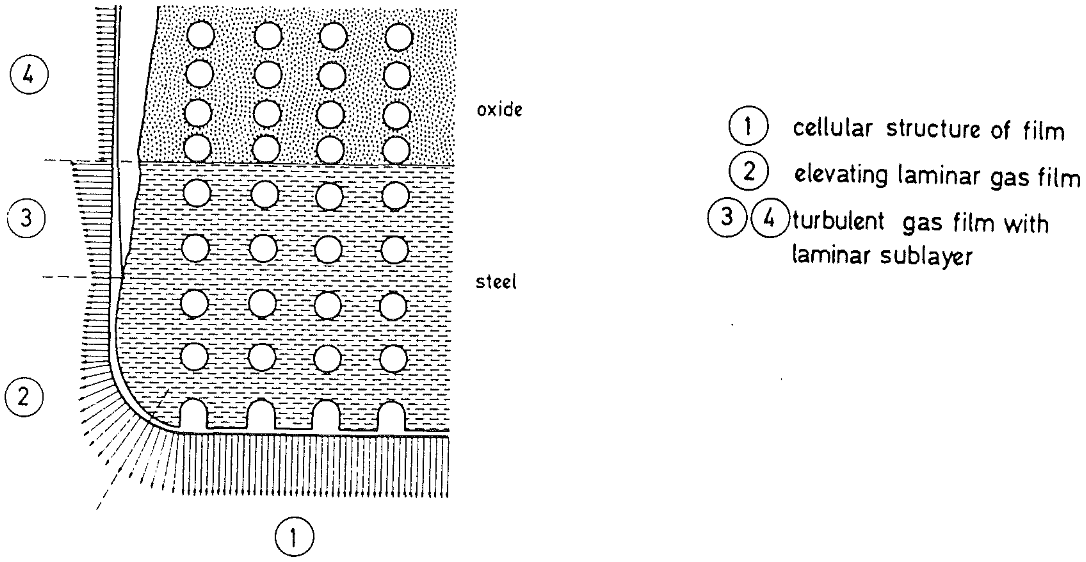

Figure 5: Schematic representation of gas film, bubble rise, and heat transfer coefficient.

For the sake of completeness, the models of heat transfer from a hot melt to concrete as derived in [13] for horizontal surfaces and in [22] for inclined and vertical surfaces will be summarized here.

At horizontal or slightly inclined surfaces, the gases give rise to an unstable gas layer at the interface of the decomposing solid with the liquid pool. This unstable gas layer breaks up into a regular pattern of bubble formation sites, where gas bubbles are growing and then leave the film. Due to the theory of stratified layers (Taylor instability), the most probable wavelength between two bubble formation sites

$$\lambda = 2\pi\sqrt{3}\,a \qquad (2.2.3\text{-}5)$$

depends on the Laplace constant

$$a=\left(\frac{\sigma}{g(\rho_\ell-\rho_g)}\right)^{1/2}. \qquad (2.2.3\text{-}6)$$

In Figure 6 a time averaged rotational symmetric flow cell of the area

$$A_{tot}=\lambda^2 \qquad (2.2.3\text{-}7)$$

around a centre of bubble formation is shown. The quantities r_i and δ^* are connected with the wavelength λ by

$$r_i=\frac{\lambda}{4}; \quad \delta^*=\frac{\lambda}{3}. \qquad (2.2.3\text{-}8)$$

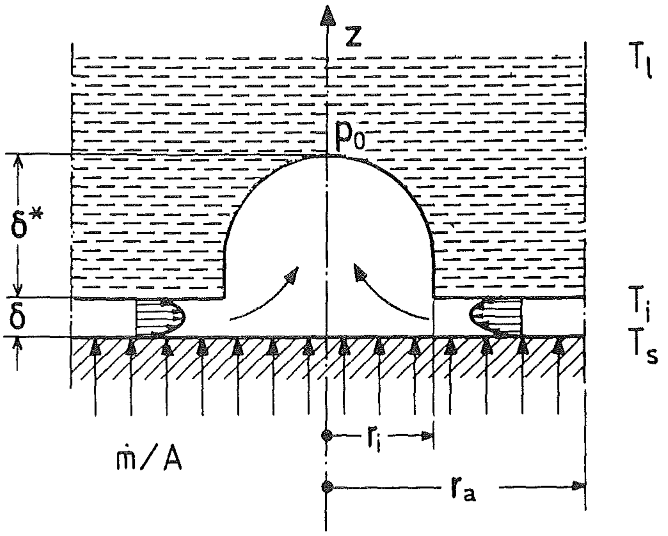

Figure 6: Flow cell on a horizontal wall.

The mean film thickness δ is determined from the balances of mass and momentum under the assumption that the gaseous decomposition products enter the film in z-direction with a constant specific mass flux $\dot{m}/A_{tot}$. The mass balance

$$\frac{1}{r}\frac{d}{dr}(r\rho_g w_m \delta)=\left(\frac{\dot{m}}{A}\right) \qquad (2.2.3\text{-}9)$$

is integrated in radial direction to give

$$w_m = -\frac{1}{2}\left(\frac{\dot{m}}{A}\right)\frac{1}{\rho_g \delta}\left(\frac{r_a^2}{r} - r\right) \qquad (2.2.3\text{-}10)$$

for the mean velocity of the gas flowing in radial direction.

The momentum balance in the radial direction taking into account pressure forces and friction forces reads

$$\frac{\partial p}{\partial r} = \mu_g \frac{\partial^2 w}{\partial z^2}. \qquad (2.2.3\text{-}11)$$

The integration of this equation results in

$$w_m = -\frac{(3\phi-2)}{12}\frac{\delta^2}{\mu_g}\frac{\partial p}{\partial r}. \qquad (2.2.3\text{-}12)$$

Combining (2.2.2-10, 12) and performing a radial integration one gets

$$p_a - p_i = \frac{6}{(3\phi-2)}\frac{\mu_g}{\rho_g \delta^3}\left(r_a^2 \ell n \frac{r_a}{r_i} - \frac{r_a^2 - r_i^2}{2}\right). \qquad (2.2.3\text{-}13)$$

In the above equation, the parameter ϕ characterizes the boundary condition at the gas/liquid interface. In Eq. (2.2.2-12) $\phi = 1$ applies to the liquid acting as a solid wall and $\phi = 2$ applies to a slip condition. In practice, the boundary condition will lie somewhere between these two conditions.

A hydrostatic pressure balance around the flow cell gives

$$p_a - p_0 = g\,\delta^*\,\rho_\ell, \qquad (2.2.3\text{-}14)$$

$$p_i - p_0 = g\,\delta^*\,\rho_g + \frac{2\sigma}{r_i}. \qquad (2.2.3\text{-}15)$$

The combination of Eqs. (2.2.2-8, 13, 14, 15) yields

$$\left(\frac{\dot{m}}{A}\right)_{tot} = 0.3724\,\frac{(3\phi-2)}{12}\,\frac{g\,\rho_g\,\Delta\rho\,\delta^3}{\mu_g\,a} \qquad (2.2.3\text{-}16)$$

for the specific mass flux of the gases released from the concrete and entering the flow cell.

In the idealized flow cell, the heat transfer by conduction through the gas film of thickness δ is effective on the area given by the ratio

$$A_{eff}/A_{tot}=(1-\frac{\pi}{16})=0.804 \qquad (2.2.3\text{-}17)$$

By combining Eqs. (2.2.2-1, 2.2.3-1, 2, 3 and 16, 17) and by introducing the dimensionless quantities

$$\tilde{\delta}=\delta/L$$

$$Nu=\frac{(Q/A)L}{k_g(T_i-T_{d0})}$$

$$Gr=\frac{g\,\rho_g\,\Delta\rho\,L^3}{\mu_g^2} \qquad (2.2.3\text{-}18)$$

$$Pr\,Ste=\frac{\mu_g\,\Delta H_c}{k_g(T_i-T_{d0})}$$

the dimensionless film thickness can be determined from the following equation as

$$\frac{1}{\tilde{\delta}}=0.825\left\{\frac{3\phi-2}{12}\;\frac{Gr\,Pr\,Ste}{\psi_g}\;\frac{L}{a}\;\frac{1}{1+1.244\,\tilde{\delta}\,Nu_{rad}}\right\}^{1/4}. \qquad (2.2.3\text{-}19)$$

The Nusselt number based on the total heat transfer rate for the horizontal surface is obtained as

$$Nu_{tot}=Nu_{rad}+\frac{A_{eff}}{A_{tot}}\,\frac{1}{\tilde{\delta}}\,. \qquad (2.2.3\text{-}20)$$

It is now assumed that the wavelength λ is small compared to the radius of curvature while going from a horizontal to a strongly inclined concrete surface. It was seen in model experiments with dry ice slabs that up to an inclination $\alpha=30^{\circ}$, the unstable gas film with bubbles breaking away was the governing mechanism of gas release. So, in this intermediate region the heat transfer is assumed to be constant as given by Eqs. (2.2.3-19, 20).

If the inclination goes beyond 30°, a continuous gas layer is formed which flows along the wall. Now, the conductive heat transport across the gas film is effective on the whole surface, i.e.

$$\frac{A_{eff}}{A_{tot}} = 1 . \tag{2.2.3-21}$$

With the denotations of Figure 7, the mass balance reads

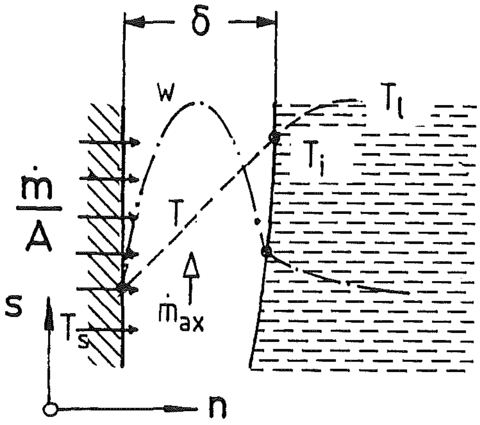

Figure 7: Laminar gas film on an inclined or vertical wall.

$$\frac{d}{ds}(\dot{m}_{ax}) = \left(\frac{\dot{m}}{A}\right) \tag{2.2.3-22}$$

with

$$\dot{m}_{ax} = \rho_g w_m \delta \tag{2.2.3-23}$$

and the integration of the simplified momentum equation taking into account friction forces and buoyancy forces yields

$$\mu_g \frac{d^2 w}{dn^2} = -g \, \Delta\rho \, sin\alpha \tag{2.2.3-24}$$

or, after integration

$$w_m = \frac{(3\phi - 2)}{12} \delta^2 \frac{g \, \Delta\rho}{\mu_g} \, sin\alpha . \tag{2.2.3-25}$$

By introducing the dimensionless variable

$$\zeta = s/L \tag{2.2.3-26}$$

and by using the dimensionless groups as defined in Eqs. (2.2.3-18), the combination of Eqs. (2.2.2-1, 2.2.3-1, 2, 3, 22, 23, 26) results in a differential equation for determining the film thickness $\tilde{\delta}$:

$$\frac{d\tilde{\delta}}{d\zeta}=\frac{4}{(3\phi-2)}\,\frac{\psi_g}{Gr\,Pr\,Ste\,sin\alpha}\,\frac{1+Nu_{rad}\tilde{\delta}}{\tilde{\delta}^3}\,, \tag{2.2.3-27}$$

and the total heat transfer is evaluated again with Eq. (2.2.3-20).

The thickness of the laminar gas film increases up to a critical value for which transition to turbulence must be expected and which can be determined from the relations for a single-phase fluid (see i.e. Schlichting [23]). By introducing the wall shear velocity

$$v=(\tau_w/\rho_g)^{1/2}\,, \tag{2.2.3-28}$$

the dimensionless velocity

$$w^+=w/v\,, \tag{2.2.3-29}$$

and the dimensionsless distance

$$y^+=n\,\frac{\rho_g v}{\mu_g} \tag{2.2.3-30}$$

can be defined. Within the framework of a two-layer concept for a single-phase fluid flow, a limiting value for the layer thickness is

$$y^+=10\,. \tag{2.2.3-31}$$

By assuming a linear velocity profile

$$w^+=y^+\,, \tag{2.2.3-32}$$

the critical Reynolds number is defined as

$$Re^*=\frac{\rho_g\,w_m\,\delta}{\mu_g}=w^+\,y^+=100\,. \tag{2.2.3-33}$$

This results in a critical film thickness given by

$$\delta_{crit}=\left\{\frac{12}{(3\phi-2)}\,\frac{Re^*}{Gr\,sin\alpha}\right\}^{1/3}. \tag{2.2.3-34}$$

Above this point, a turbulent core (subscript c) with a laminar sublayer (subscript g) is present as indicated in Figures 5 and 8. The mass flux through the film is

$$\dot{m}_{ax} = \rho_c w_c \left\{ \delta_c - \delta\left(1 - \frac{1}{2}\frac{\rho_c}{\rho_g}\right) \right\} \tag{2.2.3-35}$$

with the velocity w_c in the turbulent core as

$$w_c = y^{+2}\frac{\mu_g}{\rho_g \delta}. \tag{2.2.3-36}$$

Inserting Eqs. (2.2.3-35, 36) in Eq. (2.2.2-22) and combining the result with Eqs. (2.2.2-1, 2.2.3-1, 2) yields

$$\frac{d}{d\zeta}\frac{\tilde{\delta}_c}{\tilde{\delta}} = \frac{\rho_g}{\rho_c}\frac{\psi_g}{y^{+2} Pr\, Ste}\frac{1}{\tilde{\delta}}\left(1 + Nu_{rad}\tilde{\delta}\right) \tag{2.2.3-37}$$

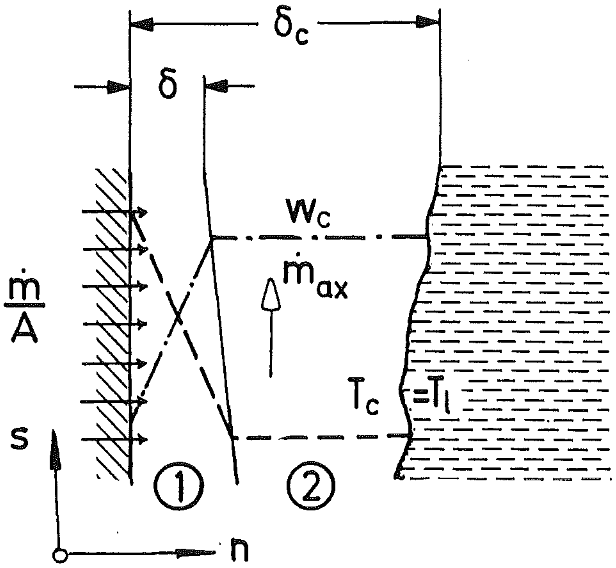

Figure 8: Turbulent gas film on an inclined or vertical wall.

In a second step, a momentum balance is applied to a control element as shown in Figure 9:

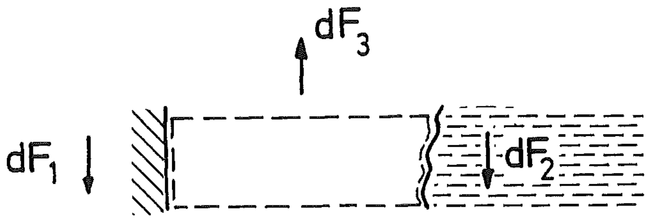

Figure 9: Forces acting on an element of the turbulent gas film.

$$\rho \int_{(K)} \vec{w}\, dQ - dF_1 - dF_2 + dF_3 = 0\,. \qquad (2.2.3\text{-}38)$$

(Q: volume flux in the film; F: forces)
Evaluating the momentum integral yields

$$\rho \int_{(K)} w\, dQ = -\frac{\rho_c}{\rho_g} y^{+4} \frac{\mu_g^2}{\rho_g} \frac{d}{ds}\left(\frac{1}{\delta}\left\{\frac{\delta_c}{\delta} - (1 - \frac{1}{3}\frac{\rho_g}{\rho_c})\right\}\right) ds\,. \qquad (2.2.3\text{-}39)$$

The forces acting in direction of the flow are the wall friction force

$$dF_1 = \tau_w ds = y^{+2} \frac{\mu_g^2}{\rho_g} \frac{1}{\delta^2}\, ds\,, \qquad (2.2.3\text{-}40)$$

the interface friction force

$$dF_2 = \tau_i\, ds = \frac{\rho_c}{\rho_g} y^{+4} \frac{\mu_g^2}{\rho_g} \frac{f_{TP}}{2} \frac{1}{\delta^2}\, ds\,, \qquad (2.2.3\text{-}41)$$

and the buoyancy force

$$dF_3 = g\, \Delta\rho\, \delta_c\, sin\alpha\, ds \qquad (2.2.3\text{-}42)$$

Combination of Eqs. (2.2.3-38, 39, 40, 41, 42) and use of Eq. (2.2.3-37) results in

$$\frac{d\tilde{\delta}}{d\zeta} = \frac{\dfrac{\rho_g}{\rho_c} \dfrac{\Psi_g}{y^{+2} Pr\, Ste}(1 + Nu_{rad}\tilde{\delta}) + \left(\dfrac{f_{TP}}{2} + \dfrac{\rho_g}{\rho_c} \dfrac{1}{y^{+2}}\right) - \dfrac{\rho_g}{\rho_c} \dfrac{Gr\, sin\alpha}{y^{+4}} \tilde{\delta}_c \tilde{\delta}^2}{\dfrac{\tilde{\delta}_c}{\tilde{\delta}} - \left(1 - \dfrac{1}{3}\dfrac{\rho_g}{\rho_c}\right)} \qquad (2.2.3\text{-}43)$$

Eqs. (2.2.3-37, 43) are a system of differential equations for the total layer thickness δ_c and the laminar sublayer thickness δ. This system of differential equations as well as the differential equation (2.2.3-27) for laminar flow may be integrated numerically by means of a Runge-Kutta method.

In the turbulent film model, the heat is assumed to be transferred by conduction through the laminar sublayer of thickness δ and by radiation from the liquid/gas interface to the concrete surface. Consequently, the total heat transfer can again be evaluated by Eq. (2.2.3-20).

As the computation of the heat transmission through the vertical gas film by solving the complete system of differential equations using a Runge-Kutta method is rather time consuming, an approximate solution has been developed by Reinecke [24] which reproduces with sufficient accuracy the results of modeling described above. By this measure, the computer time required by the WECHSL code has been reduced considerably. The relevant approximation equations and sets of constants are given in Section 2.4.2.

2.2.4 Pool Boundary Layer

In all flow regimes of the gas film model, the temperature difference T_i-T_{d0} is decisive for the heat transfer, where T_i is the temperature of the melt at the interface with the gas film and T_{d0} is the surface temperature of the decomposing concrete. In the bottom region of the pool, a thin boundary layer driven by micro-convection between bubble release sites is assumed to exist. Along the inclined walls, a boundary layer is created by drag forces exerted by the gas flowing in the film. Both boundary layers result in a temperature drop of the pool bulk temperature T_m to the interface temperature T_i. Because of the excellent thermal conductivity and the low viscosity of the metals which, normally, occur at the bottom of the pool, this temperature drop across the boundary layer in the metal is only on the order of few degrees. However, in the oxide region (region 4 in Figure 5), the temperature drop across the boundary layer is quite significant because of the low thermal conductivity and the high viscosity of the oxides. This reduces considerably the total heat transfer from the molten pool to the concrete. To describe the attack of a two-phase melt on the concrete properly, a boundary layer analysis, especially for inclined and vertical walls in the oxide region, is important. The results of this approach can also be applied as a first-order approximation on the bottom region where the metallic melt interacts.

In reference [25], the complete analysis is given of the boundary layer formation at a laminar gas film/liquid interface. Boundary layer calculations were carried out for vertical plates of sublimating dry ice in water and water-glycerine mixtures as well as for concrete slabs attacked by metallic or oxidic melts.

In all of these computations, the coefficient ϕ in Eq. (2.2.3-27) which determines the coupling of the gas film with the liquid was found to be almost unity. Consequently, the use of

$$\phi = 1 \qquad (2.2.4\text{-}1)$$

in Eqs. (2.2.3-19, 22) is appropriate to obtain heat transfer results.

Following a proposal of Lock [26], the ratio of the hydrodynamical boundary layer thickness between two fluids is

$$\frac{\delta_{h1}}{\delta_{h2}} = 0.844 \left(\frac{\mu_1}{\mu_2} \right)^{2/3} \left(\frac{\rho_2}{\rho_1} \right)^{1/3} \qquad (2.2.4\text{-}2)$$

when fluid 2 is at rest. In the gas film, the thermal boundary layer thickness equals the film thickness, and the hydrodynamic boundary layer thickness can be set as the thickness of the layer where the velocity drops from the maximum to the interface value. This is

$$\frac{\delta_{hg}}{\delta_{tg}} = \frac{1}{2} \qquad (2.2.4\text{-}3)$$

for $\phi = 1$. On the other hand, the ratio of the hydrodynamical and the thermal boundary layer thickness in the liquid is approximated by

$$\frac{\delta_{h\ell}}{\delta_{t\ell}} \sim Pr_{\ell}^{\,1/2} . \qquad (2.2.4\text{-}4)$$

(see e.g. Schlichting [23]).

With these assumptions made, a good approximation for the heat transfer results of all boundary layer calculations could be found by

$$\frac{\delta_{t\ell}}{\delta_{tg}} = 1.236\, Pr_{\ell}^{-1/2} \left(\frac{\mu_{\ell}}{\mu_{g}} \right)^{2/3} \left(\frac{\rho_{g}}{\rho_{\ell}} \right)^{1/3} . \qquad (2.2.4\text{-}5)$$

The comparison of this equation with the results of the boundary layer theory is shown in Figure 10.

The boundary layer analysis was carried out for laminar film flow. However, in the model experiments with dry ice slabs of 25 cm length sublimating in water and water/glycerine mixtures, transition to turbulent gas film flow occurred. As shown in [25], a good representation of the heat transfer results of these model experiments could be found when calculating the interface temperature

$$T_i = \frac{T_{\ell} + \dfrac{\delta_{t\ell}}{\delta_{tg}} \dfrac{k_g}{k_{\ell}} T_{d0}}{1 + \dfrac{\delta_{t\ell}}{\delta_{tg}} \dfrac{k_g}{k_{\ell}}} \qquad (2.2.4\text{-}7)$$

from the laminar analysis (Eq. 2.2.4-5), applying this result also to the turbulent gas film region and setting the friction coefficient f_{TP} in the turbulent film zone as a function of the viscosity ratio (μ_{ℓ}/μ_{g}) determined at the interface temperature T_i.

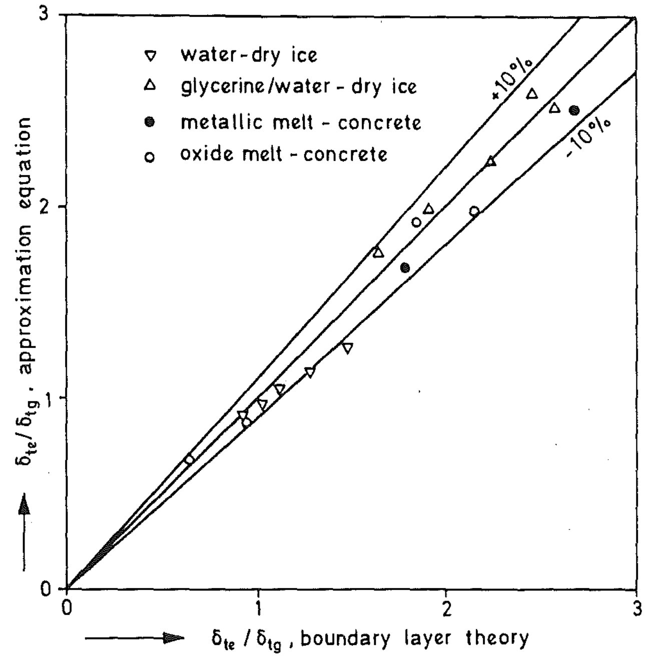

Figure 10: Comparison of Eq. (2.2.4-4) with the results of boundary layer theory.

$$f_{TP} = 3.414 \cdot 10^{-4} (\mu_\ell/\mu_g)^{2/3} \tag{2.2.4-7}$$

This comparison is given in Fig. 11.

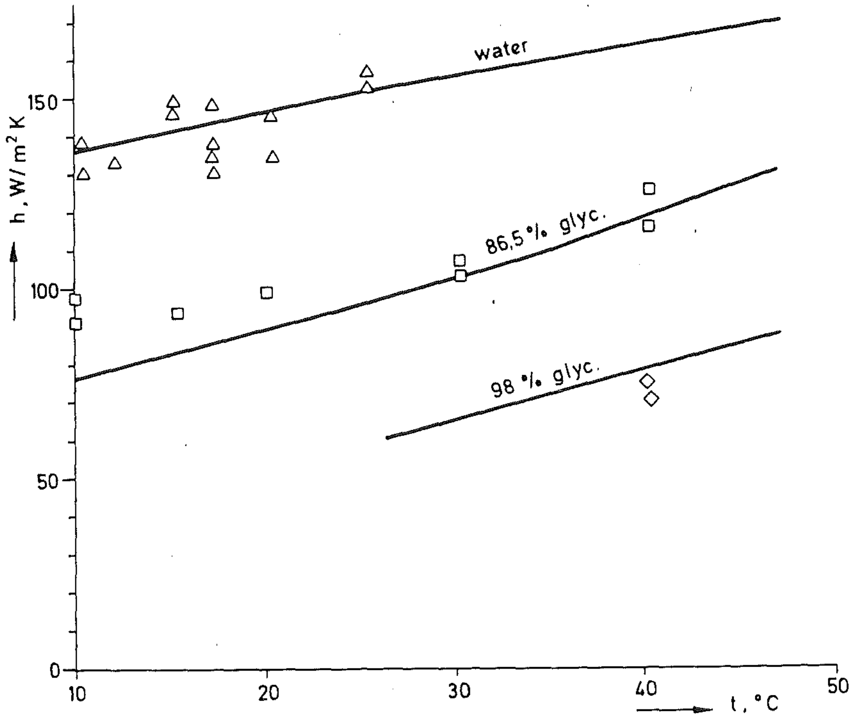

Figure 11: Comparison of experimental and calculated heat transfer results of vertical dry ice slabs sublimating in liquid pools.

2.2.5 Discrete Bubble Model

During the interaction of a core melt with concrete the pool temperature of the melt drops continuously. Moreover, other types of concrete with a lower weight fraction of gaseous decomposition would release lower gas rates when attacked by the melt. So, the mass flux density of the released gases as defined in Eq. (2.2.2-1) could drop to a value at which a stable gas film can no longer exist. With a Reynolds number based on the mass flux defined by

$$Re = \frac{(\dot{m}/A)a}{\mu_g} \tag{2.2.5-1}$$

and the approach of Berenson [17] for film boiling on horizontal surfaces followes the minimum Reynolds-number for a stable gas film:

$$Re_{min} = 0.09\left(Gr \frac{\rho_g}{\rho_\ell + \rho_g} \right)^{1/2}. \tag{2.2.5-2}$$

According to the results of the BETA experiments, this minimum value will be modified in Section 2.2.7. From the Zuber criterion for the maximum gas flow at departure from nucleate boiling (DNB), the maximum Reynolds number yields

$$Re_{max} = 0.09\left(Gr \frac{\rho_\ell}{\rho_\ell + \rho_g} \right)^{1/2}. \tag{2.2.5-3}$$

After the Reynolds number has dropped below the minimum value, the melt will get into direct contact with the concrete surface and the heat will be transferred through a boundary layer on the melt/concrete interface driven by microconvection between the sites of gas bubble formation. Such a discrete bubble model was derived by Reineke et al. [27] for horizontal surfaces and extended later to include inclined and vertical walls [28].

In terms of the dimensionless quantities based on the properties of the melt

$$Nu_\ell = \frac{(Q/A)a}{k_\ell(T_\ell - T_{d0})}$$

$$Pr_\ell = \frac{\mu_\ell c_{p\ell}}{k_\ell} \tag{2.2.5-4}$$

$$(Pr\,Ste)_\ell = \frac{\mu_\ell \Delta H_c}{k_\ell(T_\ell - T_{d0})}$$

the heat transfer is determined by

$$Nu_{\ell 1} = \frac{C^2(\alpha)}{6^{1/2}} \psi_g \frac{Pr_\ell^{0.84}}{(Pr\,Ste)_\ell} \tag{2.2.5-5}$$

with an expression taking into account the angle of inclination α

$$C(\alpha) = 1.65 + 7.47\alpha - 8.77\alpha^2 + 3.65\alpha^3 . \tag{2.2.5-6}$$

As due to an argument given in [29] the bubble density at the decomposing surface cannot exceed a limiting value, the upper boundary for the Nusselt number is

$$Nu_{\ell 2} = 4.63\, Pr^{0.38} . \tag{2.2.5-7}$$

The governing Nusselt number is evaluated by

$$Nu_\ell = Min\{Nu_{\ell 1}, Nu_{\ell 2}\} \tag{2.2.5-8}$$

If the Reynolds number Re_{max} given in Eq. (2.2.5-3) is exceeded, a stable gas film must exist. Between destabilization of the gas film and departure from discrete bubble heat transfer, transition heat transfer is the governing mechanism (see 2.2.7).

2.2.6 Transient Crust Model

Crust formation is governed by the following mechanisms:

- Heat transfer at the crust internal side with the driving temperature difference $T_{bulk} - T_{freez}$
- Heat conduction through the crust; the bounding temperatures of the crust are T_{freez} and T_i
- Heat transfer at the crust external side with the driving temperature difference T_i and T_{surr}.

Figure 12 illustrates the concept of crust formation with an electrical analogy model.

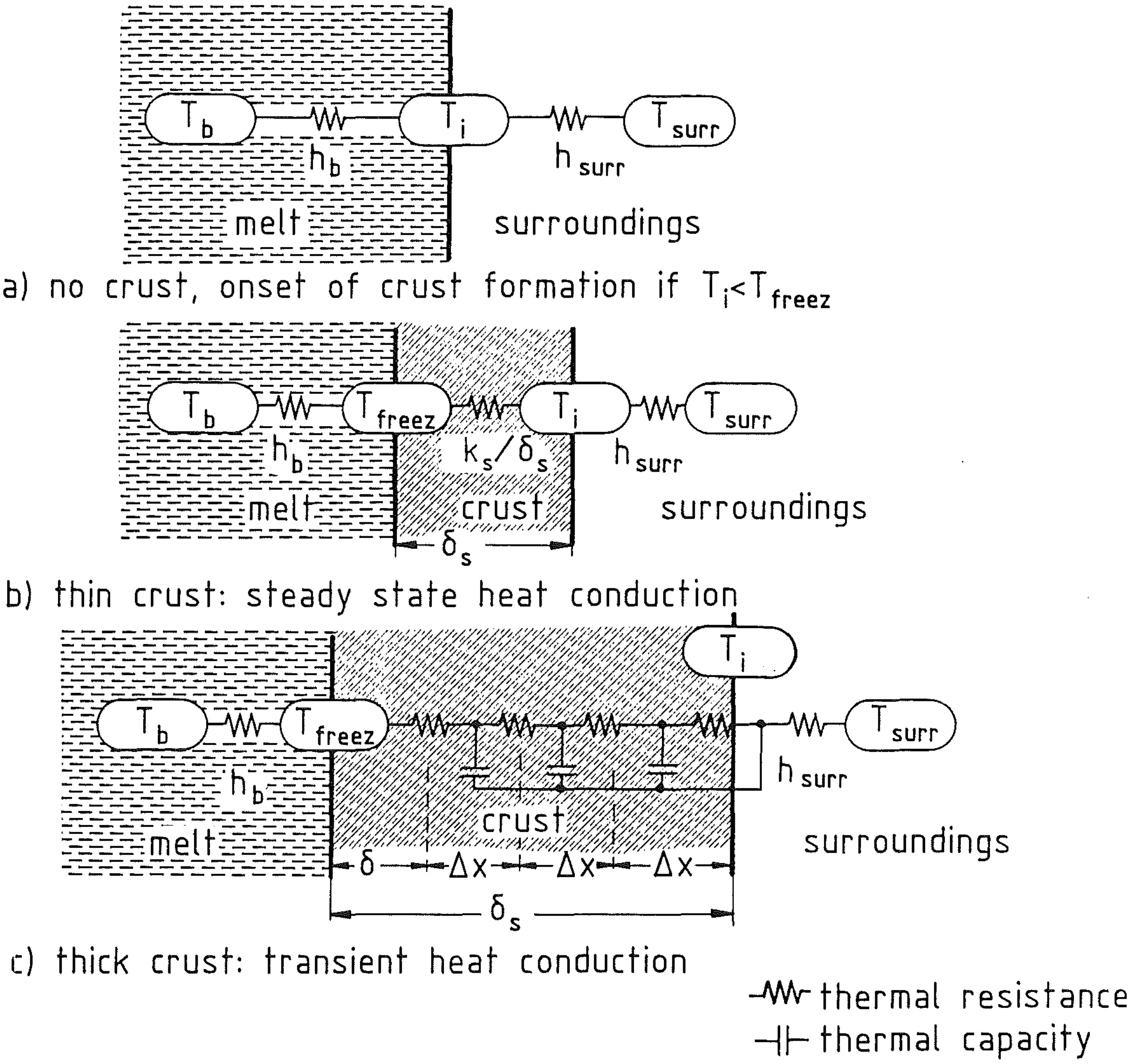

Figure 12: Electrical analogon for crust formation.

In the case of a crust facing the concrete surface, the surrounding temperature T_{surr} is equal to the concrete ablation temperature T_{d0} and the heat transfer coefficient is h_{film}.

After the onset of crust formation, thin solid layers which are formed float with the liquid of the melt bulk. Hence, it is plausible to assume steady-state heat conduction through the crust for this situation . In that case, all three heat flux densities are equal and the situation corresponds to Figure 12b. Thus,

$$h_b(T_b - T_{b,freez}) = \frac{k_s}{\delta_s}(T_{b,freez} - T_i) = h_{surr}(T_i - T_{surr}) . \qquad (2.2.6\text{-}1)$$

From this equation, the unknown quantities
- crust thickness δ_s and
- surface temperature of the crust T_i

can be evaluated.

In the next time step, the mesh width of the relevant bulk material is fixed. If the crust thickness exceeds this value, transient heat conduction is applied in the first complete mesh and the next mesh starts growing. The situation then corresponds to that in Figure 12c (where the effect of internal heat sources is not considered). The one-dimensional, transient heat conduction inside the crust can be treated with an explicit calculation scheme according to [30] inside the mesh n for the time characterized by j + 1, viz,

$$T_{n,j+1} = \bar{p}\,(T_{n+1,j} + T_{n-1,j}) + (1 - 2\,\bar{p}\,)T_{n,j} + \frac{(\Omega_b/V_b)}{\rho_b c_b} \qquad (2.2.6\text{-}2)$$

where Ω_b/V_b is the heat source density of the bulk, containing nuclear decay, chemical reaction heat, and energy contributions from the liquid and gaseous concrete decomposition products flowing through the solid crust.

The module $\bar{p}$ is defined by

$$\bar{p} = \frac{k_b}{\rho_b c_b}\,\frac{\Delta t}{(\Delta x)^2} \qquad (2.2.6\text{-}3)$$

This module is fixed.with the given mesh width Δx and time increment $\Delta\tau$. Care must be taken that the stability criterion

$$\bar{p} < 1/3 \tag{2.2.6-4}$$

is fulfilled in the explicit calculation scheme given by Eq. (2.2.6-2).

The temperature of the first fictitious mesh n = 1 at the outside of the crust can be evaluated by

$$T_{1,j} = \frac{1 - Bi^*}{1 + Bi^*} T_{2,j} + \frac{2\,Bi^*}{1 + Bi^*} T_{surr,j} \tag{2.2.6-5}$$

with the sourrounding temperature $T_{surr,j}$. The special Biot-number Bi* contains the external boundary condition and is defined by

$$Bi^* = \frac{h_{surr}}{k_b} \frac{\Delta x}{2} \tag{2.2.6-6}$$

where h_{surr} is the external heat transfer coefficient.

At the phase change interface between crust and melt at freezing temperature T_{freez}, the change of the crust thickness δ_s is given by the heat flux balance

$$\rho_b h_{fus} \frac{d\delta_s}{d\tau} = (Q/A)_{out} - (Q/A)_{in} \tag{2.2.6-7}$$

with the specific latent heat of phase change of the bulk material h_{fus}. The heat flux density $(Q/A)_{out}$ is carried away by heat conduction into the last mesh of the crust and

$$(Q/A)_{in} = h_\ell (T_\ell - T_{freez}) \tag{2.2.6-8}$$

is transported by convective mechanisms to the phase change interface. Hence, the crust thickness is changed in a time increment $\Delta\tau$ by

$$\Delta\delta = \frac{\Delta\tau}{\rho_b h_{fus}} \left\{ \frac{T_{freez} - T_{n,j}}{(\frac{\Delta x}{2} + \delta^*)} k_b - h_\ell (T_\ell - T_{freez}) \right\} \tag{2.2.6-9}$$

If the residual crust thickness ($\delta^* + \Delta x/2$) exceeds 1.2 Δx, a further mesh is added to the region of transient heat conduction inside the crust. In the opposite case of crust melting, a mesh is subtracted from the region of transient heat conduction, when the residual crust thickness δ^* drops below 0.3 Δx.

2.2.7 Application of the Models in the WECHSL Code

The BETA high power tests, in which completely liquid layers must be anticipated, showed a strong downward penetration of the metal bulk into the concrete of the crucible and a very limited side-wall erosion. Consequently, an enhanced heat transfer mode must exist in the bottom region of the crucible which leads to the conclusion that at higher superficial gas velocities, as given by the BERENSON criterion Eq. (2.2.5-2), a partial destabilization of the horizontal gas film may occur. Thus, a factor F for multiplication of the BERENSON criterion has been introduced in the post-test calculations.

$$Re_{min\ mod} = F\, Re_{min} \tag{2.2.7-1}$$

which leads to an increase in the minimum superficial gas velocity at which quenching sets in at the bottom of the crucible. The bottom aerea covered by the gas film is then linearly reduced until the heat transfer is governed completely by the discrete bubble model.

The Reynolds number of the gas film is

$$Re_{film} = \frac{Nu_{film}}{Pr\, Ste} \tag{2.2.7-2}$$

whith Nu_{film} given by Eqs. (2.2.3-19, 20).

If $Re_{film} < Re_{min\ mod}$ (Eq. (2.2.7-1))and $Re_{bubble} < Re_{max}$(Eq. (2.2.5-3)), the Nusselt number based on the gas properties is

$$Nu = f\, Nu_{film} + (1-f)\, Nu_{bubble}\, \frac{k_\ell}{k_g}\, \frac{T_\ell - T_{d0}}{T_i - T_{d0}} \tag{2.2.7-3}$$

where

$$f=\frac{Re_{film}-Re_{min}}{Re_{min\,mod}-Re_{min}} \tag{2.2.7-4}$$

and Nu_{bubble} is given by Eqs. (2.2.5-5, 6, 7, 8) with $a=0$ in Eq. (2.2.5-6). As in Eq.(2.2.7-2) Re_{bubble} is defined on the basis of liquid properties.

As shown in Figure 13, an earlier destabilization of the gas film is likely to occur, as, in contrast to boiling phenomena, the gases during concrete decomposition are released in the depth of the solid material beneath the ablating concrete surface, while the heat flux causing the gas release has to be transported by thermal conduction through a layer of degassed concrete. This may lead to temporal oscillations of gas emission. Moreover, the aggregate stones may form a barrier to the released gases which may lead to local discontinuities in the gas flow. To reproduce the erosion data of the high power BETA tests with WECHSL, a factor

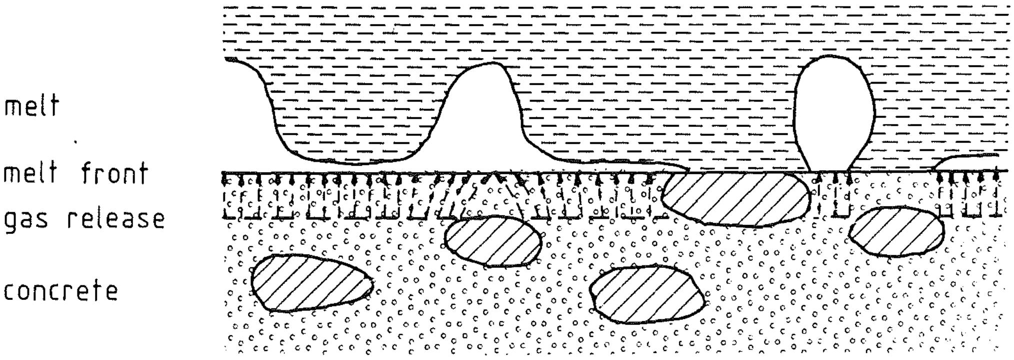

Figure 13: Destabilization of the gas film.

$$F=25 \tag{2.2.7-5}$$

was found to be convenient and was fixed in WECHSL.

If a crust is formed in the bottom region, the quenched regions of the concrete surface are reduced again. At a defined minimum crust thickness δ_{min}, the crust will close completely so that no quenched regions exist any longer. This behavior is taken into account by defining a new factor

$$f^{*}=(1-f)f_c+f \tag{2.2.7-6}$$

where

$$f_c=\frac{\delta_s}{\delta_{min}}\,. \tag{2.2.7-7}$$

and by replacing the factor f in Eq. (2.2.7-3) by f*.

At the side walls, the gas film is more stable than in the bottom region of the concrete structure. Consequently, the gas film is retained in WECHSL in all situations occurring .

When the melt layer is completely liquid or has only thin crusts with $\delta_s < \delta_{min}$, the bulk boundary layer heat transfer is calculated as described in Section 2.2.4. When the crust thickness exceeds a defined value δ_{max}, a situation as shown in Figure 3c has established: The gases released from the concrete flow through tubular holes in the crust and form gas bubbles detaching from the inner crust surface. The inside heat transfer from the melt bulk to the crust is then given, in principle, by a discrete bubble type heat transfer relation as recommended in [27]

$$Nu_\ell = C\,Re^{0.5}\,Pr_\ell^{0.42} \tag{2.2.7-8}$$

which is also the basis of Eq. (2.2.5-5). The Reynolds number is defined by Eq. (2.2.5-1) and the Prandtl number by Eq. (2.2.5-4). The constant C was fixed empirically to be

$$C = 0.40\,. \tag{2.2.7-9}$$

Between δ_{min} and δ_{max}, the heat transfer is averaged linearly in WECHSL.

When the metal layer has solidified completely, direct contact of the frozen slug with the concrete is assumed. Then, the surface temperature of the metal block facing the concrete is assumed to be at the concrete decomposition temperature T_{d0}.

2.3 Pool Behavior

2.3.1 Bubble Size and Velocity of Rise

Gas bubbles rising through the melt are responsible for melt stirring. They also cause swelling of the melt so that the surface area for heat transfer is effectively increased. The bubble behavior is important because of the large volume fluxes of gas released, and a considerable void fraction may develop in the melt.

It has been assumed in the gas film model that bubbles of uniform size and spacing are formed. This is well confirmed by experiments with simple materials such as water over dry ice. However, also in experiments with water over inhomogeneous materials, i.e. frozen xylene and carbon dioxide snow simulating the liquid and gaseous decomposition products of the concrete [13], it was seen that the gas bubbles have an average diameter similar to that in the experiments with pure materials.

The mean equivalent sphere radius of the bubbles detatching from the gas film has been estimated in Eq. (2.2.3-8) to be

$$r_{eq} = \frac{\lambda}{4} = 2.74a\,. \tag{2.3.1-1}$$

The bubble radius as estimated in the discrete bubble model is of the same order of magnitude.

The Reynolds number of the bubble

$$Re_{\ell} = \frac{\rho_{\ell} r_{eq} u_{b}}{\mu_{\ell}} \tag{2.3.1-2}$$

is important to the behavior of rising bubbles. For small Reynolds-Numbers, i.e. for small bubble dimensions or for a high kinematic viscosity of the fluid, buoyancy forces are balanced by the friction forces:

$$\frac{4\pi}{3} r_{eq}^{3} g\,\Delta\rho = \zeta \pi r_{eq}^{2} \frac{\rho\, u_{b}^{2}}{2} \tag{2.3.1-3}$$

where ζ is the friction coefficient. From this equation, the bubble velocity can be written as

$$u_{b} = \left(\frac{8\, g\, \Delta\rho\, r_{eq}}{3\, \rho_{\ell} \zeta} \right)^{1/2}. \tag{2.3.1-4}$$

For very small bubbles - which are not of interest here - the friction coefficient for a rigid sphere is applicable (Stokes flow and transition region). For higher Reynolds numbers, the friction coefficient is twice that for Stokes flow around a rigid sphere as proposed by Levich [31]:

$$\zeta = \frac{24}{Re_\ell} \tag{2.3.1-5}$$

and the velocity of bubble rise is obtained as

$$u_{b1} = \frac{1}{9}\, g \, \frac{\Delta\rho}{\rho_\ell}\, r_{eq}^2 \, \nu^{-1} . \tag{2.3.1-6}$$

In low viscous fluids, the velocity of rise increases up to a maximum value. Beyond this value, the rise behavior changes completely.

The sperical cap bubbles start oscillating and rise along zig-zag or helical lines. With increasing bubble radius, the rise velocity decreases to a minimum value. Then, the rise velocity increases again. Mendelson [32] formulated this complicated behavior in a single equation by balancing basically the inertia forces with the gravity and capillary forces. By introducing the dimensionless groups

$$\left.\begin{aligned} E\ddot{o} &= \frac{g\,\rho_\ell r_{eq}^2}{\sigma} \\ We &= \frac{r_{eq}\,\rho_\ell\, u_b^2}{\sigma} \end{aligned}\right\} \tag{2.3.1-7}$$

it results

$$We = E\ddot{o} + 1 , \tag{2.3.1-8}$$

or, for the velocity of bubble rise

$$u_{b2} = \left(g\, r_{eq} + \frac{\sigma}{\rho_\ell\, re_{eq}} \right)^{1/2} . \tag{2.3.1-9}$$

For large bubbles, the capillary forces can be neglected and the rise velocity approaches

$$u_{b2}^{*} = (g\, r_{eq})^{1/2} . \tag{2.3.1-10}$$

In highly viscous fluids, the bubbles rise straight without oscillations. Here, the rise velocity increases continuously with increasing bubble radius and, finally, approaches Eq. (2.3.1-10).

The effective bubble rise velocity is determined by

$$u_b = min(u_{b1}, u_{b2}) . \qquad (2.3.1\text{-}11)$$

Some data from the experimental work of Habermann and Morton [33] are shown in Figure 14, along with the values computed by Eq. (2.3.1-11).

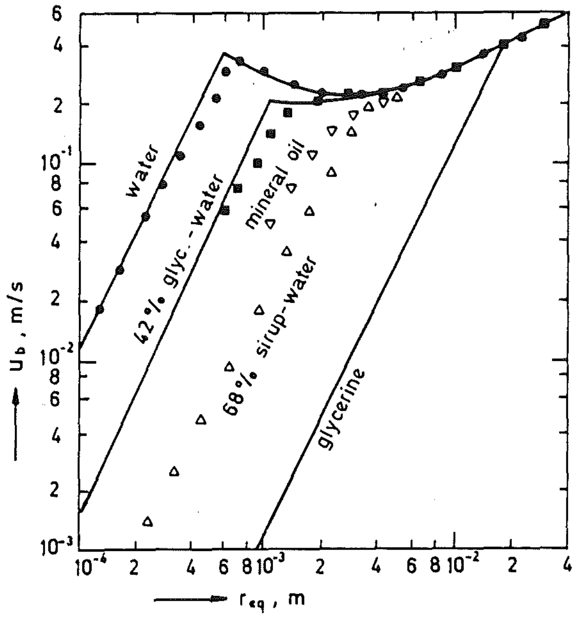

Figure 14: Velocity of rise for air bubbles in a tank of stagnant liquid [33].

The maximum possible equivalent bubble radius is given by Levich [31] to be

$$r_{eq\,max} = \frac{\sigma}{u_b^2}\left(\frac{12}{\rho_g\,\rho_\ell^2}\right)^{1/3} . \qquad (2.3.1\text{-}12)$$

When a bubble exceeds this dimension, it bursts into smaller bubbles.

The formation of a foamy oxide with very small gas bubbles but very high voids, as observed in some of the simulant tests, is not considered in WECHSL because of lack of information about the conditions under which a foamy melt would exist.

2.3.2 Void Fraction

In the foregoing section, the rise behavior of a single bubble in a stagnant liquid was discussed. However, when large numbers of bubbles rise, the rise velocity is reduced to u_{bs}. Le Clair and Hamielec [34] gave a plot of the ratio u_{bs}/u_b over the void fraction ε of the liquid with the single bubble Reynolds number Re_b as the parameter. Their figure can be closely approximated by

$$\frac{u_{bs}}{u_b} = (1-\varepsilon)^n \tag{2.3.2-1}$$

with

$$Re_b \leq 50: n = -1.14 \, log(Re_b) + 4.11$$

$$Re_b > 50: n = -0.52 \, log(Re_b) + 3.05 \tag{2.3.2-2}$$

The values of the exponent n are restricted. By introducing the superficial gas velocity as

$$v_g = \frac{(\dot{m}/A)}{\rho_g} , \tag{2.3.2-3}$$

the maximum exponent n_{max} is a function of the ratio u_b/v_g. The criterion of estabilishing this function is to avoid numerical overflow in WECHSL.

The void fraction, the artificial gas velocity and the velocity of bubble swarm rise velocity of a bubble swarm are correlated according to Nicklin [35] by

$$\frac{v_g}{\varepsilon} = u_{bs} + v_g \tag{2.3.2-4}$$

By inserting Eq. (2.3.2-1), the void fraction can be evaluated from

$$\varepsilon = \frac{1}{\left(1 + (1-\varepsilon)^n \frac{u_b}{v_g}\right)} \tag{2.3.2-5}$$

In WECHSL, the void fraction is arbitrarily limited to $\varepsilon_{max} = 0.85$.

2.3.3 Phase Segregation

It has been experimentally observed [7, 8] that a melt containing metal and lighter oxidic phases may undergo a rapid, density driven phase segregation. The BETA tests [4], however, showed that under certain conditions, mainly characterized by high viscosity of the oxide phase and by high gas flow, the melt phases may intermix. As the dispersed state of the metallic and the oxidic phases will segregate when the gas flow is reduced after the initial, relatively short and intense phase of interaction modeling by WECHSL is limited to the assumption of two separated layers: an upper oxide layer and a lower metal layer. In a core melt, the oxide is initially composed of a mixture of ZrO_2 and UO_2, which, according to Ondracek [36], has a slightly lower density than the metallic phase. This is the maximum possible density for the oxide. The accretion of molten concrete constituents in the oxide layer causes the density to become significantly lower.

2.3.4 Heat Transfer between the Molten Layers

Wehrle [37] studied the heat transfer between liquid layers in the presence of gas percolation using simulant materials. In liquid layers without gas percolation, heat is transferred by natural convection. Haberstroh and Reinders [38] performed an analysis of this case based on the heat transport through a single layer heated from below and they obtained

$$Nu = 0.0535 \{Gr\,Pr\}^{1/3} Pr^{n} \tag{2.3.4-1}$$

If an odd symmetric temperature profile is assumed to exist in each layer, the heat flux transferred from the high temperature (index h) to the low temperature (index l) layer is

$$\left(\frac{Q}{A}\right)_{i,0} = \left(\frac{2}{\left(\frac{1}{h_h^{*}k_h}\right)^{3/4} + \left(\frac{1}{h_l^{*}k_l}\right)^{3/4}}\right)^{4/3} (T_h - T_l)^{4/3}, \tag{2.3.4-2}$$

where T_h and T_l are the different bulk temperatures and

$$h_{h,l}^{*} = 0.0535 \cdot 2^{4/3} \left(\frac{g\,\beta_{h,l}}{\nu_{h,l}^{2}}\right)^{1/3} Pr_{h,l}^{0.417}\, k_{h,l} \tag{2.3.4-3}$$

is a special quantity related to the heat transfer coefficient by

$$h_{h,l} = h_{h,l}^{*} (T_{h,l} - T_i)^{1/3}. \tag{2.3.4-4}$$

The interface temperature is determined by

$$T_i = T_h + \frac{\left(\frac{1}{h_h^* k_h}\right)^{3/4}}{\left(\frac{1}{h_h^* k_h}\right)^{3/4} + \left(\frac{1}{h_l^* k_l}\right)^{3/4}} (T_h - T_l). \tag{2.3.4-5}$$

Wehrle evaluated his model experiments using silicone oil/water and silicone oil/wood metal systems by determination of the factor

$$\gamma = \frac{(Q/A)_i}{(Q/A)_{i,0}} \tag{2.3.4-6}$$

describing the enhancement of heat transfer by gas percolation in comparison with pure thermal convection. A reasonable fit of his data is

$$\gamma = 1 + 608\,(\frac{v_g}{u_b})\,Ar^{-0.43} \tag{2.3.4-7}$$

with the Archimedes number

$$Ar = \left| \frac{\rho_l - \rho_h}{\rho_l} \right| \tag{2.3.4-8}$$

In Figure 15, a comparison of the experimental data with Eq. (2.3.4-7) is given.

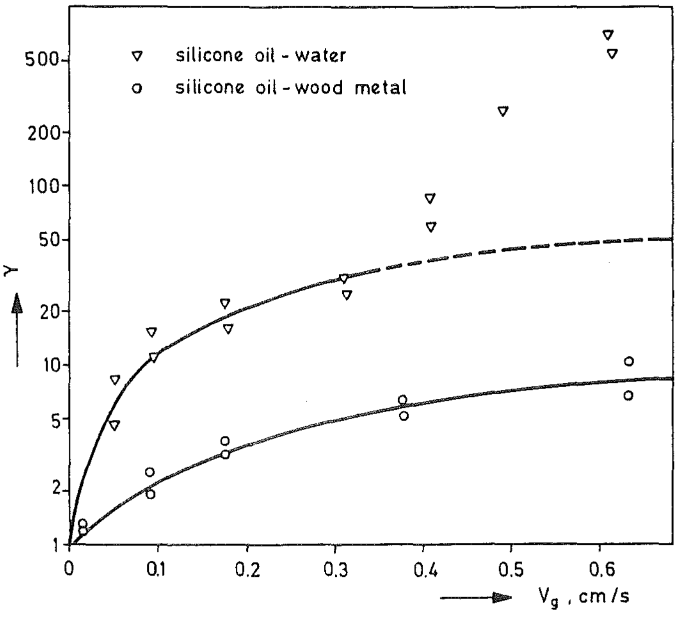

Figure 15: Enhancement of heat transfer between liquid layers percolated by gas bubbles.

The equation above holds as long as a distinct interface exists between the liquid layer and emulsifying effects are not decisive. The formation of emulsions was observed when the densities of the liquid layers were nearly equal or the viscosity of the oxide liquid was very high and the gas velocity was high. In Figure 11, the onset of emulsion formation is marked by a further increase in heat transfer in the oil/water system. In the oil/wood metal system, such a behavior could not be observed up to the maximum superficial gas velocity. In a core meltdown accident emulsification may occur at an intermediate stage, as was discussed above. On the other hand, the heat exchange between the molten layers is rather intense, even if the emulsifying effects are left out of consideration so that the temperature differences between the layers are generally small. A further improvement of heat transfer modeling would produce only a minor effect.

In the late phase of low-power BETA experiments, the metal bulk has a higher temperature than the oxide bulk. In that case, $T_m > T_o$, a metal crust may occur at the interface between metal and oxide. On the other hand, in the course of a core melt accident, the oxide bulk may have a higher temperature than the metal bulk. Thus, when $T_m < T_o$, an oxide crust may develop at the interface between metal and oxide. The metal is then either liquid at the interface, or the metal bulk is completely frozen so that a hot solid block of metal acts on the concrete structure.

This means, that a crust can only be formed at the metal/oxide interface in the high temperature phase. The heat conduction inside the crust is modeled in agreement with Section 2.2.6 either as a steady-state process (Figure 12b) for thin crusts or a transient process if the crust thickness exceeds the predefined mesh width (Figure 12c). The heat transfer coefficient at the interface between the melt layers and at the solidified interface is determined according to Eq. (2.3.4-1). For the first case, the driving temperature difference is T_i-T_l, whereas for the latter case, T_h-$T_{freez,h}$ is valid.

If the metal layer has completely solidified, the discrete bubble type heat transfer equation given in Eq. (2.2.7-8, 9) is used again.

2.3.5 Heat Transfer from the Top of the Melt

The gas bubbles rise through the oxide layer and break through the surface. By this mechanism, heated liquid is "pumped" to the free surface and a thermal boundary layer is formed.

From the top of the melt, the heat is carried away mainly by thermal radiation or - if the melt is flooded by water as may occur in core melt accidents with sump water ingression - by boiling heat transfer.

The heat transfer through the boundary layer under the melt surface is then represented by an expression similar to microconvective heat transport induced by a discrete bubble detaching from a gas emitting wall [27], again in agreement with Eq. (2.2.7-7, 8)

$$Nu_{o,s} = 0.040\, Re_b^{1/2}\, Pr_o^{0.42} \,. \tag{2.3.5-1}$$

with

$$Nu_{o,s} = \frac{h_{o,s}\, r_{eq}}{k_o} \tag{2.3.5-2}$$

and the Reynolds-number of the bubble as defined in Eq. (2.3.1-2).

If the heat is carried away from the melt surface by thermal radiation, the resulting heat flux density

$$(Q/A)_{o,s} = h_{o,s}\,(T_o - T_{o,s}) \tag{2.3.5-3}$$

is balanced with the heat radiation from the surface to the surroundings

$$(Q/A)_{rad,s} = \varepsilon_{s\infty}\, c_0\, (T_{o,s}^4 - T_\infty^4) \tag{2.3.5-4}$$

with

$$\varepsilon_{s\infty} = \frac{1}{\dfrac{1}{\varepsilon_{o,s}} + \dfrac{1}{\varepsilon_\infty} - 1} \tag{2.3.5-5}$$

The resulting equation is solved for the surface temperature.

If a crust is formed at the top of the melt, the additional heat resistance due to heat conduction in the crust has to be taken into account; the heat conduction is considered again to be stationary for a thin crust or transient for a thick crust, as described in Section 2.2.6. When a crust is present, the surface temperature $T_{o,s}$ must be replaced by T_{freez} in Eq. (2.3.5-3).

In the BETA tests, strong splashout of oxide melt was observed in high power tests with high superficial gas velocities. To take into consideration this effect in WECHSL, an empirical model was established. It is assumed that splashout acts on an annular region adjacent to the side wall of the concrete structure of width λ, where λ is the wavelength defined by Eq. (2.2.3-5). Thus, the effective surface area for splashout is

$$A_{eff}=(d_o-\lambda)\lambda\pi \ . \tag{2.3.5-6}$$

If the superficial gas velocity

$$v_g>0.04\ m/s\ , \tag{2.3.5-7}$$

the mass flux of oxides splashed out onto the side wall is given by the equation

$$\frac{\dot{m}_o}{C_o A_{eff}}=\left(\frac{v_g}{0.04}-1\right)^{1.8} \tag{2.3.5-8}$$

where

$$C_o=600\ \frac{kg}{m^2 s}\ . \tag{2.3.5-9}$$

The material is splashed out at oxide bulk temperature and returns into the pool at the mean temperature

$$T=(T_o+T_{freez})/2\ . \tag{2.3.5-10}$$

By this empirical model, the strong cooling effect caused by splashout due to the violent gas evolution in the high-power BETA tests could be reproduced adequately in the WECHSL code. In a core melt accident, the surface area ratio A_{eff}/A_{tot} is very small and, consequently, the cooling effect due to splashout is only of minor importance.

If the liquid oxide pool is flooded by water at high temperature, oxide droplets may be entrained into the water bulk. This may cause steam explosions, as reported in [39]. Of course, agitation of the gas bubbles breaking through the pool surface enhances the entrainment of oxide and the possibility of steam explosions as well. In a core melt accident in a large German standard PWR, it is very likely that sump water ingression occurs only in the late phase of core melt/concrete interaction, several hours after the start of interaction. In that situation either solid crusts have been formed at the pool surface or the melt is highly viscous with a bulk temperature near the solidification temperature. This excludes serious steam explosions resulting from late sumpwater ingression, but also prevents substantial fragmentation of the oxide surface so that a coolable particle bed has not to be expected [40, 41].

For the evaluation of heat transfer from the melt pool surface to the bulk of water it was considered sufficient to take into account in WECHSL boiling phenomena at a rigid horizontal surface. The correlations given below are taken from the "Handbook of Heat Transfer" [42].

Initially, when the water floods the melt surface, the surface temperature is around 1000 K. Hence, film boiling occurs. The heat transfer through the vapor film is given by

$$Nu_{fb}=0.425\left[Gr_{v}\,Pr_{v}\,\frac{h_{wv}+0.4c_{pv}\Delta T}{c_{pv}\Delta T}\right]^{1/4} \tag{2.3.5-11}$$

with the driving temperature difference

$$\Delta T=T_{o,s}-T_{w} \tag{2.3.5-12}$$

Here and in the following equations, the index v characterizes vapor properties, whereas the index w indicates sump water properties in the state of saturation. $T_{o,s}$ is again the melt pool surface temperature.

The dimensionless groups in Eq. (2.3.5-11) are

$$Nu_{fb}=\frac{h_{fb}'\;a}{k_{v}}$$

$$Gr_{v}=\frac{\rho_{v}g(\rho_{l}-\rho_{v})a^{3}}{\mu v^{2}} \tag{2.3.5-13}$$

$$Pr_v = \frac{\mu_v c_{pv}}{k_v}$$

The characteristic length is the Laplace constant

$$a = \left[\frac{\sigma}{g(\rho_w - \rho_v} \right]^{1/2} \tag{2.3.5-14}$$

The heat transfer coefficient is given by

$$h_{fb} = 0.425 \left[\frac{k_v^3 \rho_v (\rho_w - \rho_v) g (h_{hw} + 0.4 c_{pv} \Delta T)}{\mu_v a \Delta T} \right]^{1/4} \tag{2.3.5-15}$$

The heat transmission by thermal radiation through the vapor film is given by

$$h_{rad} = \varepsilon_{sw} c_o \left(\frac{T^4_{o,s} - T^4_w}{T_{o,s} - T_w} \right) \tag{2.3.5-16}$$

with

$$\varepsilon_{sw} = \frac{1}{\frac{1}{\varepsilon_s} + \frac{1}{\varepsilon_w} - 1} . \tag{2.3.5-17}$$

The total heat flux density is evaluated by the approximation equation

$$(Q/A)_{fb} = (h_{fb} + \frac{3}{4} h_{rad})(T_{0,s} - T_w) \tag{2.3.5-18}$$

The minimum heat flux density for destabilization of the gas film is again

$$(Q/A)_{min} = 0.09 \, \rho_v h_{wv} \left[\frac{\sigma g (\rho_w - \rho_v)}{(\rho_w + \rho_v)^2} \right]^{1/4} \tag{2.3.5-19}$$

The region of instable boiling is situated between the minimum heat flux density for film boiling and the maximum heat flux for nucleate boiling given by

$$(Q/A)_{max} = 0.18 \, \rho_v h_{wv} \left[\frac{\sigma g (\rho_w - \rho_v)}{\rho_v^2} \right]^{1/4} \left(\frac{\rho_w}{\rho_w + \rho_v} \right)^{1/2} \tag{2.3.5-20}$$

If the surface temperature $T_{o,s}$ is further reduced, the region of nucleate boiling is entered. The heat transfer is described e.g. by Rohsenow [42] by

$$Ste = \bar{C}\, Re_{bubble}^{1/3}\, Pr_w^s \tag{2.3.5-21}$$

with

$$\left.\begin{aligned} Ste &= \frac{h_{wv}}{c_{pw}\,\Delta T} \\ Re_{bb} &= \frac{(Q/A)a}{\mu_w h_{wv}} \end{aligned}\right\} \tag{2.3.5-22}$$

For water, s = 1 and $\bar{C} = 0.006$ are recommended. Thus, the heat flux density due to bubble boiling yields

$$(Q/A)_{bb} = \left[166.7\, \frac{k_w \Delta T}{a} \left(\frac{a}{\mu_w h_{wv}} \right)^{2/3} \right]^{1/3}. \tag{2.3.5-23}$$

For the sake of completeness, natural convection at very small temperature differences is also considered. The heat transfer is characterized by

$$Nu_{conv} = 0.14\,(Gr_w Pr_w)^{1/3} \tag{2.3.5-24}$$

leading to

$$(Q/A)_{conv} = 0.14\,\Delta T \left[\frac{k_w \rho_w^2 g \beta_w \Delta T c_{pw}}{\mu_w} \right]^{1/3} \tag{2.3.5-25}$$

The boundary between natural convection and bubble boiling is fixed by

$$(Q/A) = Max\,\{(Q/A)_{bb}, (Q/A)_{conv}\} \tag{2.3.5-26}$$

With this set of equations, the complete boiling curves can be evaluated with the aid of a system of equations of state for equilibirium properties [43] and transport properties including the surface tension [44].

Figure 16 is a plot of the results obtained in the relevant pressure region between 1 and 10 bar. The computations have been carried out with a separate computer program BOIL.

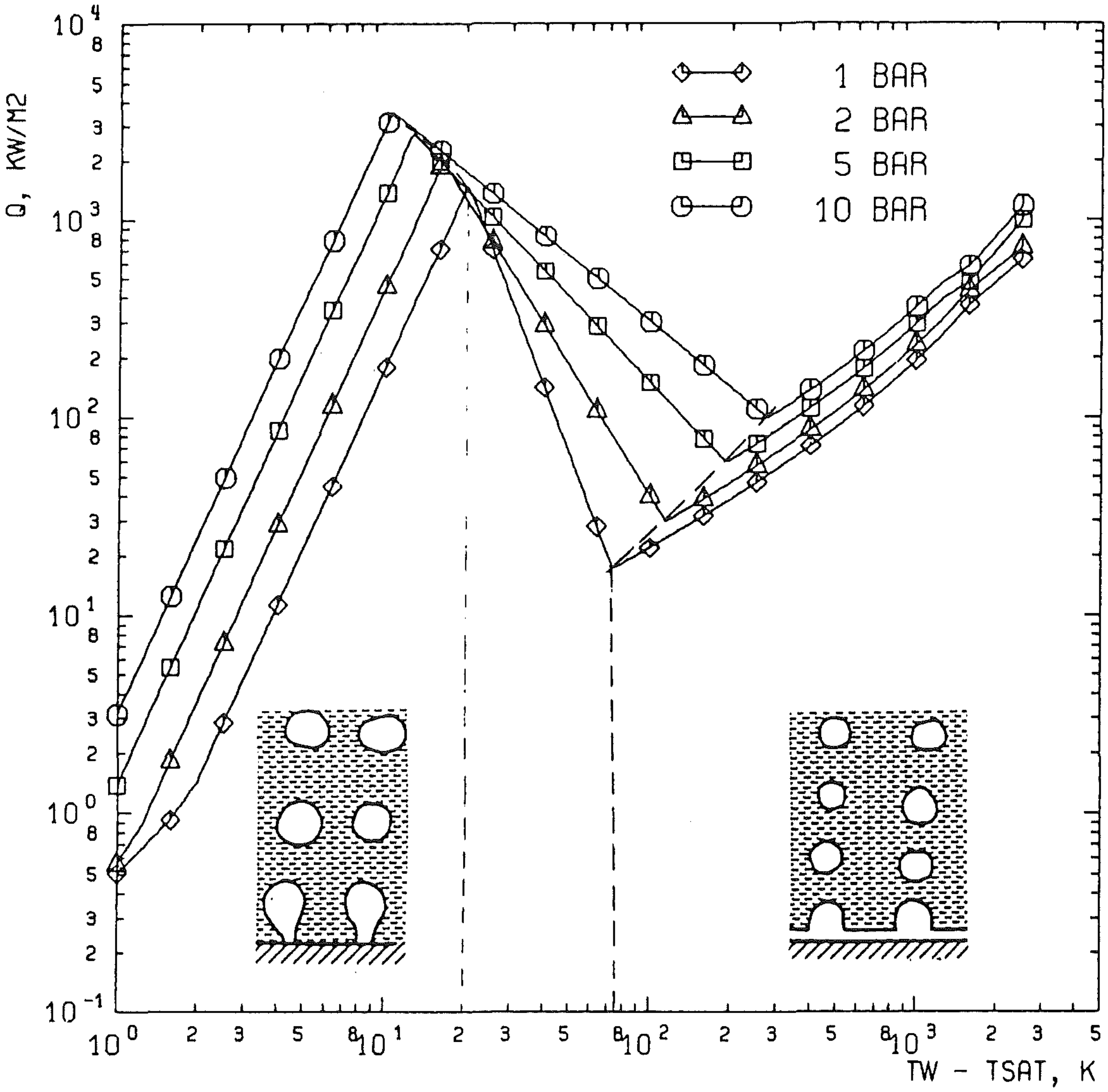

Figure 16: Boiling curves for water as a function of the system pressure.

The results as a function of equidistant logarithmic steps of the temperature difference ΔT are compiled in a set of data which is implemented into the subroutine SIEDE of the WECHSL code. Thus, the actual values for boiling heat transfer on the melt pool surface are determined by interpolation.

2.3.6 Oxidation Reactions

It has been observed that a large fraction of the steam and carbon dioxide bubbling through a metallic melt is reduced according to the reactions and enthalpies given below:

$$\left.\begin{aligned} & Zr + 2H_2O \rightarrow ZrO_2 + 2H_2 + r_{Zr,H_2O} \\ & r_{Zr,H_2O} = 7760 + 1.15(T_m - 2000) \text{ in } J/g\ Zr \end{aligned}\right\} \qquad (2.3.6\text{-}1)$$

$$\left.\begin{aligned} & Zr + 2CO_2 \rightarrow ZrO_2 + 2CO + r_{Zr,CO_2} \\ & r_{Zr,CO_2} = 5926 \text{ in } J/g\ Zr \end{aligned}\right\} \qquad (2.3.6\text{-}2)$$

$$\left.\begin{aligned} & 2Cr + 3H_2O \rightarrow Cr_2O_3 + 3H_2 + r_{Cr,H_2O} \\ & r_{Cr,H_2O} = 3504 + 2.79\,(T_m - 2000) \text{ in } J/g\ Cr \end{aligned}\right\} \qquad (2.3.6\text{-}3)$$

$$\left.\begin{aligned} & 2\,Cr + 3CO_2 \rightarrow Cr_2O_3 + 3CO + r_{Cr,CO_2} \\ & r_{Cr,CO_2} = 2780 \text{ in } J/g\ Cr \end{aligned}\right\} \qquad (2.3.6\text{-}4)$$

$$\left.\begin{aligned} & Fe + H_2O \rightarrow FeO + H_2 + r_{Fe,H_2O} \\ & r_{Fe,H_2O} = 56.7 - 2.24 \cdot 10^{-5}\,(T_m - 2000) \text{ in } J/g\ Fe \end{aligned}\right\} \qquad (2.3.6\text{-}5)$$

$$\left.\begin{aligned} & Fe + CO_2 \rightarrow FeO + CO + r_{Fe,CO_2} \\ & r_{Fe,CO_2} = -377 + 0.0271(T_m - 2000) \text{ in } J/g\ Fe \end{aligned}\right\} \qquad (2.3.6\text{-}6)$$

Other reactions are also possible theoretically, but it can be found in the literature that the equilibrium constants for reactions yielding Fe_2O_3, Fe_3O_4 and NiO are such that only a very small fraction of the gases can be reduced in these reactions.

Calculations based on a diffusion model [45] show that the above reactions proceed rapidly towards equilibrium. The equilibrium constants for the reactions (2.3.6-1) through (2.3.6-4) lie very near to complete reduction of H_2O and CO_2. For the reactions (2.3.6-5, 6), equilibrium constants are given in the relevant literature, they do not suggest that the reaction of the gases is complete. However, the composition of the gas recorded in the BETA tests could be reproduced much better under the assumption of complete reduction of steam and carbon dioxide to hydrogen and carbon monoxide by oxidation of iron.

The reactions are assumed to proceed in the order Zr:Cr:Fe so that Fe is oxidized only when all available Zr and Cr has been burnt out.

The reaction enthalpies per g metal are also given in Eqs. (2.3.6-1, 2, 3, 4, 5, 6). Reactions (2.3.6-1) through (2.3.6-4) are strongly exothermic. Reaction (2.3.6-5) is slightly exothermic and reaction (2.3.6-6) is slightly endothermic.

It is assumed that each bubble contains a single gas constituent; therefore, the water-gas reactions do not compete with the gas-metal reactions within the melt. The rationale for this assumption is that each bubble is probably generated from a relatively small area of concrete. Some bubbles are expected to contain mostly CO_2, from decomposition of a lump of limestone; other bubbles will contain mostly H_2O, from decomposition of the cement matrix. However, above the melt the gases will be well mixed, and the water-gas reaction can be expected to be homogeneous:

$$H_2O + CO \rightleftharpoons H_2 + CO_2 . \tag{2.3.6-7}$$

The equilibrium constant depending on the reaction temperature T_{reac} is given by

$$log_{10} K_p = -1.7778 + \frac{2010}{T_{reac}} \tag{2.3.6-8}$$

where

$$K_p = \frac{p_{H_2}\, p_{CO_2}}{p_{H_2O}\, p_{CO}} \tag{2.3.6-9}$$

An additional reaction considered in the WECHSL code is the thermite reaction

$$Zr + 2FeO \rightarrow ZrO_2 + 2Fe + r_{Zr\,FeO}$$

$$r_{Zr\,FeO} = 5124 \; in\, J/g\, Fe \tag{2.3.6-10}$$

This reaction is strongly exothermic and extremely rapid. In combination with the reactions (2.3.6-1, 2) any metallic zirconium present would be depleted within a short period of time.

2.3.7 Material Properties

Powers and Frazier have described in [46] the VISRHO subroutine, i.e. a method of accurate computation of densities and viscosities of magmatic melts containing silicates. This method is applied in WECHSL to the constituents of a core melt in a core melt accident and a thermite melt in a simulation test, respectively. The formation of $CaAl_2O_4$ is taken into account if CaO and Al_2O_3 are constituents of the melt.

The density of each phase is computed from the mole fraction X_i, the molecular weight M_i, the partial molar volume V_{Mi}, the thermal coefficient of volumetric expansion β_i, and the bulk temperature T by

$$\rho = \frac{\sum_{i=1}^{n} X_i M_i}{\sum_{i=1}^{n} X_i V_{Mi}\left(1+\beta_i(T-1673)\right)} \tag{2.3.7-1}$$

The values of the molar mass M_i; best estimate values of the molar volume V_{Mi} and the thermal coefficient of volumetric expansion β_i at a reference temperature of 1400 °C are compiled in Table 3.

In VISRHO the dynamic viscosity of a magmatic melt in Poise is obtained from

$$\mu = exp\left\{ \sum_{i=1}^{n} X_i D_i \right\} \tag{2.3.7-2}$$

where the coefficients D_i are tabulated in [46] for different ranges of silica contents between 35 mole% and 85 mole% and for temperatures ranging between 1200 °C and 1800 °C. From these tables, Arrhenius coefficients A_i, B_i are evaluated and used in WECHSL. They describe the temperature dependence of the coefficients D_i by

$$D_i = A_i + \frac{B_i}{T} \, . \tag{2.3.7-3}$$

No data are available in [46] for the constituents UO_2 and ZrO_2 . For these substances, the coefficients for TiO_2 are used. The Arrhenius coefficients are extrapolated for low silica fractions to give reasonable results for pure corium and

Component	M_i g/mole	V_i cm³/mole	β_i (K⁻¹)
UO_2	270	26.76	1.2×10^{-5}
ZrO_2	123.2	23.32	5.88×10^{-5}
FeO	71.85	12.8	16×10^{-5}
CaO	56.08	16.5	18×10^{-5}
SiO_2	60.09	26.8	0.9×10^{-5}
Al_2O_3	101.96	37.96	2.6×10^{-5}
Cr_2O_3	152	30.11	2.6×10^{-5}
$CaAl_2O_4$	158.04	54.5	20.6×10^{-5}
Fe	55.85	7.7	3.1×10^{-5}
Zr	91.22	15.7	1.65×10^{-5}
Cr	52.0	8.67	1.8×10^{-5}
Ni	58.71	7.55	3.9×10^{-5}

Table 3: Masses and densities of oxidic and metallic constituents, reference temperature 1400 °C.

pure Al_2O_3, respectively, and for high silica fractions to reproduce the viscosity data of pure silicate.

In the method originally described in [46] coefficients were used which were considered to be constant within a range of silica contents. However, it has been found that the jumps in viscosity in passing from one silica range to the next may cause severe numerical disturbances under some circumstances. Therefore, linear interpolation is used to give smooth transitions.

Skoutajan et al. [47] investigated experimentally the viscosity of corium/silicate melts at temperatures between 1300 °C and 1600 °C. They found that the VISRHO calculations give values far below the experimental data. A much better representation of their experimental data can be found by presuming the precipitation of solid particles of the high melting oxides (i.e. UO_2, ZrO_2, CaO) between the liquidus and the solidus temperatures of the melt. The empirical Kunitz-formula [48] for liquid/solid mixtures

$$\frac{\mu_{LS}}{\mu} = \frac{1 + 0.5\,\Gamma}{(1 - \Gamma)^4} \qquad (2.3.7\text{-}4)$$

with

$$\Gamma = \frac{T_L - T_{LS}}{T_L - T_S} \sum_{i=1}^{n_h} \psi_i \qquad (2.3.7\text{-}5)$$

is used, where μ_{LS} is the viscosity of the liquid/solid mixture at a temperature T_{LS} between the liquidus temperature T_L and the solidus temperature T_S, and $\Sigma\psi_i$ is the sum of weight fractions of the high melting constituents (i.e. UO_2, ZrO_2, CaO).

In Figure 17, the results of the modified VISRHO calculations are compared with the experimental data. As can be seen, most of the measurements are made between case A (reactor concrete as given in [47] with 73.1 wt.-% SiO_2) and case B (87.2 wt.-% SiO_2). For 0%/100 % and 10 %/90 % corium/concrete mixtures, the measurements carried out beyond the liquidus temperature, for the 30 %/70 % and 50 %/50 % corium/concrete mixtures the measurements have been carried out between the solidus and the liquidus temperature where Eq. (2.3.7-4) is applicable.

In the simulation experiments performed in the BETA test facility, the oxidic corium melt is replaced by the oxidic part of a thermite melt which is usually Al_2O_3. Consequently, the knowledge of the viscosity of mixtures containing Al_2O_3 and SiO_2 is also important in the evaluation of the simulation tets. In [46], measurements of the dynamic viscosity of Al_2O_3/SiO_2 mixtures are compiled from the literature. They were performed at temperatures between 1900 °C and 2350 °C which is always beyond the relevant liquidus temperature. Figure 18 gives the comparison of the modified VISRHO calculation with the experimental data.

For the metallic phase, the viscosity is assumed to be that of pure iron, the major metallic constituent. According to the data of [49], the metal viscosity is equated by

$$log_{10}\left(\frac{\mu}{\mu_o}\right) = \frac{2385.2}{T} - 0.5958 \qquad (2.3.7\text{-}6)$$

Specific heat, latent heat of freezing, thermal conductivity and surface tension are computed with the simple mixture theory.

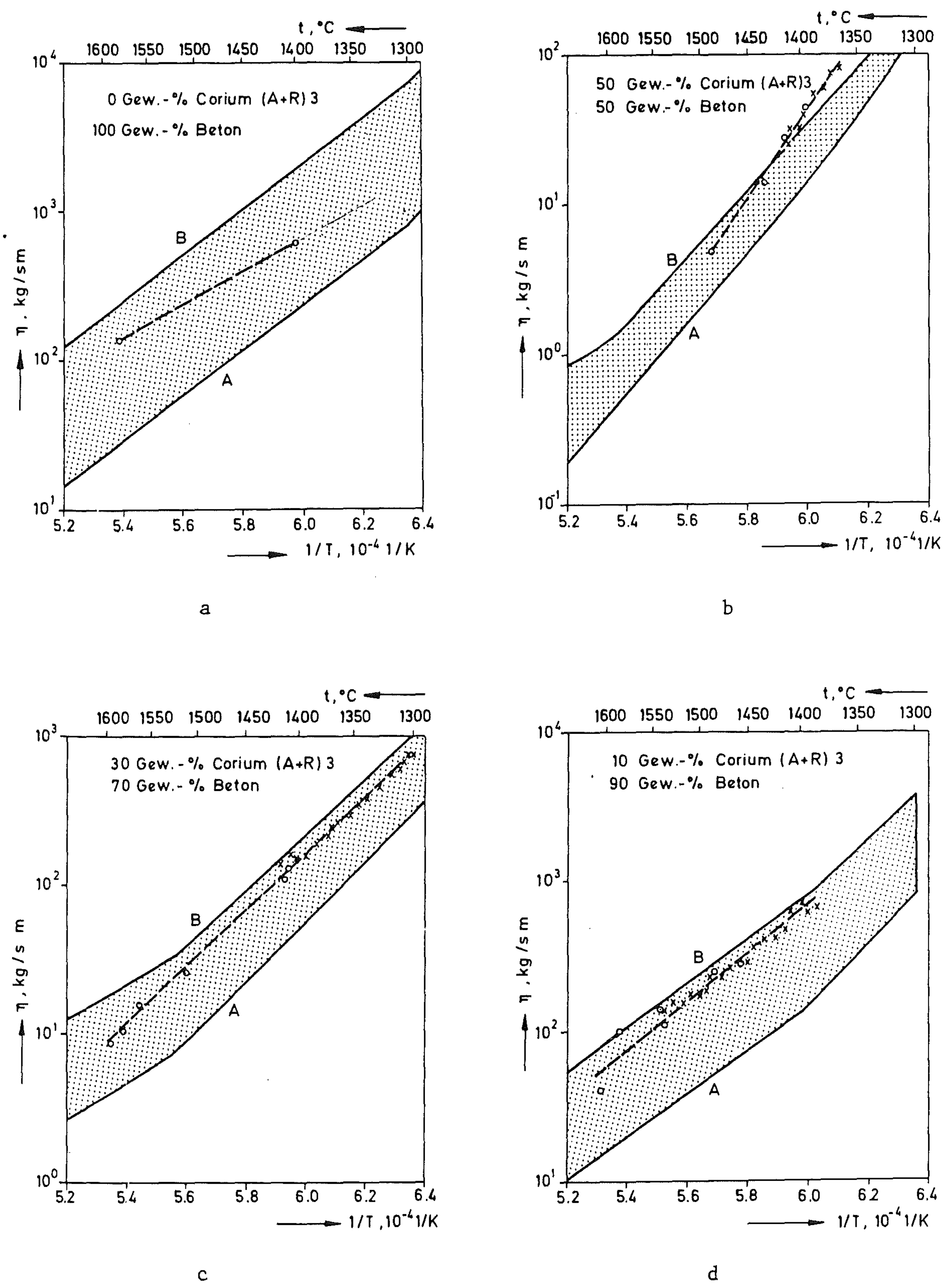

a

b

c

d

Figure 17: Comparison of viscosity measurements with calculated results of corium mixed with siliceous concrete.

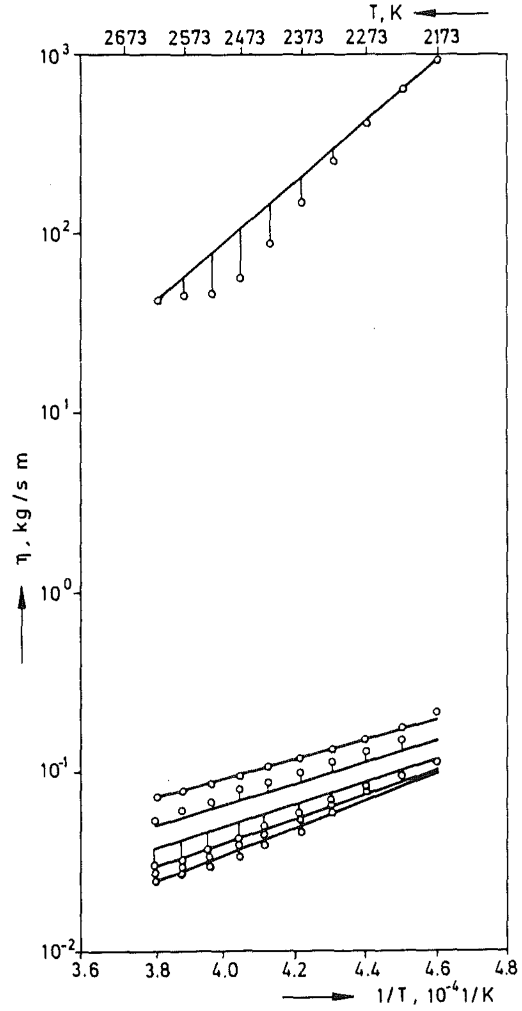

Figure 18: Comparison of viscosity measurements with computed results for molten Al_2O_3/SiO_2 mixtures.

Enthalpies are determined as shown in Figure 19. The enthalpy is approximated by

$$h = c\,T \tag{2.3.7-7}$$

in the solid region,

$$h = cT + \Delta h_{LS} \frac{T - T_S}{T_L - T_S} \tag{2.3.7-8}$$

in the region between liquidus and solidus temperatures and

$$h = cT + \Delta h_{LS} \tag{2.3.7-9}$$

in the liquid region of each molten layer. Note that the specific heat capacity is assumed to be constant over the temprature range of interest. This approximation

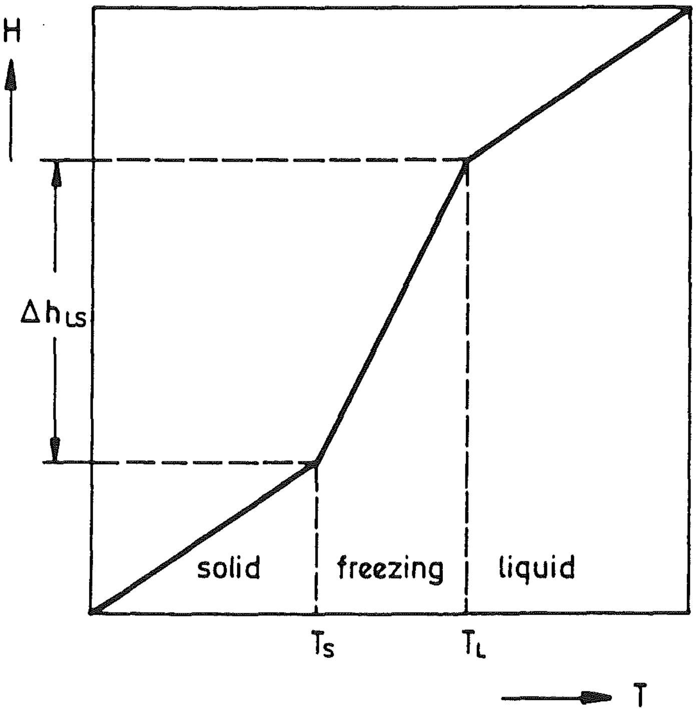

Figure 19: Enthalpy determination for each layer of the melt.

is reasonably good for liquid metal, but it is not very accurate for some of the oxide constituents.

For the description of the gas behavior (i.e. in the gas film or discrete bubble model), properties of the steam/carbon dioxide mixture released from the concrete must be provided. The properties of the individual species, namely specific volume v_1 at reference pressure

$$p_1 = 1\ bar \qquad (2.3.7\text{-}10)$$

specific heat capacity c_p, dynamic viscosity μ, and thermal conductivity k, are evaluated in WECHSL from tables given in [50] within the temperature range

$$373\,K < T < 3600\,K \qquad (2.3.7\text{-}11)$$

For determining the density of the gas mixture, the gas species are considered as perfect gases.

Then, for a given temperature, the actual gas constant for each species i is:

$$R_i = \frac{p_1 v_{1i}}{T} \tag{2.3.7-12}$$

and the actual molecular weight is

$$M_i = \frac{\mathbb{R}}{R_i} \tag{2.3.7-13}$$

For a given mass fraction γ_i, the molar fraction X_i is

$$X_i = \frac{\gamma_i / M_i}{\sum_i \gamma_i / M_i} \tag{2.3.7-14}$$

Then, the gas constant of the mixture is

$$R_{mix} = \frac{\mathbb{R}}{\sum_i \gamma_i M_i} \tag{2.3.7-15}$$

and the density of the mixture yields

$$\rho_{mix} = \frac{p}{R_{mix} T} \tag{2.3.7-16}$$

The specific heat capacity is

$$c_p = \sum_i \gamma_i c_{pi} \tag{2.3.7-17}$$

The transport properties of the gas mixture are derived by a method described in reference [51]. The dynamic viscosity of the mixture is

$$\mu_{mix} = \sum_{i=1}^{n} \frac{X_i \mu_i}{\sum_{j=1}^{n} X_j \phi_{ij}} \tag{2.3.7-18}$$

and the thermal conductivity

$$k_{mix} = \sum_{i=1}^{n} \frac{X_i k_i}{\sum_{j=1}^{n} X_j \Phi_{ij}} \qquad (2.3.7\text{-}19)$$

where

$$\Phi_{ij} = \frac{1}{2\sqrt{2}} \left(1 + \frac{M_i}{M_j}\right)^{-1/2} \left\{1 + \left[\frac{\mu_i}{\mu_j} \left(\frac{M_j}{M_i}\right)^{1/2}\right]^{1/2}\right\}^{2} \qquad (2.3.7\text{-}20)$$

2.3.8 Freezing Behavior

The solidus and liquidus temperatures of the oxide phase are computed by a method suggested by Ondracek [52]. In this procedure, the multiphase melt is reduced to a binary system with a high melting point component (the molten corium oxides UO_2, ZrO_2 and CaO, Cr_2O_3 with melting temperatures between 2700 K and 3000 K, index 1) and a low melting point component (SiO_2, FeO, $CaSiO_3$ with melting temperatures around 1800 K, index 2).

If ideal mixing of the liquid components and formation of ideal mixture crystals are assumed, the van Laar Equations (see i.e. [53]) are valid:

$$X_L = \frac{exp(N_L) - 1}{exp(N_L) - exp(M_L)} \tag{2.3.8-1}$$

and

$$X_S = \frac{exp(N_S) - 1}{exp(N_S + M_S) - 1} \tag{2.3.8-2}$$

with

$$N_{L,S} = \frac{\Delta H_{LS,2}}{\mathbb{R}} \left(\frac{1}{T} - \frac{1}{T_{(L,S),2}} \right) \tag{2.3.8-3}$$

and

$$M_{L,S} = \frac{\Delta H_{LS,1}}{\mathbb{R}} \left(\frac{1}{T_{(L,S),1}} - \frac{1}{T} \right), \tag{2.3.8-4}$$

where

X - molar concentration,
ΔH_{LS} - molar latent heat of freezing,
$T_{L,S}$ - liquidus and solidus temperatures, resp.,
T - melt bulk temperature,
$\mathbb{R}$ - universal ideal gas constant.

The data for the molar latent heat of freezing ΔH_{LS} given in the literature ranges for the constituents of the oxide melt between 7680 J/mol for SiO_2 and 138 000 J/mol for FeO.

By selecting values for ΔH_{LS} and $T_{L,S}$ of the low and high melting point components and by solving the above equations, the composition dependent liquidus and solidus temperatures of the fictitious two-phase melt with ideal mixing behavior are found.

Skokan et al. [9] measured the composition dependent solidification temperature for mixtures of corium at different oxidation levels with different types of concrete. As shown in Figure 20, their experimental data for siliceous concrete can be reproduced with sufficient accuracy when selecting for completely oxidized corium (A + R, E + R) 3 is selected:

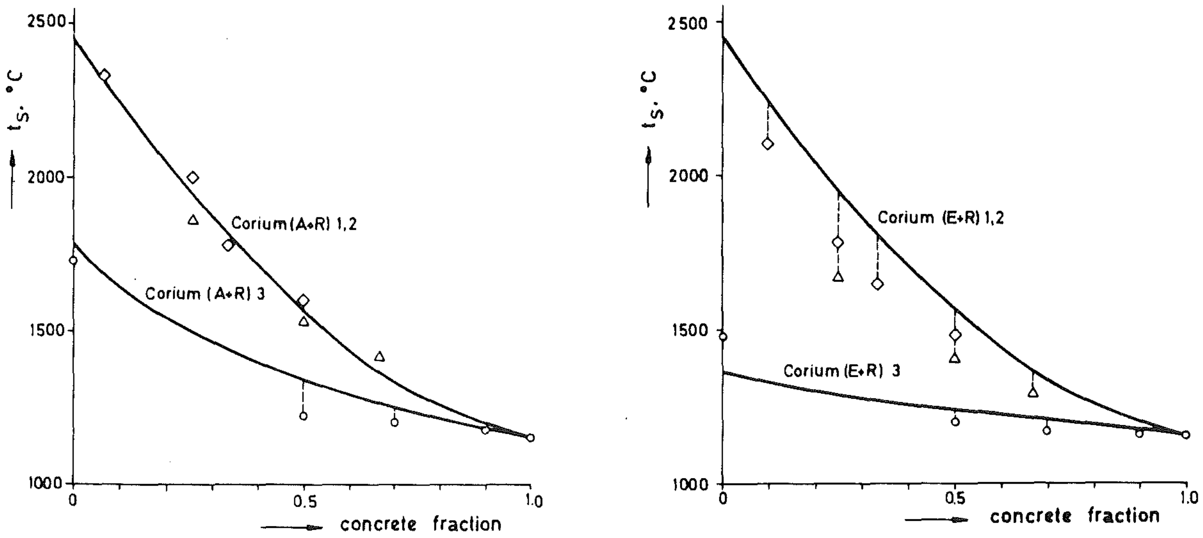

Figure 20: Solidification temperature of corium/concrete mixtures: comparison of measured and calculated values.

$$T_{S,1} = 2323\,K,\ \Delta H_{LS,1} = 80\,000\ J/mol,$$

$$T_{S,2} = 1423\,K,\ \Delta H_{LS,2} = 24\,840\ J/mol, \qquad (2.3.8\text{-}5)$$

For partly or not oxidized corium (A + R, E + R) 1,2 the following equations hold:

$$T_{S,1} = 2723\,K,\ \Delta H_{LS,1} = 110\,000\ J/mol,$$

$$T_{S,2} = 1423\,K,\ \Delta H_{LS,2} = 14\,000\ J/mol. \qquad (2.3.8\text{-}6)$$

It should be noted that the liquidus and solidus points in the oxide phase are being constantly lowered as the siliceous concrete constituents dilute the oxide material. At the same time, the melt temperature drops because of cooling. The apparent specific heat of the melt is higher between the solidus and liquidus temperatures because of partial solidification of the melt; this, evidently, decreases the cooling rate.

The concept of ideal mixing is not applicable to calcareous concrete without any silicates. The measurements [9] show a minimum for the solidification temperature at 50 wt.-% corium/50 % wt.-% calcareous concrete indicating strong deviations from the ideal mixing behavior.

The principal constituents of the metal melt are Cr, Fe, and Ni. The metal melt may freeze during an accident. Consequently, the phase diagram of this ternary system must be considered for the solidification process. A single fit to the ternary Cr-Fe-Ni phase diagram was constructed by Bartel et al. [54]. The liquidus and solidus temperatures, expressed in Kelvin, are approximated by

$$\begin{aligned} T_L = max\,(&2130 - 510\,\psi_{Fe} - 1140\,\psi_{Ni}, \\ &1809 - 90\,\psi_{Cr} - 440\,\psi_{Ni}, \\ &1728 - 200\,\psi_{Cr} - 40\,\psi_{Fe}, \\ &1793 - 230\,\psi_{Cr} - 130\,\psi_{Ni}) \\ T_L = max\,(&2130 - 730\,\psi_{Fe} - 3310\,\psi_{Ni}, \\ &1809 - 90\,\psi_{Cr} - 560\,\psi_{Ni}, \\ &1728 - 250\,\psi_{Cr} - 100\,\psi_{Fe}, \\ &1783 - 310\,\psi_{Cr} - 140\,\psi_{Ni}, 1613) \end{aligned} \qquad (2.3.8\text{-}7)$$

where ψ_{Cr}, ψ_{Fe}, and ψ_{Ni} are the weight fractions of the metal melt. The current coding ignores the presence of other elements in the metallic phase, and renormalizes so that

$$\psi_{Cr} + \psi_{Fe} + \psi_{Ni} = 1 \qquad (2.3.8\text{-}8)$$

In general, the surface temperatures of the molten pool are below the bulk temperatures. Consequently, these temperatures will drop at first below the freezing temperature of the melt and crust formation will occur. The process of onset of crust formation and crust growth with transient heat conduction inside the crust is described in Section 2.2.6.

For the oxide phase, the criterion of crust formation is that the temperature in the boundary layer drops below the solidus temperature of the oxide.

For the metal phase, the criterion of crust formation is that the boundary layer temperature drops below a freezing temperature situated between the solidus and liquidus temperatures of the mutal phase as defined below:

$$If\ T_m < T_{m,sol}: T_{m,freez} = T_{m,sol};$$

$$If\ T_{m,sol} < T_m < T_{m,liq}: T_{m,freez} = \frac{2T_m + T_{sol}}{3}; \qquad (2.3.8\text{-}9)$$

$$If\ T_m > T_{m,liq}: T_{m,freez} = \frac{2T_{m,liq} + T_{sol}}{3}.$$

With this criterion of freezing, a reasonable behavior was obtained of the WECHSL computations compared with the low power BETA test results.

2.4 Supplementary Features of the WECHSL Code

2.4.1 Cavity Shape

The cavity is constrained to be axially symmetric; except for this constraint, any shape may be selected. Because of the variation in erosion rate around the periphery and the constantly changing level of the melt, the cavity shape undergoes permanent alteration.

The pool is divided into segments which are chosen such that the peripherial lengths Δ_S are equal with the exception that the phase boundary and the upper surface always occur at the segment boundaries. Each segment has the form of a (conical) frustum between two nodes (Figure 21).

The heat fluxes and the resulting erosion velocity are computed at the nodes; it is assumed that the velocity vector at each node in the outward direction normal to the rotational symmetric segment is limited by a circle passing through that node and the two adjoining nodes. New node positions are computed, and the periphery is rezoned so that all nodes are again equidistant from each other (except for the nodes at the phase boundary and at the free surface). This rezoning introduces a rough form of filtering so that bizarre cavity shapes caused by numerical problems are inhibited.

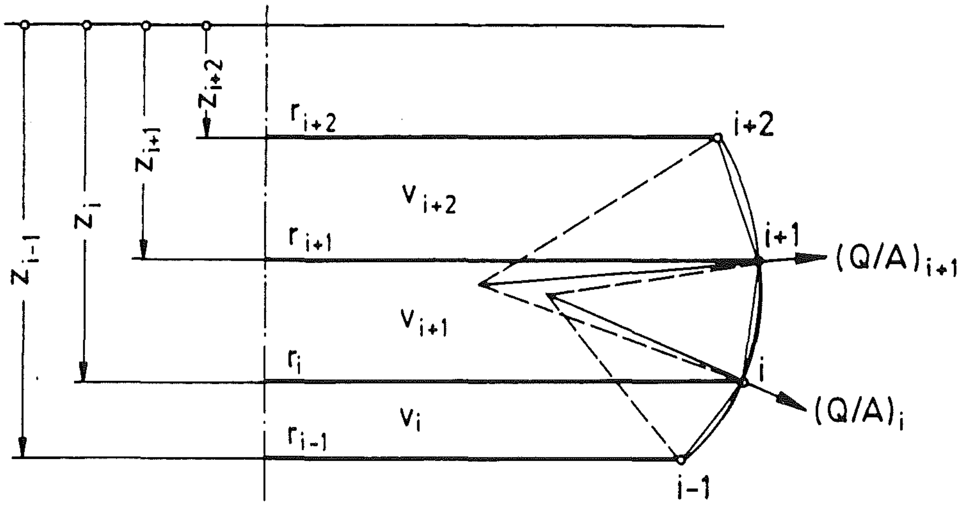

Figure 21: Cavity geometry.

It should be pointed out that the velocity vector is based on a rotational symmetric segment limited by a circle passing through three adjacent nodes, whereas the surface integral of heat flux and the new volumes are computed as if the cavity were composed of conical frusta. The new positions of the nodes are based on the assumptions first made. This could lead to discrepancies between the mass and volume. The mass discrepancy has been checked for a number of typical runs and found to amount to less than 1 % after several thousand time steps if cavity zoning is sufficiently fine.

During a core melt accident, crust formation and freezing is calculated to start at the metal layer, whereas the freezing temperature of the oxide layer is continuously being reduced. Thus, the situation occurs where the rate of melt front propagation of the oxide layer is higher than that of the metal slug. Consequently, the oxide pool starts to bypass the metal slug, as shown in Figure 22. Geometrical modeling in the WECHSL code was extended to cover also that situation.

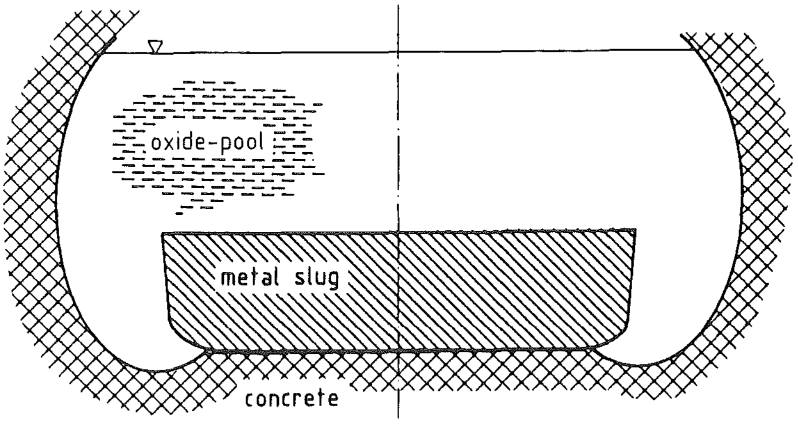

Figure 22: Cavity formation for a heavily encrusted or solidified metal layer.

2.4.2 Simplified Calculation Scheme for the Gas Film Model

2.4.2.1 Laminar Flow Regime

Calculations with the WECHSL code proved that numerical integration of the differential equations (2.2.3-27) for the laminar gas film and (2.2.4-27,43) for the turbulent gas film by means of a RUNGE-KUTTA-method required too much computation time compared with other parts of the code. Therefore, Reinecke [24] developed a simplified calculation scheme both for the laminar and turbulent gas films which shall be summarized here.

Equation (2.2.3-27) (valid for the laminar gas film) can be rearranged to give

$$\frac{\tilde{\delta}^3}{1+Nu_{rad}\tilde{\delta}}\,d\tilde{\delta}=\frac{4}{3\phi-2}\,\frac{\Psi_g}{Gr\,Pr\,Ste\,\sin\alpha}\,d\zeta \qquad (2.4.2\text{-}1)$$

As Nu_{rad} depends only on the temperatures at the melt surface and at the concrete surface which are constant for each melt layer, Nu_{rad} is constant in Eq. (2.4.2-1). The other dimensionless groups, namely Gr, Pr, and Ste, depend only on material properties and are again constant between the melt layer and the concrete. However, the angle of inclination α of the melt front with respect to the horizontal can change very strongly according to the shape of the cavity. Therefore, Eq. (2.4.2-1) cannot be integrated in a closed form but only stepwise with constant angle of inclination α. In WECHSL, the interval is given as the distance $\Delta\zeta$ between two nodes i, i + 1. This integration yields

$$6(Nu_{rad}\tilde{\delta})_{i+1}-3(Nu_{rad}\tilde{\delta})^2_{i+1}+2(Nu_{rad}\tilde{\delta})^3_{i+1}-6ln(1-Nu_{rad}\tilde{\delta})_{i+1}= \tag{2.4.2-2}$$

$$\frac{4}{3\phi-2}\frac{\Psi_g}{Gr\,Pr\,Ste\,\sin\alpha}6Nu^4_{rad}\Delta\zeta+6(Nu_{rad}\tilde{\delta})_i-3(Nu_{rad}\tilde{\delta})^2_i+2(Nu_{rad}\tilde{\delta})^3_i-6ln(1-Nu_{rad}\tilde{\delta})_i$$

or, abbreviated

$$A_{i+1}=\frac{4}{3\phi-2}\frac{\Psi_g}{Gr\,Pr\,Ste\,\sin\alpha}6Nu^4_{rad}\Delta\zeta+A_i \tag{2.4.2-3}$$

where A is a function of the parameter $Nu_{rad}\,\tilde{\delta}$. The inverse function is

$$Nu_{rad}\tilde{\delta}=f(A) \tag{2.4.2-4}$$

and it is attempted now to find an analytical approximation function in the possible range of values of the quantity A. After some trials, the function

$$Nu_{rad}\tilde{\delta}=10^bA^n \tag{2.4.2-5}$$

was found to be most convenient. The parameters b and n can be derived from Table 4 by interpolation

A	b	n
$4.21532\cdot10^{-4}$	$-1.38655\cdot10^{-2}$	0.255701
$4.59945\cdot10^{-3}$	$-4.57386\cdot10^{-5}$	0.260525
$1.01591\cdot10^{-2}$	$4.40342\cdot10^{-3}$	0.262577
$5.00419\cdot10^{-2}$	$1.26954\cdot10^{-2}$	0.267651
0.101325	$1.58377\cdot10^{-2}$	0.270342
0.502209	$2.05461\cdot10^{-2}$	0.277689
1.00494	$2.10744\cdot10^{-2}$	0.281254
4.97413	$1.79809\cdot10^{-2}$	0.290184
200.0766	$8.05687\cdot10^{-3}$	0.299708

Table 4: Parameters for laminar gas film.

To compute the melt front propagation, the mean value of the film thickness in the considered interval $\Delta\zeta$ must be evaluated. For that purpose, the exponents b and n are determined from Table 4 for the mean value of A_i and A_{i+1}. Then, the integrated mean value of the gas film thickness yields by integrating Eq. (2.4.2-5)

$$\tilde{\delta}_{i+\frac{1}{2}} = \frac{10^b}{Nu_{rad}} \frac{A_{i+1}^{n+1} - A_i^{n+1}}{(n+1)(A_{i+1} - A_i)} \qquad (2.4.2\text{-}6)$$

Equation (2.2.3-20) applies again for calculating the total heat transfer, with the mean film thickness $\tilde{\delta}$ as given by Eq. (2.4.2-6).

2.4.2.2 Turbulent Flow Regime

In the turbulent regime, the increase in the laminar sublayer characterizing the heat transfer is described by the system of coupled differential equations (2.2.3-27,43). An analytical solution in an interval as derived for the laminar flow regime is not possible in the turbulent region. Some substantial simplifications must be introduced in order to obtain an approximative solution.

The basic idea in solving the problem comprises again a stepwise integration of the differential equation over an interval. At first, the ratio of the total film thickness to the thickness of the laminar sublayer,

$$\Theta_{i+1} = \left(\frac{\tilde{\delta}_c}{\tilde{\delta}} \right)_{i+1} \qquad (2.4.2\text{-}7)$$

is calculated with the value $\tilde{\delta}_i$ kept constant over the interval i→i + 1 to give, in principle

$$\Theta_{i+1} = \Theta_i + A_1 \frac{1 + Nu_r \tilde{\delta}_i}{\tilde{\delta}_i} \Delta\zeta \qquad (2.4.2\text{-}8)$$

Equation (2.2.3-43) may be written in a simplified form as

$$\frac{d\tilde{\delta}}{d\zeta} = \frac{A_1(1 + Nu_r \tilde{\delta}) + A_2 + A_3 \Theta \tilde{\delta}^3}{\Theta - A_4} \qquad (2.4.2\text{-}9)$$

This non-linear differential equation cannot be solved analytically. In order to establish an approximative solution, the variable thickness of the laminar sublayer is written as

$$\tilde{\delta}_{i+1}=\tilde{\delta}_{i}+\Delta\tilde{\delta})$$

or (2.4.2-10)

$$\tilde{\delta}_{i+1}=\tilde{\delta}_{i}(1+\varepsilon)$$

Consequently, Eq. (2.4.2-9) yields

$$\frac{d}{d\zeta}(\Delta\tilde{\delta})=\frac{A_1(1+Nu_r\tilde{\delta}_i)+A_2-A_3\Theta\tilde{\delta}_i^3}{\Theta-A_4} \tag{2.4.2-11}$$

$$+\frac{A_1Nu_r-A_3\Theta\tilde{\delta}_i^2(3+3\varepsilon+\varepsilon^2)}{\Theta-A_4}\Delta\tilde{\delta}$$

If the factor ε is kept constant inside the interval, Eq. (2.4.2-11) is transferred into a linear differential equation with the solution

$$\Delta\tilde{\delta}=\frac{B_2}{B_1}[1-exp(-B_1\Delta\zeta)]. \tag{2.4.2-12}$$

The constants in the equation above are defined as

$$\left.\begin{aligned} A_1&=\frac{\rho_g}{\rho_c}\,\frac{g}{y^{+2}PrSte}\\ A_2&=\frac{f_{TP}}{2}+\frac{\rho_g}{\rho_c}\frac{1}{y^{+2}}\\ A_3&=\frac{\rho_g}{\rho_c}\,\frac{Gr\,sina}{y^{+4}}\\ A_4&=1-\frac{1}{3}\,\frac{\rho_g}{\rho_c}\end{aligned}\right\} \tag{2.4.2-13}$$

$$\left.\begin{aligned} B_1&=\frac{3A_1\Theta\tilde{\delta}_i^2(1+\varepsilon+\frac{\varepsilon^2}{3})-A_1Nu_r}{\Theta-A_4}\\ B_2&=B_1\frac{A_1(1+Nu_r\tilde{\delta}_i)+A_2-A_3\Theta\tilde{\delta}_i^3}{3A_3\Theta\tilde{\delta}_i^2(1+\varepsilon+\frac{\varepsilon^2}{3})-A_1Nu_r}\end{aligned}\right\} \tag{2.4.2-14}$$

Extensive numerical investigations revealed that the accuracy of the result is dependent on a convenient estimation of the parameter ε, especially in the regime of transition from laminar to turbulent flow. Finally, the following attempt proved to be successful:

By division of Eq. (2.4.2-12) by $\tilde{\delta}_i$ and using the definition of the constants (2.4.2-13, 14)

$$\varepsilon_{i+1}=\frac{A_1(1+Nu_r\tilde{\delta}_i)+A_2-A_3\Theta\tilde{\delta}_i^3}{3A_3\Theta\tilde{\delta}_i^3(1+\varepsilon_i+\frac{\varepsilon_i^2}{3})-A_1Nu_r\tilde{\delta}_i}\cdot\left[1-exp(-B_1\Delta\zeta)\right] \qquad (2.4.2\text{-}15)$$

is obtained. Under the assumption

$$\varepsilon_{i+1}=\varepsilon_i=\varepsilon, \qquad (2.4.2\text{-}16)$$

Eq. (2.4.2-15) yields

$$\varepsilon\left[a_2(1+\varepsilon+\frac{\varepsilon^2}{3})-a_3\right]=a_1\left\{1-exp\left[[a_4(1+\varepsilon+\frac{\varepsilon^2}{3})-a_5]\Delta\zeta\right]\right\} \qquad (2.4.2\text{-}17)$$

with the constants being defined by

$$a_1=A_3\Theta\tilde{\delta}_i^2-\frac{A_1(1+Nu_r\tilde{\delta}_i)+A_2}{\tilde{\delta}_i}$$

$$a_2=3A_3\Theta\tilde{\delta}_i^2$$

$$a_3=A_1Nu_r \qquad (2.4.2\text{-}18)$$

$$a_4=\frac{a_2}{\Delta-A_4}$$

$$a_5=\frac{a_3}{\Delta-A_4}$$

Equation (2.4.2-17) must be solved by an iteration scheme based on regula falsi. Test calculations involving variation of all parameters revealed a systematic underestimation on the order of 6.5 % of the heat transfer rate by the approximative solution when compared with the values obtained by direct integration of the differential equation using a RUNGE-KUTTA-method. Consequently, a correction factor f was introduced

$$f=\frac{1}{1-(1-c)f_T} \tag{2.4.2-19}$$

where

and

$$\left.\begin{aligned} f_T&=1 \; for\, T-T_{freez}\geq 200 \\ f_T&=\frac{T-T_{freez}}{200} \; for\, T-T_{freez}<200. \end{aligned}\right\} \tag{2.4.2-20}$$

The constant c is defined by

$$c=1-0.0642\cdot\left|1-exp(-3.89\cdot\;\Delta\zeta)\right| \tag{2.4.2-21}$$

To evaluate the melt front propagation, a mean thickness of the laminar sublayer characteristic of heat transfer in the turbulent flow regime is needed. The relevant equations are

$$\overline{\Delta\tilde{\delta}}_{i\rightarrow i+1}=\frac{B_2}{B_1}-\frac{\Delta\tilde{\delta}_{i+1}}{B_1\Delta\zeta} \tag{2.4.2-22}$$

$$\overline{\tilde{\delta}}_{i\rightarrow i+1}=\tilde{\delta}_i+\overline{\Delta\tilde{\delta}}_{i\rightarrow i+1}$$

With the approximative calculation scheme for gas film heat transfer as described above for the laminar and turbulent flow regimes, the melt front propagation as calculated by direct integration of the differential equations by means of a RUNGE-KUTTA-method has been reproduced with sufficient accuracy. As an example, Figure 23 shows a comparison of both methods of cavity formation during a core melt accident in the cylindrical cavity of a German standard PWR.

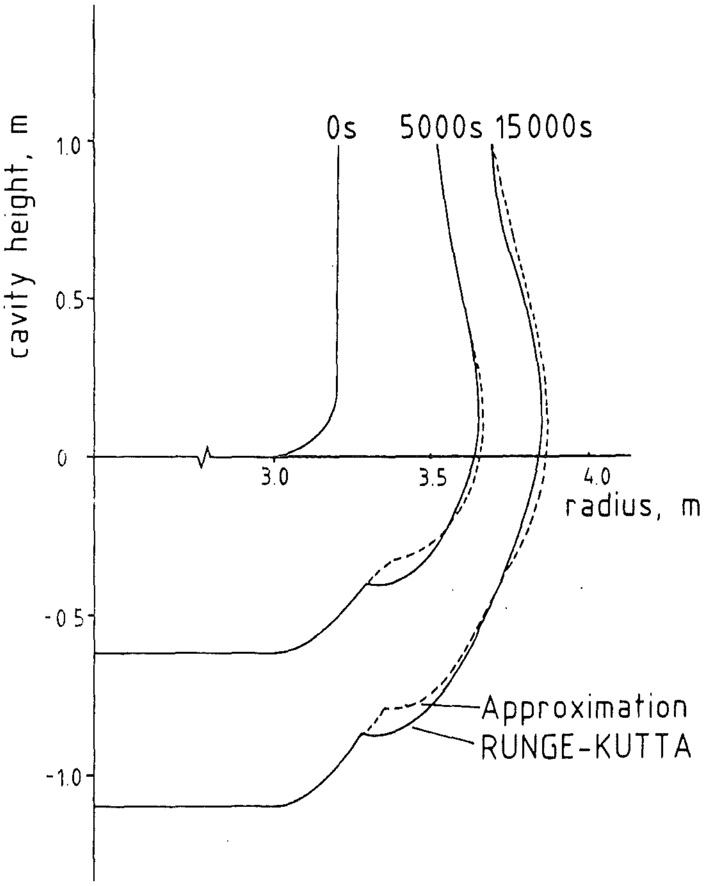

Figure 23: Comparison of cavity formation during a core melt accident:
a) by approximative gas film calculation scheme;
b) by integration of the differential equations by means of a RUNGE-KUTTA-method.

2.4.3 Energy Balance

The internal heat sources from the decay heat can be prescribed in WECHSL as a function of time for each layer of the melt. The energy flux balance considers the energy gain by these internal sources from chemical reactions, and by the enthalpy fluxes into each phase; the energy gain or loss by exchange of energy between the phases and by exothermal or endothermal chemical reactions, and the energy losses from each phase by heat transfer to the concrete, enthalpy fluxes out of the phase, and heat radiation from the upper surface to the environment yields an energy flux balance for an isobaric system:

$$\frac{dH_b}{dt} = \sum_k \dot{m}_k h_k + \sum_\ell \dot{Q}_l + \Omega_{chem} + \Omega_{decay} \qquad (2.4.3\text{-}1)$$

where H_b is the bulk enthalpy of the melt layer under consideration, Ω_{decay} is the heat source due to nuclear decay, Ω_{chem} is the heat gain or loss due to exothermal or endothermal chemical reactions inside this layer, $\dot{m}_k$ are the mass fluxes of material entering or leaving the layer and carrying the specific enthalpy h_k, and $\dot{Q}_l$ are the convective heat fluxes passing the boundaries of the layer.

At each time step, properties are computed with the bulk temperatures and the melt composition from the previous time step; heat transfer rates are computed on the basis of these properties.
The new bulk enthalpy for the time $\tau_{j+1} = \tau_j + \delta\tau$ is then computed by

$$H_{bj+1} = H_{bj} + \left[\sum_k \dot{m}_k h_k + \sum_\ell \dot{Q}_l + \Omega_{chem} + \Omega_{decay} \right] \delta\tau \qquad (2.4.3\text{-}2)$$

and the new mass of the melt layer is

$$m_{bj+1} = m_{bj} + \sum_k \dot{m}_k \delta\tau \qquad (2.4.3\text{-}3)$$

New temperatures are then computed by

$$T_{bj+1} = \left(\frac{H_{b\,j+1}}{m_{b\,j+1}} + \Delta \right) / c \qquad (2.4.3\text{-}4)$$

where

$$for \quad T < T_{sol}\text{:}\ \Delta = 0,\ c = c_p$$

$$for \quad T_{liq} \geq T \geq T_{sol}\text{:}\ \Delta \frac{h_{fus}}{T_{liq} - T_{sol}} T_{sol};\ c = c_p + \frac{h_{fus}}{T_{liq} - T_{sol}} \qquad (2.4.3\text{-}5)$$

$$for \quad T > T_{liq}\text{:}\ \Delta = -h_{lat};\ c = c_p$$

The new melt layer temperatures are determined by Eqs. (2.4.3-4,5) for homogeneous layers (completely liquid, slurry, or solid). At the surfaces of the metal layer facing the concrete and the oxide layer, crusts of substantial thickness may be formed. In that case, the metal bulk mass is split up into a liquid and a solid fraction.

As for the crust formation only a one-dimensional model is used, the actual fraction of the solid material is unknown. In order to get an appropriate first estimation of the fractions of solid and liquid materials, the surface areas of the metal layer covered by crusts, i.e., the area facing the concrete and the interface area between the metal and the oxide layer, are multiplied by the relevant increase in the crust thickness, as determined by the one-dimensional transient crust growth model, and the density, to give the solid mass change Δm_S. With the solid fraction ϕ_S evaluated by adding the mass increase to the solid mass and dividing by the total metal mass m_b, energy balances are established to give the new enthalpies for the liquid fraction

$$H_{l\,j+1} = H_{l\,j} + \left[\left(\sum_i \dot{m}_i h_i + \Omega_{chem} + \Omega_{decay} \right) \left(1 - \phi_s \right) + \dot{Q}_{int} - \gamma \cdot \dot{Q}_{conc} \right] \delta\tau - \Delta m_s h_{fus} \qquad (2.4.3\text{-}6)$$

and for the solid fraction

$$H_{s\,j+1} = H_{s\,j} + \left[\left(\sum_i \dot{m}_i h_i + \Omega_{chem} + \Omega_{decay} \right) \phi_s - (1-\gamma) \dot{Q}_{conc} \right] \delta\tau + \Delta m_s h_{fus} \qquad (2.4.3\text{-}7)$$

where $\dot{Q}_{int}$ is the heat gain through the metal-oxide interface, $\dot{Q}_{conc}$ is the heat consumed by the highly endothermal concrete decomposition process, and γ is the ratio of heat fluxes entering the crust by thermal conduction at the metal melt/solid interface and leaving the crust to cause concrete decomposition. The total bulk enthalpy is the sum of the liquid and solid enthalpies as given in Eqs. (2.4.3-6,7).

The temperature of the solid fraction is evaluated as being the mean temperature of the crusts by using the temperature distribution inside the crusts as evaluated with the transient heat conduction model. With these temperatures, $H_{l\,j+1}$ is recalculated by

$$H_{l\,j+1} = H_{b\,j+1} - c_p (T_{sw} \cdot m_{sw} + T_{si} \cdot m_{si}) \qquad (2.4.3\text{-}8)$$

where subscript "sw" assigns the metal crust facing the concrete and subscript "si" the metal crust at the metal/oxide interface. The temperature of the liquid fraction is then computed by means of Eqs. (2.4.3-4,5).

For complete freezing of the metal layer, two cases are considered:

- the solid mass fraction exceeds the total mass of the metal layer, or
- the temperature of the liquid bulk drops below the thermodynamic freezing temperature.

After complete freezing, one-dimensional, transient heat conduction is considered in vertical direction inside the metal slug and a correction is used for taking into account sidewall effects.

An integrated energy balance and an integrated mass balance are maintained and can be printed out periodically. Because of numerical roundoff and approximations, the enthalpy or mass at any time will not be equal to that computed from the inital enthalpy or mass and the integrated gains and losses. However, the errors are always less than 1 % and normally insignificantly small.

3. Instructions for the Use of the Code

3.1 WECHSL Code Characteristics

The WECHSL code is at present operational on the IBM/3090-Siemens 7890 computer system at Kernforschungszentrum Karlsruhe. The code is written in FORTRAN IV, input and output data are in SI units. The amount of printout and of plot output data is user controlled.

The WECHSL code is capable of restart. The following input and output files are provided:

Content	Dataset reference number
- control parameters	1
- initial input data	3
- cleaned data (auxiliary)	4
- restart input (unformatted)	2
- print detailed results	6
- print tables	30, 31, 32
- plot data for diagrams	8
- plot data for cavity shape	9
- output for next restart (unformatted)	22

The principal structure of the MAIN program operating the WECHSL subroutine is shown in Figure 24. The program starts by reading the variable ISTEU from the control parameter file.

For an initial WECHSL run, ISTEU = 0.
Then the initial input data are read and handled with the help of an auxiliary dataset, which may be temporary.

For a restart run, i.e. continuing the execution of the same problem, ISTEU has to be greater than 0. In that case, the new end time is read from the control parameter file and the actual values as well as the input tables are restored from the restart file. The initial input file itself is no longer used. As the print and plot options chosen for the initial run remain unchanged, they must be carefully selected for the initial data set.

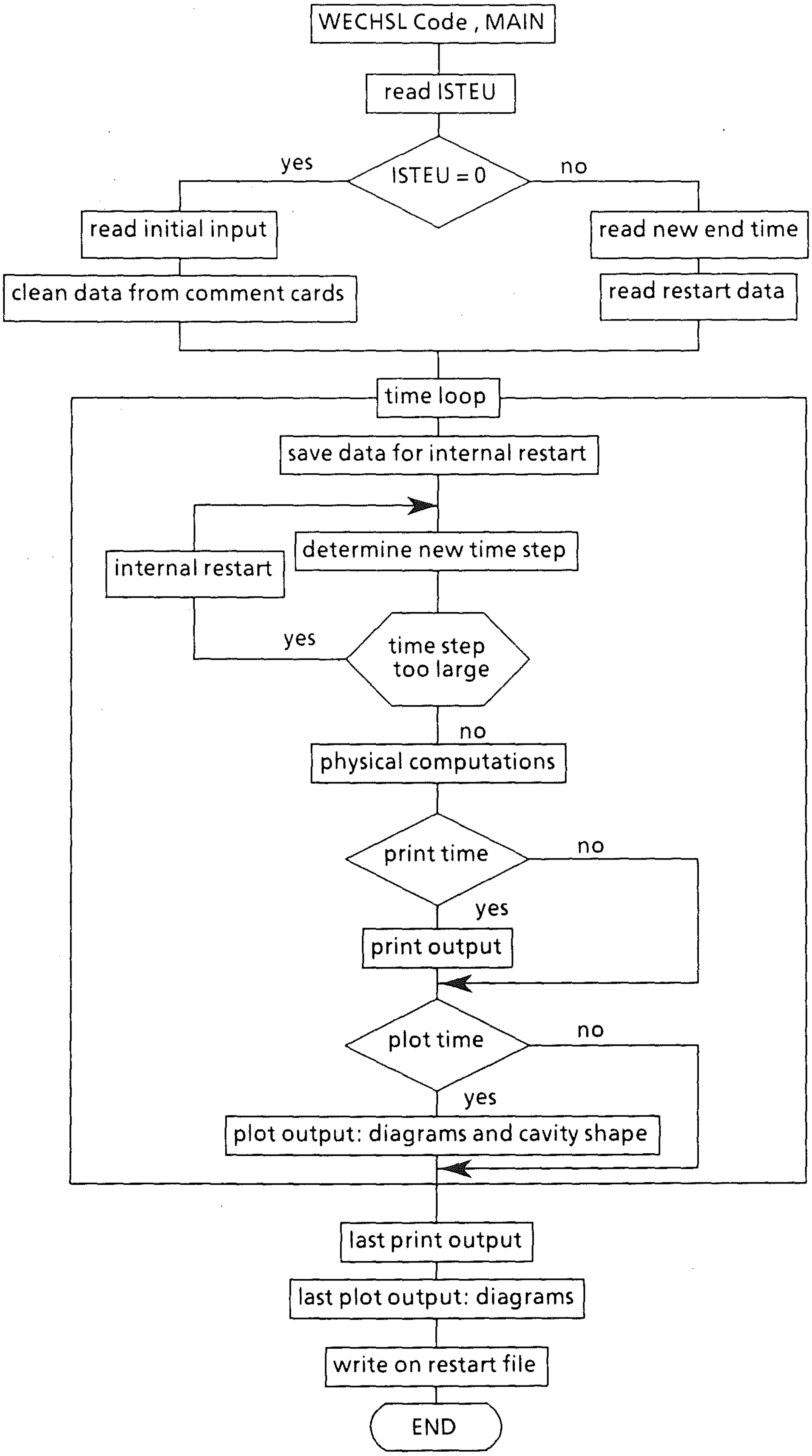

Figure 24: Simplified layout of data handling in the WECHSL code.

Subsequently, the time loop is executed until the prespecified time limit is exceeded. It will be aborted before the end time is reached, if one of the following events occurs:

- The boundary temperature drops below the concrete ablation temperature.
- The single oxide layer is frozen.
- The basemat is penetrated by the melt.

The size of the time step is governed by the heat from oxide to concrete within the limits given by the user.

In the time loop, the output for print (detailed at particular times and summarized in tables) and the output of plot data (separately for diagrams and cavity shape) are made at intervals specified by the user. In order to reduce the amount of data, the list does not contain all the cavity coordinates but only those that were changed during the last time step.

After termination of the time loop, a final printout with a complete set of cavity points and plot output for diagrams is created. The cavity plot output is omitted if it does not match the prescribed time inteval. Finally, all the variables and arrays used for the calculation of this problem are stored in the restart output dataset. The problem can be restarted as many times as desired.

In the next sections, the input data are described in detail. Furthermore, the WECHSL output on the print and plot files are presented.

3.2 Input Description

3.2.1 Control Parameters

The first card has to be present in any case.

Card 1:	free format
ISTEU	$=0$ means initial run
	>0 means restart run

If ISTEU $=0$, the next card may be omitted and the code proceeds by reading the initial input data. Additionally, the cleaned data file has to be allocated.

If ISTEU > 0, the next card gives the new end time and a restart input file must be available.

Card 2:	free format - not used if ISTEU = 0.
TF	final problem time for the restart run in seconds

3.2.2 Initial Input Data

These data are necessary for the first run of a problem only. The number of input data cards is variable and depends on the type of the problem. Those cards, which must always be present, are marked with the symbol ' ! '. To copy some of the input data, the "cleaned data file" must be allocated (see Section 3.3).

Comment Cards

It is convenient to insert comment cards in order to achieve a better readability. The symbol ' * ' in the first column identifies a card as a comment. It may be used at any place.

Data Cards

Problem identification:

! Card 1:	format (18A4) 72 characters for text of problem identification

Thermite Addition:

! Card 2:	format (2E10.3) WTHEM - rate of thermite addition, kg/s THERM - final time for thermite additions, s

Thermite is assumed to be added at a constant rate of WTHEM kg/s over THERM seconds. This card is used for some simulation tests in which a certain quantity of thermite is poured into the crucible at the beginning of the test. For calculation of melt down accidents, the variables can be entered as zeroes.

Metal and Oxide Addition

! Card 3:	free format NADD - number of material (melt) additions to the crucible (0-10)

If NADD is not equal to zero, the set of the following 3 cards has to be available NADD times.

Card 4: free format : addition characteristics
TADDB - initial time for addition, s
TADDE - final time for addition, s
TEMADD - temperature of added materials, K

Card 5: free format : added oxides
KGADD (1) - added mass of UO_2 during this time, kg
KGADD (2) - added mass of ZrO_2 during this time, kg
KGADD (3) - added mass of FeO during this time, kg
KGADD (4) - added mass of CaO during this time, kg
KGADD (5) - added mass of SiO_2 during this time, kg
KGADD (6) - added mass of Al_2O_3 during this time, kg
KGADD (11) - added mass of Cr_2O_3 during this time, kg

Card 6: free format : added metals
KGADD (7) - added mass of Fe during this time, kg
KGADD (8) - added mass of Zr during this time, kg
KGADD (9) - added mass of Cr during this time, kg
KGADD (10) - added mass of Ni during this time, kg

The input of the material is at a constant rate during each addition. The materials may be solid or liquid.
Note: TADDB (I + 1) must be greater than or equal to TADDE (I), for all values of I.

Concrete Characteristics

! Card 7: format (4E10.3)
FC1 - weight fraction of $CaCO_3$ in concrete
FC2 - weight fraction of $Ca(OH)_2$ in concrete
FC3 - weight fraction of SiO_2 in concrete
FC4 - weight fraction of free water in concrete

Note: The weight fraction of Al_2O_3 is assumed to be FC5 = 1.-FC1-FC2-FC3-FC4.
The fractions are related to concrete without steel reinforcement.

! Card 8: format (4E10.3)

	RBR	- fraction of reinforcing steel: kg steel per kg concrete without reinforcement
	TSB	- melting temperature of concrete without steel, K
	HC	- decomposition enthalpy of concrete without steel, J /kg
	RHC	- density of concrete without steel, kg/m^3

Liquidus - Solidus Curves

Cards 9 to 13 constitute the liquidus and solidus curves for the oxide phase. A group of high melting points and a group of low melting points are considered.

Note: To simulate a core meltdown accident, the high temperature group would normally be UO_2 and ZrO_2. Note, however, that very small amounts of iron oxide drastically reduce the melting point and the reduced melting point should be used here. The low temperature group would normally be the concrete constituents, i.e. CaO and SiO_2. The latent heat is due to phase change only, and is not equivalent to the decomposition enthalpy of concrete.

The curves can either be given as an input table or calculated by the code with the help of the Schröder-van Laar equation (Eq. 2.3.8-1) with two components. The latter case requires the input of the effective latent heat, the solidus and the liquidus temperatures.

! Card 9: format (I5): switch for liquidus-solidus curves for the oxide phase

IMAT
- =1 means calculation with Schröder van Laar equation
- >1 means table input with IMAT points (IMAT$\leq$11)

! Card 10: format (10I5): low temperature material group

NCOM1	- number of components in this group (1$\leq$NCOM1$\leq$6)
ICOM1(1)	- index of the first component
ICOM1(2)	- index of the second component

Repeat up to ICOM1(NCOM1), as required.

The indices for the components are as follows:

1 = UO_2	4 = CaO
2 = ZrO_2	5 = SiO_2
3 = FeO	6 = Al_2O_3

The calculation with the Schröder-van Laar equation (IMAT = 1) calls for the following card.

(!) Card 11a: format (3E10.3) : properties of the low temperature group

DHS1	- effective latent heat of melting, J/mol
TS1	- solidus temperature for 'pure' low temperature group
TL1	- liquidus temperature for 'pure' low temperature group

Table input for the low temperature group ($1 < \text{IMAT} \leqq 11$):

(!) Card 11b: format (6E10.3) : input table with IMAT points

CCL (1)	- molar concentration for liquidus
TLL (1)	- liquidus temperature, K
CCL (2)	- as above
TLL (2)	- as above
CCL (3)	- as above
TLL (3)	- as above

Repeat Card 11b until IMAT couples are reached.

! Card 12: format (10I5) : high temperature material group

NCOM2	- number of components ($1 \leqq \text{NCOM2} \leqq 6$)
ICOM2(1)	- index of the first component
ICOM2(2)	- index of the second component

Repeat up to ICOM2(NCOM2), as required.

Indices for the components are the same as for the low temperature group.

The calculation with the Schröder-van Laar equation (IMAT = 1) calls for this card:

(!) Card 13a:	format (3E10.3) : properties of the high temperature group	
	DHS2	- effective latent heat of melting, J/mol
	TS2	- solidus temperature for 'pure' high temperature group
	TL2	- liquidus temperature for 'pure' high temperature group

The table input for the high temperature group is analogous to that of the low temperature group:

(!) Card 13b:	format (6E10.3) : input table with IMAT points (max. 11)	
	CCS(1)	- molar concentration of solidus
	TSS(1)	- solidus temperature, K
	etc.	

Repeat card 13b until IMAT couples (up to 3 per card) are reached.

Description of the Oxide Phase of the Melt

! Card 14:	format (8E10.3) : initial oxide masses, kg	
	WT(1)	mass of UO_2
	WT(2)	mass of ZrO_2
	WT(3)	mass of FeO
	WT(4)	mass of CaO
	WT(5)	mass of SiO_2
	WT(6)	mass of Al_2O_3
	WCR2O3	mass of Cr_2O_3

Note: The problem must start with a finite mass of oxides.

! Card 15:	format (E10.3)	
	TO	- initial temperature of oxides, K

Cards 16 through 18 give the internal heat sources in the oxide as a function of time.

! Card 16:	format (I5)	
	NIO	number of couples in the internal power table for oxide ($0 \leqq NIO \leqq 80$)

Note: If NIO = 0, the internal power of oxide is assumed to be zero.

Card 17: format (E10.3)- must not be used if NIO = 0
TSH - shift time for internal heat generation, s

The code shifts the time scale given in the table below for TSH seconds. This is to take into account the time difference between the time origin of the internal heat source and the contact time of the melt and concrete.

Card 18: format (6E10.3) - must not be used if NIO = 0
TIO(1) - time for first point, s
QIO(1) - power for first point, W
TIO(2) - time for second point, s
QIO(2) - power for second point, W
etc.

Repeat up to NIO points, (up to 3 per card), using additional cards if required.
Note: TIO(I + 1) must be greater than TIO (I), for all values of I.

Description of the Metal Phase of the Melt

! Card 19: format (4E10.3) : initial metal masses, kg
WT(7) - mass of Fe
WT(8) - mass of Zr
WT(9) - mass of Cr
WT(10) - mass of Ni

Note: The initial mass of metal is allowed to be zero.

! Card 20: format (E10.3)
TFM - initial temperature of metals, K

Card 21 and 22 give the internal energy sources in the metal as a function of time.

! Card 21: format (I5)
NIM - number of couples in the internal power table for metal ($0 \leqq NIM \leqq 80$)

Note: If NIM = 0, the internal power of the metal is assumed to be zero.

Card 22: format (6E10.3) - must not be used if NIM = 0
TIM(1) - time for first point, s
QIM(1) - power for first point, W, etc.

Repeat up to NIM points (up to 3 couples per card) using additional cards, if required.

Note: TIM (I + 1) must be greater than TIM (I), for all values of I.

Time Characteristics for Execution of the Calculation

! Card 23: format (4E10.3)
DT - initial time step, s
TF - final time for calculation, s
DTMIN - minimum time step allowed, s.
DTMAX - maximum time step allowed, s.

Note: The initial time step should be chosen so that the temperature change is small, say $\leqq$ 5 K. It is suggested that an initial trial be made with a roughly estimated time step. The code optimizes the time step in the range given by DTMIN and DTMAX.

Printout Times

! Card 24: format (I5)
NTPR - number of different printout intervals ($NTPR \leqq 80$)

! Card 25: format (6E10.3) : table of printout intervals
TPR(1) - start time for the first printout interval, s
DPR(1) - time step for printout in first interval, s
etc.

Repeat as necessary up to TPR (NTPR), DPR (NTPR), (up to 3 couples per card). Use additional cards, if required.

Note: TPR(I + 1) must be greater than TPR(I), for all values of I.

Ambient Atmospheric Pressure

! Card 26: format (I5)
NPP - number of couples in time-pressure table (NPP $\leqq$ 80)

! Card 27: format (6E10.3): pressure table
TP(1) - time for first point, s
PP(1) - pressure for first point, bar
etc.

Repeat up to TP(NPP), PP(NPP), up to 3 couples per card. Use additional cards, if required.

Note: TP(I + 1) must be greater than TP(I), for all values of I.

Ambient Temperature for Radiation from the Top of the Corium

! Card 28: format (I5)
NTT - number of couples in time-temperature table (NTT $\leqq$ 80)

! Card 29: format (6E10.3): temperature table
TIT(1) - time for first point, s
TAM(1) - temperature for first point, K
etc.

Repeat up to TIT (NTT), TAM (NTT), up to 3 couples per card. Use additional cards as required.

Note: The time points must be written in ascending order.

Cavity Shape

There are different ways of defining the initial cavity shape. The type of card 31 and the use of card 32 depend on the option selected on card 30.

Note: The cavity must be deep enough to accommodate the entire melt including the effects of level swell. The program will not allow the cavity to run over. The maximum allowable number of points is 300. The initial shape should not consist of more than 150 points in order to allow for cavity growth. However, if it is too small, details will be lost. As the cavity is axisymmetric, only the right part of the cavity is defined in cylinder coordinates with the ordinate as the center line. The initial bottom of the cavity is defined as $y = 0$.

! Card 30: format (I5)
NB - indicates the desired option and, in addition, the initial number of points for option I

If $NB < 1000$: arbitrary shape with NB points - Option I
If $1000 \leq NB < 1500$: cylinder with rounded corners - Option II
If $1500 \leq NB < 2000$: conical section on cylinder with rounded corners - Option IIa
If $NB \geqq 2000$ cylinder with hemispherical bottom - Option III

The next card has to be coded according to the selected option.

Option I - Arbitrary shape:

(!) Card 31/I format (6E10.3)
RCAV(1) - radius of the first point, m
YCAV(1) - height of the first point, m
etc.

Continue up to RCAV(NB), YCAV(NB), with 3 points per card.
Use as many continuation cards as necessary.

Note: NB should not exceed 150 (see above)

Option II - Cylinder with rounded corners:

(!) Card 31/II format (2I5, 4E10.3)
NR - initial number of points on the horizontal part of the floor
NC - initial number of points on the rounded corner
RO - initial radius of the cylinder, m
RKL - initial radius of the corner, m

DELZ - initial interval between the points in cylindr. section, m
ZMX - initial height of the cavity, m

Option IIa - Additional input for conical section on the top of the cylinder, if option IIa is selected:

Card 32: format (2E10.3)
ZMXE - total height of the cavity, m
WIN - angle of inclination, deg.

Note: WIN is the angle between the conical part and the vertical center line of the crucible.

Option III - Cylinder with hemispherical bottom

(!) Card 31/III: format (4E10.3)
DPHI - initial central angle between points in the hemisphere, degrees
DELZ - initial interval between points in cylinder, m
RO - initial radius of hemisphere, m
ZMX - initial total height of cavity, m

(End of Option III)

! Card 33: format (E10.3)
SMX - interval between cavity points during the execution of the program, m

All points are automatically set to be equidistant.

Note: If SMX is too small, an excessive number of cavity points will be used. If SMX is too large, much of the cavity detail will be lost.

! Card 34: format (3E10.3)
RSUMP - radius for sump water ingression, m
ZMIN - erosion depth for basemat penetration, m
TSUMP - time for sump water ingression, s

Sump water floods the melt, if the radial erosion exceeds RSUMP or if the current time exceeds TSUMP. Flooding is avoided by choosing large values for RSUMP and TSUMP, respectively.

Print Options

! Card 35: format (4I10) : switches for printout
KTEM - temperatures
KPROP - properties
KINT - interface
KMAS - masses

! Card 36: format (4I10) : switches for printout (cont.)
KBAL - heat balance
KGAS - gas release
KCAV - cavity shape
KDIAG - diagnostics

If any of the quantities is not equal to zero, the corresponding print option will be exerciced. A zero value bypasses this print option.

Options for Output on Plot File

Note: The user has to provide his own plot programs.
For KfK-configuration standard programs are available.

! Card 37: format (2I10) : switch for plot output
JCUR - plot of diagrams
JCAV - plot of cavity shape

Any value unequal to zero specifies that plot data are written to the plot files.

! Card 38: format (2E10.3)
TPL - start time to write plot file for diagrams, s
DPL - time step for writing diagram data, s

Note: DPL is only valid for the first 3600 seconds. Then it is set to 3600 s by the code in order to limit the amount of data.

! Card 39: format (2E10.3)
TPLC - start time to write plot file for cavity shape, s
DPLC - time step for writing cavity data, s

Note: Cards 38 and 39 must be present even if no plot output is desired.

3.3 Cleaned Data File

This file must be allocated for the duration of the initial run of a problem. The program copies data to this file which serves as a temporary storage for the input data, from which the comments were removed.
The records are written with FORMAT (72A1).

3.4 Restart Files

As these files are not planned to be read by the user, they contain data unformatted.

At the end of a normal run, i.e. if it is not aborted, the data required for program continuation are always stored on the restart output file.

If restart is desired, this former output file has to be used as input.

3.5 Output Description

3.5.1 Detailed Printout

At the beginning of an initial run, the input data are printed for control.

At the beginning of a restart run, the restart time is given.

Then, the actual values are printed at intervals defined by the user. The following data are given at each print time: time, next time step for computation, and cavity dimensions. Additional data output depends on the options selected on input cards 35 and 36.

KTEM$\neq$0:

- pool (bulk) temperatures of metal and oxide
- temperatures at the interface of metal and oxide with concrete
- temperatures of the metal/oxide interface and the surface of oxide
- actual liquidus and solidus temperatures of metal and oxide layers
- temperatures of the gases leaving the melt
- temperature of the water-gas reaction
  This temperature is a constant predefined value in WECHSL.

KPROP$\neq$0:

Bulk properties: density, thermal conductivity, specific heat, surface tension, and viscosity of metal and oxide.

KINT$\neq$0:

- erosion velocities for the pool/concrete interface
- energy fluxes at the pool bottom, sidewalls and surface
- information about the gas film model used

KMAS$\neq$0:

- integrated mass balance in the melt
- masses, volumes, void fractions
- heights of the melt
- weight fraction of each constituent in each layer
- crust thickness, if crust is formed at the boundaries of the melt layers

KBAL≠0:

- internal energy source, entering and leaving enthalpy fluxes, heats of chemical reactions, heat released to concrete, heat interchanged between the phases, heat radiated or evaporated from surface, and net heat gain or loss (denoted 'sensible heat')
- an energy balance integrated from t=0, the initial enthalpy, internal energy, entering and leaving enthalpy fluxes, reaction energy, energy to concrete, energy radiated from the top of the melt, sums of positive and negative energy, and the error in energy resulting from numerical balance

KGAS≠0:

- temperature of leaving gases
- heat flux, mass and molar rates, weight and molar fractions, total mass and moles released since t=0 for each species of gas
- if sump water has flooded the corium: temperature, mass flow, enthalpy and total mass of the evaporated water. The reference point for the vapor enthalpy is 0 °C, liquid water.

KCAV≠0:

- number of cavity coordinates relevant to the calculation
- coordinates as couples of radius and height

Note:

- The output at the start of a problem and at the end of each run contains the whole amount of cavity points.
- The bypassing of metal by oxide can be recognized by a decrease of radius and height in the same table.

KDIAG≠0:

- diagnostics indicating numerical problems.

The occasional appearance of these diagnostics does not necessarily indicate a severe problem.

3.5.2 Table Printout

There are three time dependent tables printed during the program execution to give a general view of the process. The time intervals are the same as for the detailed output.

Table 1:

- time, s
- heat flux radiated or evaporated at the top of the melt, W
- release of CO_2, kg/s
- release of CO, kg/s
- release of H_2O, including evaporated sump water, kg/s
- release of H_2, kg/s
- release of sump water, kg/s
- integrated mass of released CO_2, kg
- integrated mass of released CO, kg
- integrated mass of released H_2O, without sump water, kg
- integrated mass of released H_2, kg
- integrated mass of released sump water, kg

Table 2:

- time, s
- temperature of liquid metal, K
- temperature of solid metal, K
- temperature of oxide, K
- temperature of oxide surface, K
- temperature of released gases, K
- enthalpy stream of CO_2 gas, W
- enthalpy stream of CO gas, W
- enthalpy stream of H_2O gas, W
- enthalpy stream of H_2 gas, W
- enthalpy stream of all gases, W

The reference point for the gas enthalpies is 0 K. To determine the energy fluxes into the containment, it is recommended to use instead of enthalpy fluxes the gas mass fluxes and associated gas temperatures as input for the containment code in order to avoid inconsistencies of enthalpy tables in different codes.

Table 3:

- time, s
- cavity radius at the top of the melt, m
- temperature of the oxide phase, K
- total mass of released CO, kg
- total mass of released CO_2, kg
- total mass of released H_2, kg
- total mass of released H_2O, without sump water, kg
- content of SiO_2 in the melt, kg

3.5.3 Diagram Plot File

If an output for diagram plots is desired (option on input card 37), selected data are collected and written on this file so that the user can use them as input for his own plot program.

The time intervals are controlled by the content of card 38.

At the beginning of an initial run, the following records are written:

Section 1:

Record 1: Format (18A4) - see input card 1
72 characters for problem identification

Record 2: Format (6E12.4) - see input card 11b
CCL(1), ... CCL(6) - molar concentration for liquidus curve

Record 3: Format (5E12.4) - as record 2
CCL(7),... CCL(11)

Record 4: Format (6E12.4) - see input card 11b
TLL(1), ... TLL(6) - liquidus temperature corresponding to CCL, in K

Record 5: Format (5E12.4) - as record 4
TLL(7),... TLL(11)

Record 6: Format (6E12.4) - see input card 13b
CCS(1),... CCS(6) - molar concentration for solidus curve

Record 7: Format (6E12.4) - as record 6
CCS(7), ... CCS(11)

Record 8: Format (6E12.4) - see input card 13b
TSS(1), ... TSS(6) - solidus temperature corresponding to CCS, in K

Record 9: Format (6E12.4) - as record 8
TSS(7), ... TSS(11)

Section 2:

At the end of each time interval records 10 to 25 are written on the plot file.
Note: The user should take care that for a restart run these data are appended to the preceding data.

Record 10: Format (I5)
NPARM - indicates the number of data to follow
NPARM is actually set to 88 by the code.

Record 11 to 24: Format (6E12.4)

Record 11:
time, s
integrated number of released moles of H_2
integrated number of released moles of H_2O
integrated number of released moles of CO
integrated number of released moles of CO_2
integrated number of released moles of all gases

Record 12:

power of released H_2, W
power of released H_2O, W
power of released CO, W
power of released CO_2, W
mass flow of H_2, g/s
mass flow of H_2O, g/s

Record 13:

mass flow of CO, g/s
mass flow of CO_2, g/s
surface temperature, K
power upward, W/m^2
internal energy, kW
power due to oxidation, kW

Record 14:

power released from the top of the melt, kW
power due to concrete decomposition, kW
power due to gas and oxides, kW
lost power in % of total power loss: upward
lost power in % of total power loss: downward
lost power in % of total power loss: gas release

Record 15:

temperature of liquid metal, K
temperature of oxide, K
conduction between metal and oxide, MW
concrete erosion speed metal - bottom, cm/h
concrete erosion speed metal - wall, cm/h
energy flux oxide - wall, kW/m^2

Record 16:

- energy flux metal - wall, kW/m^2
- energy flux at the bottom, kW/m^2
- temperature of liquid metal, K
- solidus temperature of metal, K
- power from metal to concrete, MW
- axial erosion depth, cm

Record 17:

- radial erosion depth, cm
- mass of Zr in % of actual metal mass
- mass of Cr in % of actual metal mass
- mass of Fe in % of actual metal mass
- mass of Ni in % of actual metal mass
- temperature of oxide phase, K

Record 18:

- solidus temperature of oxide, K
- power from oxide to concrete, MW
- thickness of oxide crust: surface, cm
- thickness of oxide crust: oxide/metal, cm
- thickness of oxide crust: oxide/concrete, cm
- mass of U_2O in % of actual oxide mass

Record 19:

- mass of ZrO_2 in % of actual oxide mass
- mass of SiO_2 in % of actual oxide mass
- mass of CaO in % of actual oxide mass
- temperature of liquid metal, K
- temperature of oxide, K
- temperature at the surface of the melt, K

Record 20:

pool height from initial bottom, cm
height of metal phase, cm
maximum vertical erosion, cm
actual mass of metal, t
actual mass of oxide, t
mass of eroded concrete, t

Record 21:

crust thickness in metal phase: metal / oxide, cm
crust thickness in metal phase: metal /concrete, cm
void fraction in oxide phase
void fraction in metal phase
molar ratio H_2/H_2O (without sump water)
molar ratio CO/CO_2

Record 22:

molar ratio H/C
internal power in melt, kW
molar flow of released H_2, mol/s
molar flow of released H_2O, mol/s
molar flow of released CO, mol/s
molar flow of released CO_2, mol/s

Record 23:

mass of released H_2, kg
mass of released H_2O (without sump), kg
molar flow of released CO, mol/s
molar flow of released CO_2, mol/s
integrated number of released moles of $(H_2 + CO + CO_2)$
zero (not used)

Record 24:

mass of FeO in % of actual oxide mass
mass of Al_2O_3 in % of actual oxide mass
mass of Cr_2O_3 in % of actual oxide mass
erosion speed oxide/wall, cm/h
temperature of solid metal, K
internal power in metal phase, kW

Record 25:

internal power in oxide phase, kW
total mass of released CO, kg
total mass of released CO_2, kg
total mass of released H_2O from sump water, kg

3.5.4 Cavity Plot File

The coordinates of the cavity shape can be stored on this file for further processing by a user provided plot program (option on input card 37). The time interval of the output is set by the user on input card 39.

By analogy with the diagram plot output, this output is divided into two sections: the first section is written once at the beginning of an initial run and the second is repeated at each time interval.

Section 1:

Record 1: Format (18A4) - see input card 1
72 characters of problem identification

Record 2: empty

Record 3: Format (E12.4)
DPLC - time interval between outputs, s

Record 4: Format (7I5)
0, 0, 0, 0, 0, 0, 1 - required for KfK - plot program

Section 2:

Record 5: Format (I5, E12.4)

NB	number of cavity points to follow
TIME	time of output, s

Record 6: Format (6E12.4)

RCAV(1)	radius for point 1, cm
YCAV(1)	height for point 1, cm
	etc.

Record 6 is repeated until all NB points are written

Note: As for the print output, the whole cavity shape is given only at the start of a problem. For the next intervals, only those points are written, which are used during the calculation, i. e., which change their positions.

3.6 Compilation of the Subroutines and Functions Used in the WECHSL Code

This section is a brief description of the coding in WECHSL and its subroutines.

MAIN

MAIN contains

- initialization of variables;
- data input for new start or restart;
- time loop for WECHSL calculation;
- integrated mass balance;
- heat flux balance and integrated energy balance;
- data output for printout, plot data for property - time - diagrams, for the cavity shape, and for restart.

SUBROUTINE WECHSL is called by MAIN;
calls PROPS, VIS, FIND, CAVITY, INTEG, BUBBLE, VOID, QINFAC, SOLWET, QTOP, REACT, ENTH, WASG, LATH, TMELT;
uses SIGMET, SIGOXI, HMELT.

WECHSL is called for each time step by MAIN and contains computations for

- initialization of variables for each time step;
- equilibrium and transport properties of the melt layers depending on temperature and composition;
- change of the cavity shape;
- gas bubble size and rise velocity;
- voiding of the melt layers;
- heat exchange between the melt layers;
- heat transfer from the top of the melt pool;
- chemical reactions inside the metal layer;
- enthalpies of materials entering or leaving each layer;
- water-gas reaction above the melt;
- new masses and composition for each layer;
- new temperatures for each melt layer from energy flux balance

SUBROUTINE CLEAN is called by MAIN;
CLEAN removes from the input data set comments starting with '*' and generates an input data set without comments.

SUBROUTINE CPADD is called by MAIN
CPADD provides the heat capacities of metal and oxide melt added to the melt bulk

SUBROUTINE PROPS is called by WECHSL;
calls SOLID, DENX
PROPS computes densities, specific heat capacities, thermal conductivities, liquidus and solidus temperatures, latent heat of phase change, and weight and molar fractions of each melt layer.

SUBROUTINE SOLLIQ is called by PROPS
SOLLIQ computes liquidus and solidus temperatures.

SUBROUTINE DENX is called by PROPS
DENX computes densities for the metal and the oxide.

FUNCTION SIGMET is used in WECHSL
SIGMET is the surface tension of the metal.

FUNCTION SIGOXI is used in WECHSL
SIGOXI is the surface tension of the oxide.

SUBROUTINE VIS is called by WECHSL
VIS computes the dynamic viscosity of the oxide.

SUBROUTINE FIND is called by WECHSL
FIND rearranges the cavity points to equal distances and computes the level and the volume of each melt layer.

SUBROUTINE CAVITY is called by WECHSL,
calles BOULAY, SOLID, GASMIX, KONTUR;
uses ERRST

CAVITY computes the new cavity profile and evaluates the heat transferred to the concrete and the masses of the liquid and gaseous concrete decomposition products.

FUNCTION ERRST is used in CAVITY

ERRST is the freezing temperature between liquidus and solidus.

SUBROUTINE BOULAY is called by CAVITY;
calls GRENZ, GASMIX, KRUSTE;
uses CRCON

BOULAY computes the characteristics of the boundary layer at the interface of the melt facing the conrete and the interface temperature, the onset of crust formation and the characteristics when thick crusts exist.

SUBROUTINE SOLID is called by CAVITY;
calls KRUSTE

SOLID computes the transient, one-dimensional heat conduction inside the solidified metal with a correction term for the influence of radial heat conduction.

SUBROUTINE SOLWET is called by WECHSL

SOLWET computes the heat ransfer between solid metal and oxide.

SUBROUTINE GRENZ is called by BOULAY;
calls GASMIX;
uses CRCON

GRENZ computes the temperature at the melt/gas film interface and the onset of crust formation.

FUNCTION CRCON is used in BOULAY, GRENZ

CRCON gives a linear transition from gas film driven boundary layer heat transfer to gas bubble driven heat transfer after a crust with defined thickness has formed.

SUBROUTINE GASMIX is called by WECHSL, CAVITY, BOULAY,
GRENZ; calls STH2O, STCO2

GASMIX computes the equilibrium and transport properties of a gas mixture containing the species H_2O and CO_2 and depending on pressure and temperature.

SUBROUTINE STH2O is called by GASMIX

STH2O evaluates the equilibrium and transport properties of steam at 1 bar.

SUBROUTINE STCO2 is called by GASMIX

STCO2 evaluates the equilibrium and transport properties of carbon dioxide at 1 bar.

SUBROUTINE KRUSTE is called by BOULAY, QTOP, QINFAC, SOLID;
calls PREP

KRUSTE calculates the transient, one-dimensional heat conduction inside a crust and the change of crust thickness.

SUBROUTINE PREP is called by KRUSTE

PREP calculates the change of the crust thickness.

SUBROUTINE KONTUR is called by CAVITY;
calls LAMIN, TURBN

KONTUR contains the heat transfer and geometry models for computing a new cavity point.

SUBROUTINE LAMIN is called by KONTUR;
calls RECHN

LAMIN computes the gas film thickness for the laminar flow regime.

SUBROUTINE RECHN is called by LAMIN

RECHN supports the computation of the laminar gas film in LAMIN.

SUBROUTINE TURBN is called by KONTUR

TURBN computes the thickness of the laminar sublayer of the turbulent gas film characteristic for the heat transfer.

SUBROUTINE QINFAC is called by WECHSL;
calls KRUSTE

QINFAC computes the heat exchange between the metal and the oxide layer including onset and growth of crusts at the relevant interface.

SUBROUTINE QTOP is called by WECHSL;
calls QRAD, SIEDE, KRUSTE, LINIT

QTOP computes the heat extracted through the top of the melt by thermal radiation or by sump water evaporation including the onset and growth of a crust.

SUBROUTINE QRAD is called by QTOP;
calls SIEDE

QRAD computes the heat flux density and the surface temperature of the oxide melt pool by thermal radiation or by sump water evaporation including the onset of crust formation.

SUBROUTINE SIEDE is called by QTOP, QRAD,
calls LINIT;
uses BLOCK DATA

SIEDE computes the heat flux density for boiling heat transfer using pressure dependent boiling curves of water.

BLOCK DATA is used in SIEDE

BLOCK DATA contains the data sets for the pressure dependent boiling curves.

SUBROUTINE LINIT is called by SIEDE

LINIT provides linear interpolation between two points.

SUBROUTINE BUBBLE is called by WECHSL

BUBBLE computes the bubble rise velocity inside a melt layer and the coalescence or breakup of gas bubbles.

SUBROUTINE VOID is called by WECHSL;
calls ITER

VOID computes the void fraction inside a melt layer.

SUBROUTINE ITER is called by VOID;
uses FANKT

ITER executes iteration of the function FANKT.

FUNCTION FANKT is used in ITER

FANKT provides the function for the iteration.

SUBROUTINE REACT is called by WECHSL

REACT computes the exothermal or endothermal reaction enthalpies and the flows of materials changed by oxidation reactions inside the metal layer.

SUBROUTINE ENTH is called by WECHSL

ENTH computes enthalpies of gases and oxides entering or leaving a melt layer.

SUBROUTINE ENTM is called by WECHSL

ENTM computes the enthalpies of metals entering or leaving a melt layer.

SUBROUTINE WASG is called by WECHSL

WASG computes the homogeneous water gas reaction of the gases leaving the melt pool and determines the new chemical equilibrium.

FUNCTION HMELT is used in WECHSL

HMELT is the specific enthalpy for metal or oxide.

SUBROUTINE TMELT is called by WECHSL

TMELT computes the temperature of a melt layer from melt mass and enthalpy.

SUBROUTINE LATH is called by WECHSL

LATH computes the latent heat of evaporation of water and the specific enthalpy of saturated steam.

SUBROUTINE INTEG is called by WECHSL

INTEG serves for the evaluation of integral values by summation.

SUBROUTINE INOUT is called by MAIN

INOUT is the input-output subroutine for restart.

ISTEU = 1: reading from restart file;
ISTEU = 2: writing to restart file;
ISTEU = 3: reading from array for internal restart;
ISTEU = 4: writing to array for internal restart.

4. Literature

[1] Rassmussen, N.C.:
"Reactor Safety Study - An Assessment of Accident Risks in US Commercial Nuclear Power Plants," USNRC, WASH 1400 (NUREG-75/014), Oct. 1975.

[2] Der Bundesminister für Forschung und Technologie (editor):
"Deutsche Risikostudie Kernkraftwerke", Verlag TÜV Rheinland,Cologne, 1979.

[3] Alsmeyer, H., Peehs, M. and Perinić, D.:
"Untersuchung der Wechselwirkung einer Kernschmelze mit Beton in der BETA-Versuchsanlage", PNS Annual Colloquium 1982, KfK 3470.

[4] Alsmeyer, H.:
"BETA-experiments in verification of the WECHSL-Code: Experimental results on the melt-concrete interaction", Nucl. Engrg. Des. 103 (1987), pp. 115-125.

[5] Murfin, W.B.:
"A Preliminary Model for Core/Concrete Interactions", SAND77-0370, Sandia Laboratories, Albuquerque N.M., Aug. 1977.

[6] Reimann, M., Murfin, W.B.:
"The WECHSL Code: A Computer Program for the Interaction of a Core Melt with Concrete." KfK 2890, Kernforschungszentrum Karlsruhe, Nov. 1981.

[7] Powers, D.A., Dahlgren, D.A., Muir, J.F., and Murfin, W.B.:
"Exploratory Study of Molten Core Material/Concrete Interactions", SAND77-2042, Sandia Laboratories, Albuquerque N.M., Feb. 1978.

[8] Perinic, D., Kammerer, B., Knauß, H., Mack, A., and Stuka, B.:
"Betontiegelversuche mit Thermitschmelzen", KfK 2572, Kernforschungszentrum Karlsruhe, July 1979.

[9] Skokan, A., Hollek, H., and Peehs, M.:
"Chemical Reactions Between Light Water Reactor Core Melt and Concrete", Nucl. Techn. 46 (1979)2, p. 255.

[10] Alsmeyer, H., Dres, K. Reimann, M., Stiefel, S.:
"Modellentwicklung zur analytischen Beschreibung von Kernschmelzunfällen" in "Projekt Nukleare Sicherheit, Jahresbericht 1986", KfK 4100 (1986), pp. 4300-14/4300-32.

[11] Peehs, M., Skokan, A., and Reimann, M.:
"The Behavior of Concrete in Contact with Molten Corium in the Case of a Hypothetical Core Melt Accident", Nucl. Techn. 46 (1979)2, pp. 192-198.

[12] Powers, D.A.:
"Kinetics and Stochiometry of the Thermal Decomposition of Concrete", LWR Safety Program, Quaterly Report Jan.-March 1986, SAND76-9369, Sandia Laboratories, Albuquerque N.M., Sept. 1976.

[13] Alsmeyer, H., Reimann, M.:
"On the Heat and Mass Transport Processes of a Horizontal Melting or Decomposing Layer under a Molten Pool", Nucl. React. Safety Heat Transf., Winter Annual Meeting ASME, Atlanta Ga., Nov. 1977, pp. 47-53.

[14] Landau, H.G.:
"Heat Conduction in a Melting Solid", Quat. Appl. Math. 8 (1951), pp. 81-94.

[15] Höpfl, R., Peehs, M.:
"Kalorische Größen von Reaktorbeton unter dem Aspekt des hypothetischen Kernschmelzunfalls", Jahrestagung Kerntechnik, Mannheim 1982, pp. 319-322.

[16] Copus, E.R., Bradley, D.R.:
"Interaction of Hot Solid Debris With Concrete", NUREG/CR-4558, SAND-85-1739, Sandia National Laboratories, Albuquerque, W.M., June 1986.

[17] Berenson, P.J.:
"Film Boiling Heat Transfer from a Horizontal Surface", Journ. Heat Transf., 38C (1961), pp. 351-358.

[18] Bromley, L.A.:
"Heat Transfer in Stable Film Boiling", Chem. Engng. Progr. 46 (1950)5, pp. 221-227.

[19] Hsu, Y.Y., Westwater, J.W.:
"Approximate Theory for Film Boiling on Vertical Surfaces", Chem. Engng. Progr. Symp. Ser. 56 (1960) 30, pp. 15-24.

[20] Dhir, V.K., Castle, J.N., and Catton, I.:
"Role of Taylor Instability on Sublimation of a Horizontal Slab of Dry Ice", Journ. Heat Transf. 99 (1977) 3, pp. 411-418.

[21] Reimann, M., Murfin, W.B., and Alsmeyer, H.:
"On the Penetration of Hot Melts into Concrete Structures", The European Nuclear Conference, Trans.ANS 31 (1979), p. 371-373.

[22] Reimann, M., Murfin, W.B.:
"Calculations for the Decomposition of Concrete Structures by a Molten Pool", Europ. Appl. Res. Rept. 1 (1979) 6, p. 1554-1566.

[23] Schlichting, H.:
"Grenzschichttheorie", G. Braun, Karlsruhe 1975, p. 556 ff.

[24] Reineke, H.H., Hahn, K.:
"Ein vereinfachtes Rechenmodell für den Wärmeübergang von einer Schmelze an Beton bei Anwesenheit eines Dampffilms", IVA Ingenieurbüro für Berechnung und Entwicklung verfahrenstechnischer Anlagen, July 1984.

[25] Reimann, M., Alsmeyer, H.:
"Hydrodynamische und thermische Modelle zur Wechselwirkung einer Kernschmelze mit Beton" in: PNS-Halbjahresbericht 1978/2, KfK 2750, Kernforschungszentrum Karlsruhe, Oct. 1979.

[26] Lock, R.C.:
"The Velocity Distribution in the Laminar Boundary Layer Between Parallel Streams", Quart. Journ. Mech. Appl. Math. 4 (1951) 1, pp. 42-63.

[27] Reineke, H.H., Rinkleff, L., and Schramm, R.: "Heat Transfer Between Molten Core Material and Concrete", Proc. 3rd Post Accident Heat Removal Int. Exch., ANL-78-10, Argonne Ill., Nov. 2-4, 1977.

[28] Schramm, R.: "Untersuchungen zur Wechselwirkung von Kernschmelzen und Beton", BMFT-FB (RS166-79-05) Abschlußbericht Band Ib, TU Hannover, Sept. 1980.

[29] Schwarzott, W. et al.: "Detaillierung von KAVERN und Programmentwicklung zur Gasabströmung aus der Schildgrube", BMFT 150379, Abschlußbericht 1983.

[30] Grigull, U., Sandner, H.:. "Wärmeleitung", Springer, Berlin 1979.

[31] Levich, V.G.: "Physicochemical Hydrodynamics", Prentice-Hall, New York 1962.

[32] Mendelson, H.D.: A.I.Ch.E.J. 13 (1967), p. 250.

[33] Haberman, W.F., Morton, R.K.: "An Experimental Investigation of the Drag and Shape of Air Bubbles Rising in Various Liquids", Rept. 802, David, W. Taylor Basin, Sept. 1953.

[34] Le Clair, B.P., Hamielec, A.E.: "Strömung durch Teilchenansammlungen" in "Kinetik metallurgischer Vorgänge bei der Stahlherstellung", Verlag Stahleisen, Düsseldorf 1972.

[35] Nicklin, D.J.: Chem.Engng. Sci. 17 (1962), p. 693.

[36] Nikolopoulos, P. Ondracek, G.: unpublished report of the Kernforschungszentrum Karlsruhe, 1979

[37] Werle, H.: "Einfluß eines Gasstroms auf den Wärmeübergang zwischen zwei Flüssigkeitsschichten" in: PNS-Halbjahresbericht 1978/2, KfK 2750, Kernforschungszentrum Karlsruhe, October 1979, p. 4300/79-182.

[38] Haberstroh, R.D., Reinders, R.D.: "Conduction Sheet Model for Natural Convection through a Density Stratified Interface", Int. J. Heat Mass Transf. 17 (1974), pp. 307.

[39] Bermann, M.: "Light Water Reactor Safety Research Program Semiannual Report October 1983 - March 1984, NUREG/CR-4459, SAND85-2500, Sandia National Laboratories, Albuquerque, N.M., 1986.

[40] Alsmeyer, H., Dres, K.: "Modellexperimente zur analytischen Beschreibung von Kernschmelzenunfällen" in Sicherheitsorientierte LWR-Forschung, PRS-Jahresbericht 1987, KfK 4450 (1987), pp. 113-128.

[41] Blose, R.E. et al.: "SWISS: Sustained Heated Metallic Melt/Concrete Interactions with Overlying Water Pools", NUREG/CR-4727 (1977).

[42] Rohsenow, W.M., Hartnett, J.P.:
"Handbook of Heat Transfer", McGraw Hill, New York 1973.

[43] Pollak, R.:
"Eine neue Fundamentalgleichung zur konsistenten Darstellung der thermodynamischen Eigenschaften von Wasser", BWK 24 (1975) 5, p. 210.

[44] Schmidt, E.:
"Zustandsgrößen von Wasser und Wasserdampf in SI-Einheiten", 3. Edition., Springer, Berlin, 1982.

[45] Alsmeyer, H., Barleon, L., Koster, J., Michael, I., Müller, U., and Reimann, M.:
"Ein Modell zur Beschreibung der Wechselwirkung einer Kernschmelze mit Beton", KfK 2395, Kernforschungszentrum Karlsruhe, Oct. 1977.

[46] Powers, D.A., Frazier, A.W.:
"VISRHO - A Computer Subroutine for Estimating the Viscosity and Density of Complex Silicate Melts", SAND76-0649, Sandia Laboratories, Albuquerque N.M., June 1977.

[47] Skoutajan, P., Baukal, W., König, R., Wagner, W., and Walter, G.:
"Durchführung von Viskositätsmessungen an oxidischen Corium - Beton - Schmelzen", BMFT-RS214A, Battelle-Institut Frankfurt/Main, May 1979.

[48] Kunitz, W.:
Journ. General Physiology 9(1926), p. 715.

[49] Gmelin-Durrer:
"Metallurgie des Eisens", Vol. 5, Berlin-Heidelberg-New York 1978, p. 23a ff.

[50] Wargaftik, N.B.:
"Tables of the Thermophysical Properties of Liquids and Gases" 2nd edition, Hemisphere, Washington, London, 1975.

[51] Bird, R.B., Stewart, W.E., Lightfoot, E.N.:
"Transport Phenomena", J. Wiley, New York, London, 1960.

[52] Misaelidis, P., Ondracek, G.:
unpublished report of the Kernforschungszentrum Karlsruhe, 1978.

[53] Prigogine, J., Defay, R.:
"Chemische Thermodynamik", VEB Verlag für Grundstoffindustrie, Leipzig 1962, p. 378 ff.

[54] Muir, J.F.:
Sandia Laboratories, Albuquerque N.M., (private communication).

APPENDIX A

Test Sample 1:
BETA Test

```
  BETA TEST V1.8 ; WECHSL POST TEST CALCULATION.
*
*
*--------  THERMITE ADDITION:  RATE AND TIME OF REACTION
*
*  KG/S  |  SEC.   |
        0.        0.
*
*
*-------  ADDITION OF OTHER MATERIALS   ---------------------------------
*
*  NUMBER OF ADDITIONS : ( MAX. 10; IF 0, NO FURTHER CARDS )
        2
* 1. ADDITION : START TIME , END TIME (SEC), TEMPERATURE (K)
                    0.           34.           2173.
*    ADDED MASS (KG) OF EACH SPECIES DURING THIS TIME :
*    UO2 |     ZRO2 |       FEO |       CAO |     SIO2 |    AL2O3 |    CR2O3 |
      0.        0.         0.         0.         0.        0.         0.
*    FE  |     ZR   |       CR  |       NI  |
    306.        0.        17.        17.
* 2. ADDITION : START TIME , END TIME (SEC), TEMPERATURE (K)
                   34.           46.           2173.
*    ADDED MASS (KG) OF EACH SPECIES DURING THIS TIME :
*    UO2 |     ZRO2 |       FEO |       CAO |     SIO2 |    AL2O3 |    CR2O3 |
      0.        0.         0.        36.         0.       84.         0.
*    FE  |     ZR   |       CR  |       NI  |
      0.        0.         0.         0.
*
*
*-------  CHARACTERISTICS OF CONCRETE WITHOUT STEEL -------------------
*
*WEIGHT FRACTION OF THE COMPONENTS : (AL2O3 IS THE COMPLEMENT)
*  CACO3 | CA(OH)2 |     SIO2 | FREE H2O|
     .0663     .0728     .7655     .0422
*   STEEL; MELT TEMP.; DECOMP. ENTH. ; DENSITY  ( ALL WITHOUT STEEL)
*KG/KGCON|  KELVIN |    J/KG |    KG/M3 |
       0.0     1573.   1.951E6    2.25E3
*
*
*------ CHARACTERISTICS OF THE LIQUIDUS/SOLIDUS CURVE OF THE OXIDE PHASE
*       SCHROEDER-VAN LAAR EQUATION: IMAT=1
*MAT|
    1
*    LOW TEMPERATURE GROUP :
*NUMBER OF SPECIES; SPECIES:1=UO2; 2=ZRO2; 3=FEO; 4=CAO; 5=SIO2; 6=AL2O3
*---|----|----|----|----|----|----|
    3    3    4    5
*EFFECTIVE LATENT HEAT , SOLIDUS AND LIQUIDUS TEMPERATURE OF THE PHASE :
* J/MOLE |  KELVIN |  KELVIN |
    24840.     1423.     1473.
*    HIGH TEMPERATURE GROUP :
*NUMBER OF SPECIES; SPECIES:1=UO2; 2=ZRO2; 3=FEO; 4=CAO; 5=SIO2; 6=AL2O3
*---|----|----|----|----|----|----|
    1    6
*EFFECTIVE LATENT HEAT , SOLIDUS AND LIQUIDUS TEMPERATURE OF THE PHASE :
* J/MOLE |  KELVIN |  KELVIN |
   110000.     2218.     2268.
*
*
```

```
*--------  CHARACTERISTICS OF THE OXIDE PHASE  -------------------------
*
* INITIAL MASS OF OXIDES IN KG :
*    UO2 |     ZRO2 |      FEO |      CAO |     SIO2 |    AL2O3 |    CR2O3 |
       0.        0.        0.        3.        0.        7.        0.
* INITIAL TEMPERATURE OF OXIDE :
* KELVIN |
    2173.
* POWER IN THE OXIDE PHASE :
* NUMBER OF COUPLES : (TIME IN SEC. ; INTERNAL POWER IN WATT )
*---| IF THIS NUMBER IS 0,GOTO METAL PHASE(NO CARDS FOR SHIFT AND POWER)
   0
*
*
*--------  CHARACTERISTICS OF THE METAL PHASE  -------------------------
*
* INITIAL MASS OF METALS IN KG :
*     FE |       ZR |       CR |       NI |
     9.0         0.       0.5       0.5
*
* INITIAL TEMPERATURE OF METAL :
* KELVIN |
    2173.
*
* POWER IN THE METAL PHASE :
* NUMBER OF COUPLES : (TIME IN SEC. ; INTERNAL POWER IN WATT )
*---| IF THIS NUMBER IS 0,GOTO THE CARD : TIME STEP AND FINAL TIME.
   7
*COUPLES (TIME IN SEC. ; INTERNAL POWER IN WATT ) ( 3 COUPLES/CARD )
*   TIME |   POWER |     TIME |   POWER |     TIME |   POWER |
       0.        0.       30.   1.800E6      225.   1.860E6
     355.   1.000E6      475.  0.670E6       485.        0.
    3600.        0.
*
*
*--------  TIME CHARACTERISTICS  ---------------------------------------
*
*TIME STEP, FINAL TIME, MIN/MAX TIME STEP:
*  SEC.   |   SEC.   |   SEC.   |   SEC.   |
     0.05     2000.       0.03       1.0
*
* PRINTOUT :
* NUMBER OF PRINTOUT COUPLES :
   3
* COUPLES (START PRINTOUT TIME,S ; PRINTOUT INTERVAL,S) (3 COUPLES/CARD)
*   TIME |     STEP |     TIME |     STEP |     TIME |     STEP |
       0.       10.      150.       25.     1000.       50.
*
*
*--------  AMBIENT ATMOSPHERIC PRESSURE  -------------------------------
*
* NUMBER OF COUPLES
*---|
   2
* COUPLES (TIME IN SEC. ; PRESSURE, BAR ) ( 3 COUPLES/CARD )
*   TIME | PRESSURE|     TIME | PRESSURE|---------|---------|
       0.        1.     1.E6         1.
*
*
```

```
*--------  AMBIENT TEMPERATURE FOR RADIATION ON THE TOP OF CORIUM  ----
*
* NUMBER OF COUPLES
*---|
   3
* COUPLES (TIME IN SEC. ; TEMPERATURE, K ) ( 3 COUPLES/CARD )
*   TIME | TEMPERA.|     TIME | TEMPERA.|---------|---------|
        0.       300.        30.      1573.      4000.      1573.
*
*
*--------  CAVITY CHARACTERISTICS  --------------------------------------
*
* OPTION FOR INITIAL SHAPE : 1500<NB<2000 : CYLINDER WITH ROUNDED CORNER
* NB|                        WITH CONIC SECTION ON THE TOP
 1601
* NUMBER OF POINTS ON FLOOR AND CORNER, RADIUS OF CYLINDER AND CORNER,
* INTERVAL BETWEEN POINTS ON CYLINDER, CYLINDER HEIGHT.
*FLO|COR.|RADIUS,M |CORNER,M |INTERV.,M| HEIGHT,M|
   11    5      0.19       0.05       0.02       0.75
* TOTAL HEIGHT OF CAVITY,M ; ANGLE OF INCLINATION,DEG
* HEIGHT |  ANGLE  |
        3.       12.5
*
* INTERVAL BETWEEN CAVITY POINTS DURING PROGRAM RUN.
*  METER |
      .020
*
* RADIUS SUMP WATER INGRESSION, BASEMAT THICKNESS, TIME FOR SUMP WATER
*  METER |   METER |   SEC   |
     1000.      1000.       1.E7
*
*
*--------  PRINTOUT OPTIONS: ( 0 = NO  ,  1 = YES ) -------------------
*
*TEMPERAT/ PROPERT./ INTERFA./ MASS BAL/
         1         1         1         1
*ENER.BAL/ GAS REL./  CAVITY /DIAGNOST./
         1         1         1         1
*
*
*--------  PLOT FILE OPTIONS: ( 0 = NO  ,  1 = YES ) ------------------
*
* DO YOU WANT DIAGRAM PLOT ? ; DO YOU WANT THE CAVITY SHAPE ?
* PLOTS  /  CAVITY /
         1         1
* START TIME AND INTERVAL TO WRITE PLOT FILE, SEC (THIS CARD MUST STAY)
* WARNING ! FOR KFK PLOT PROGRAM, NO MORE THAN 500 TIMES CAN BE WRITTEN!
* START  | INTERVAL|
        0.       10.
* START TIME AND INTERVAL TO WRITE CAVITY PLOT, S (THIS CARD MUST STAY)
* START  | INTERVAL|
        0.       60.
*
*-------  END OF WECHSL INPUT DATA  ----------------------------------
```

```
     BETA TEST V1.8 ; WECHSL POST TEST CALCULATION.

 1. ADDITION FROM       0. TO      34. SECONDS
             AT TEMPERATURE OF 2173. K :
   FE      :     306. KG
   CR      :      17. KG
   NI      :      17. KG
 2. ADDITION FROM      34. TO      46. SECONDS
             AT TEMPERATURE OF 2173. K :
   CAO     :      36. KG
   AL2O3   :      84. KG

COMPOSITION OF CONCRETE ( INCLUDING STEEL CONTENT )
 CACO3    CA(OH)2  SIO2     H2O      AL2O3
 0.066    0.073    0.765    0.042    0.053
WEIGHT FRACTION, IN MASS UNIT OF CONCRETE, OF:
  CAO      SIO2     AL2O3    H2O      CO2
  0.092    0.765    0.053    0.060    0.029

TSB=1573. K  HB= 0.1951E+07 J/KG  RHO=2250. KG/M3 ( ALL WITHOUT STEEL )
 0.000 KG FE PER KG CONCRETE ( WITHOUT STEEL )

 HB  FOR CONC.+FE =  0.1951E+07 J/KG
 RHO FOR CONC.+FE = 2.2500 T/M3

INITIAL MASS OF OXIDES, KG
 UO2         ZRO2        FEO         CAO         SIO2        AL2O3       CR2O3
      0.          0.          0.          3.          0.          7.          0.
INITIAL OXIDE TEMPERATURE T= 2173. K

INTERNAL HEAT GENERATION IN OXIDE PHASE
 TIME,S       POWER,W
 0.0000E+00   0.0000E+00
 0.1000E+11   0.0000E+00

INITIAL MASS OF METAL, KG
 FE          ZR          CR          NI
      9.          0.          1.          1.
  INITIAL METAL TEMPERATURE T= 2173. K

 INTERNAL HEAT GENERATION IN METAL PHASE
 TIME,S       POWER,W
 0.0000E+00   0.0000E+00
 0.3000E+02   0.1800E+07
 0.2250E+03   0.1860E+07
 0.3550E+03   0.1000E+07
 0.4750E+03   0.6700E+06
 0.4850E+03   0.0000E+00
 0.3600E+04   0.0000E+00

  COMPUTATIONS MADE EVERY  0.05 SECONDS UNTIL   2000.0 SEC.
  MINIMUM TIME STEP IS =  0.030 SEC.
  MAXIMUM TIME STEP IS =  1.000 SEC.
  PRINTOUT EVERY   10.SEC., BEGINNING AT    0. SEC.
  PRINTOUT EVERY   25.SEC., BEGINNING AT  150. SEC.
  PRINTOUT EVERY   50.SEC., BEGINNING AT 1000. SEC.
```

```
 FEO    CAO    SIO2

 ALOX

LIQUIDUS TEMPERATURE OF THE OXIDE PHASE:
MOL. FRACT. H.T.GROUP  TEMPERATURE, K
 0.000                  1473.
 0.007                  1553.
 0.020                  1632.
 0.042                  1712.
 0.075                  1791.
 0.125                  1871.
 0.198                  1950.
 0.302                  2030.
 0.453                  2109.
 0.673                  2189.
 1.000                  2268.

SOLIDUS TEMPERATURE OF THE OXIDE PHASE:
MOL. FRACT. H.T.GROUP  TEMPERATURE, K
 0.000                  1423.
 0.111                  1503.
 0.205                  1582.
 0.289                  1662.
 0.367                  1741.
 0.444                  1821.
 0.524                  1900.
 0.611                  1980.
 0.712                  2059.
 0.837                  2139.
 1.000                  2218.

PRESSURE HISTORY
 TIME,S         PRESSURE,BAR
 0.0000E+00   0.1000E+01
 0.1000E+07   0.1000E+01

AMBIENT TEMPERATURE HISTORY
 TIME,S         TEMPERATURE,K
 0.0000E+00   0.3000E+03
 0.3000E+02   0.1573E+04
 0.4000E+04   0.1573E+04


============================================================
                  AT TIME =     0. SEC.
             BEGINNING OF THE OXIDATION OF CR
              2CR + 3H2O <=====> CR2O3 + 3H2
              2CR + 3CO2 <=====> CR2O3 + 3CO

============================================================
============================================================



============================================================
                     TIME =     0. SEC.
 THE HEAT TRANSFER MODEL BETWEEN BOTTOM METAL AND CONCRETE
 IS ,FROM NOW, THE MIXED MODEL (OR TRANSITION MODEL)
 THE REYNOLD NUMBER OF THIS GAS FLOW IS :    0.2925E+01
 THERE IS NO METAL CRUST..

============================================================
============================================================
```

```
************************
*                      *
*  TIME =      0. SEC  *         NEXT TIME STEP= 0.04 SEC
*                      *
************************


CAVITY DIMENSIONS, M :

       VERTICAL EROSION  :   0.000
       MAXIMAL RADIUS    :   0.190
       ZERO LEVEL RADIUS :   0.190

TEMPERATURES, K :

       POOL -      LIQ. METAL: 2169.   OXIDE     :  2149.
       SURFACES -  MET./CONC.: 2153.   OX./CONC.:  2020.
                   MET./OX.  : 2173.   OX./SURF.:  2167.
       LIQUIDUS -  METAL     : 1787.   OXIDE     :  2148.
       SOLIDUS  -  METAL     : 1777.   OXIDE     :  1934.
       GAS LEAVING THE MELT  : 2030.
       WATER GAS REACTION    : 1200.

PROPERTIES:
                                          METAL             OXIDE
       DENSITY, KG/M3                 :    7094.             2632.
       HEAT CONDUCTIVITY, W/(M.K):  46.997              7.992
       HEAT CAPACITY , J/(KG.K)  :      748.             1393.
       SURFACE TENSION, KG/S2     :   1.653              0.211
       VISCOSITY , KG/(S.M)       : 0.3176E-02        0.1162E+02

POOL-CONCRETE INTERFACE :
                                    BOTTOM      METAL/WALL   OXIDE/WALL   OXIDE/SURFACE
       EROSION SPEED, CM/S :  0.1062E+00   0.1632E-01   0.9144E-02
       EROSION SPEED, CM/H :   382.19        58.74        32.92
       ENERGY FLUX,    W/M2 :  0.4660E+07   0.7162E+06   0.4014E+06   0.6872E+06
       ENERGY FLUX,   KW/M2 :    4660.         716.         401.          687.

       HEAT TRANSFER FOR BOTTOM/CONCRETE MIXED MODE

INTEGRATED MASS BALANCE IN THE MELT, TONS :

       INITIAL MELT MASS:     0.020    ACTUAL MASS OF MELT  :     0.021
       ERODED (CONC.+FE):     0.000    MASS OF LEAVING GASES:     0.000

       SUM OF LEFT TERMS:     0.021    SUM OF RIGHT TERMS    :     0.021
       THE ERROR BETWEEN THE 2 SUMS IS  0.173E-17 TONS, I.E   0.845E-14 %

MASSES ,VOLUMES AND HEIGHTS :
                                                          METAL       OXIDE
       MASS ,TONS                                 :       0.01        0.01
       VOLUME, (INCLUDING VOID FRACTION), M3 :       0.01        0.03
       VOLUME, (WITHOUT VOID FRACTION), M3   :       0.00        0.00
       VOID FRACTION , IN PERCENT                :      85.00       85.00
       DEPTH, M                                   :       0.09        0.22
       POOL HEIGHT FROM INITIAL BOTTOM, M      :            0.31
       VOLUME OF ERODED CONCRETE, M3           :            0.00
       MASS OF ERODED CONCRETE, TONS           :           0.000

WEIGHT FRACTION OF SPECIES IN EACH PHASE, % :

        METAL PHASE:(       10. KG)    OXIDE PHASE:(      10. KG)
               ZR :  0.0                          UO2 :  0.0
               CR :  5.0                         ZRO2 :  0.0
               FE : 90.0                          FEO :  0.0
               NI :  5.0                          CAO : 30.0
                                                  SIO2 :  0.1
                                                 AL2O3 : 69.9
                                                 CR2O3 :  0.0
```

```
HEAT FLUX BALANCE IN EACH PHASE,  WATT :
                                                METAL          OXIDE
        POWER DUE TO DECAY HEAT               :   0.3000E+04     0.0000E+00
        POWER ENTERING DUE TO GAS AND OXIDES :   0.7596E+06     0.1238E+07
        POWER LEAVING DUE TO GAS AND OXIDES  :  -0.1098E+07    -0.1103E+06
        POWER DUE TO OXIDATION REACTIONS     :   0.1631E+06     0.0000E+00
        POWER DUE TO CONCRETE DECOMPOSITION  :  -0.6081E+06    -0.1121E+06
        CONDUCTION BETWEEN PHASES            :   0.0000E+00     0.0000E+00
        RADIATION OR EVAPORATED AT SURFACE   :   0.0000E+00    -0.6500E+07
        SENSIBLE HEAT                        :  -0.7805E+06    -0.5484E+07

INTEGRATED ENERGY BALANCE IN THE MELT, JOULE :

        INITIAL ENTHALPIE     0.6060E+08    INTEGRATED ENTHALPIE      0.6029E+08
        DECAY HEAT            0.1500E+03    CONCRETE DECOMPOSITION    0.3601E+05
        ENTERING(GAS,OX.)     0.4496E+05    LEAVING (GASES)           0.5515E+04
        OXIDAT. REACTIONS     0.8157E+04    RADIATION OR TO WATER     0.3250E+06

        SUM OF LEFT TERMS     0.6065E+08    SUM OF RIGHT TERMS        0.6065E+08
        THE ERROR BETWEEN THE 2 SUMS IS     0.6155E-08 J., I.E    0.1015E-13 %

GASES GOING IN THE CONTAINMENT, AT THE TEMPERATURE T= 2030. K.
AFTER THAT THE WATER-GAS REACTION OCCURED AT THE SURFACE :

                            CO2         CO          H2O         H2
        HEAT FLUX, WATT   0.3255E+04  0.1414E+05  0.2587E+05  0.6557E+05
        MASS FLUX, KG/S   0.1410E-02  0.5951E-02  0.3549E-02  0.2071E-02
        MOL. FLUX, MOL/S  0.3205E-01  0.2124E+00  0.1971E+00  0.1030E+01
        WEIGHT FRACTION   0.1086E+00  0.4584E+00  0.2734E+00  0.1596E+00
        MOLAR FRACTION    0.2177E-01  0.1443E+00  0.1339E+00  0.7000E+00
        TOTAL MASS, KG    0.7052E-04  0.2975E-03  0.1774E-03  0.1036E-03
        TOT.MOLS, MOL     0.1602E-02  0.1062E-01  0.9853E-02  0.5152E-01
```

```
THE CAVITY SHAPE HAS BEEN CALCULATED USING 163 POINTS, COORDONATES IN CM :
  R=RADIUS  ;  Z=DEPTHNESS   ;  Z-REFERENCE: INITIAL BOTTOM OF THE CAVITY

     R         Z          R         Z          R         Z          R         Z
    0.0       0.0        2.0       0.0        4.0       0.0        6.0       0.0
    8.0       0.0       10.0       0.0       12.0       0.0       14.0       0.0
   15.9       0.4       17.6       1.6       18.6       3.2       19.0       5.2
   19.0       7.2       19.0       8.9       19.0      11.2       19.0      13.2
   19.0      15.2       19.0      17.2       19.0      19.2       19.0      21.2
   19.0      23.2       19.0      25.2       19.0      27.2       19.0      29.2
   19.0      31.2       19.0      33.2       19.0      35.2       19.0      37.2
   19.0      39.2       19.0      41.2       19.0      43.2       19.0      45.2
   19.0      47.2       19.0      49.2       19.0      51.2       19.0      53.2
   19.0      55.2       19.0      57.2       19.0      59.2       19.0      61.2
   19.0      63.2       19.0      65.2       19.0      67.2       19.0      69.2
   19.0      71.2       19.0      73.2       19.5      75.1       19.9      77.1
   20.3      79.0       20.8      81.0       21.2      82.9       21.6      84.9
   22.1      86.8       22.5      88.8       22.9      90.7       23.4      92.7
   23.8      94.7       24.2      96.6       24.7      98.6       25.1     100.5
   25.5     102.5       26.0     104.4       26.4     106.4       26.8     108.3
   27.3     110.3       27.7     112.2       28.1     114.2       28.6     116.1
   29.0     118.1       29.4     120.0       29.9     122.0       30.3     123.9
   30.7     125.9       31.2     127.8       31.6     129.8       32.0     131.8
   32.5     133.7       32.9     135.7       33.3     137.6       33.8     139.6
   34.2     141.5       34.6     143.5       35.1     145.4       35.5     147.4
   35.9     149.3       36.4     151.3       36.8     153.2       37.2     155.2
   37.7     157.1       38.1     159.1       38.5     161.0       39.0     163.0
   39.4     164.9       39.8     166.9       40.2     168.9       40.7     170.8
   41.1     172.8       41.5     174.7       42.0     176.7       42.4     178.6
   42.8     180.6       43.3     182.5       43.7     184.5       44.1     186.4
   44.6     188.4       45.0     190.3       45.4     192.3       45.9     194.2
   46.3     196.2       46.7     198.1       47.2     200.1       47.6     202.0
   48.0     204.0       48.5     206.0       48.9     207.9       49.3     209.9
   49.8     211.8       50.2     213.8       50.6     215.7       51.1     217.7
   51.5     219.6       51.9     221.6       52.4     223.5       52.8     225.5
   53.2     227.4       53.7     229.4       54.1     231.3       54.5     233.3
   55.0     235.2       55.4     237.2       55.8     239.1       56.3     241.1
   56.7     243.0       57.1     245.0       57.6     247.0       58.0     248.9
   58.4     250.9       58.9     252.8       59.3     254.8       59.7     256.7
   60.2     258.7       60.6     260.6       61.0     262.6       61.5     264.5
   61.9     266.5       62.3     268.4       62.8     270.4       63.2     272.3
   63.6     274.3       64.1     276.2       64.5     278.2       64.9     280.1
   65.4     282.1       65.8     284.1       66.2     286.0       66.7     288.0
   67.1     289.9       67.5     291.9       68.0     293.8       68.4     295.8
   68.8     297.7       69.3     299.7       69.6     303.5
```

```
***********************
*                     *
*  TIME =     10. SEC *        NEXT TIME STEP= 0.03 SEC
*                     *
***********************


CAVITY DIMENSIONS, M :

       VERTICAL EROSION  :  -0.011
       MAXIMAL RADIUS    :   0.195
       ZERO LEVEL RADIUS :   0.191

TEMPERATURES, K :

       POOL -       LIQ. METAL: 1964.   OXIDE     :  1855.
       SURFACES -   MET./CONC.: 1953.   OX./CONC.:  1786.
                    MET./OX.  : 1959.   OX./SURF.:  1843.
       LIQUIDUS -   METAL     : 1787.   OXIDE     :  2070.
       SOLIDUS  -   METAL     : 1777.   OXIDE     :  1754.
       GAS LEAVING THE MELT   : 1832.
       WATER GAS REACTION     : 1200.

PROPERTIES:
                                          METAL             OXIDE
       DENSITY, KG/M3               :     7146.             2701.
       HEAT CONDUCTIVITY, W/(M.K):  46.935              6.758
       HEAT CAPACITY , J/(KG.K)  :      748.              1367.
       SURFACE TENSION, KG/S2     :   1.722               1.690
       VISCOSITY , KG/(S.M)       : 0.4157E-02         0.3505E+02

POOL-CONCRETE INTERFACE :
                                 BOTTOM     METAL/WALL  OXIDE/WALL  OXIDE/SURFACE
       EROSION SPEED, CM/S :  0.1068E+00  0.1255E-01  0.3516E-02
       EROSION SPEED, CM/H :   384.56        45.16       12.66
       ENERGY FLUX,    W/M2 :  0.4689E+07  0.5507E+06  0.1543E+06  0.3514E+06
       ENERGY FLUX,   KW/M2 :    4689.        551.        154.         351.

       HEAT TRANSFER FOR BOTTOM/CONCRETE MIXED MODE

INTEGRATED MASS BALANCE IN THE MELT, TONS :

       INITIAL MELT MASS:     0.120    ACTUAL MASS OF MELT  :     0.124
       ERODED (CONC.+FE):     0.004    MASS OF LEAVING GASES:     0.000

       SUM OF LEFT TERMS:     0.125    SUM OF RIGHT TERMS   :     0.125
       THE ERROR BETWEEN THE 2 SUMS IS  0.278E-16 TONS, I.E   0.223E-13 %

MASSES ,VOLUMES AND HEIGHTS :
                                                    METAL       OXIDE
       MASS ,TONS                                :    0.11        0.01
       VOLUME, (INCLUDING VOID FRACTION), M3 :    0.07        0.04
       VOLUME, (WITHOUT VOID FRACTION), M3   :    0.02        0.01
       VOID FRACTION , IN PERCENT              :   77.40       85.00
       DEPTH, M                                  :    0.60        0.29
       POOL HEIGHT FROM INITIAL BOTTOM, M      :         0.88
       VOLUME OF ERODED CONCRETE, M3           :         0.00
       MASS OF ERODED CONCRETE, TONS           :        0.004

WEIGHT FRACTION OF SPECIES IN EACH PHASE, % :

        METAL PHASE:(      110. KG)    OXIDE PHASE:(      15. KG)
               ZR :  0.0                          UO2 :  0.0
               CR :  4.5                         ZRO2 :  0.0
               FE : 90.5                          FEO :  0.0
               NI :  5.0                          CAO : 23.0
                                                 SIO2 : 22.5
                                                AL2O3 : 49.0
                                                CR2O3 :  5.5
```

```
HEAT FLUX BALANCE IN EACH PHASE,  WATT :
                                                  METAL           OXIDE
        POWER DUE TO DECAY HEAT                 :  0.6013E+06      0.0000E+00
        POWER ENTERING DUE TO GAS AND OXIDES    :  0.1060E+07      0.1509E+07
        POWER LEAVING DUE TO GAS AND OXIDES     : -0.1434E+07     -0.1168E+06
        POWER DUE TO OXIDATION REACTIONS        :  0.2034E+06      0.0000E+00
        POWER DUE TO CONCRETE DECOMPOSITION     : -0.8698E+06     -0.6007E+05
        CONDUCTION BETWEEN PHASES               : -0.2004E+07      0.2004E+07
        RADIATION OR EVAPORATED AT SURFACE      :  0.0000E+00     -0.1954E+07
        SENSIBLE HEAT                           : -0.2444E+07      0.1382E+07

INTEGRATED ENERGY BALANCE IN THE MELT, JOULE :

        INITIAL ENTHALPIE     0.2516E+09    INTEGRATED ENTHALPIE      0.2341E+09
        DECAY HEAT            0.3022E+07    CONCRETE DECOMPOSITION    0.8472E+07
        ENTERING(GAS,OX.)     0.1037E+08    LEAVING (GASES)           0.1127E+07
        OXIDAT. REACTIONS     0.1895E+07    RADIATION OR TO WATER     0.2325E+08

        SUM OF LEFT TERMS     0.2669E+09    SUM OF RIGHT TERMS        0.2669E+09
        THE ERROR BETWEEN THE 2 SUMS IS     0.7451E-08 J., I.E    0.2791E-14 %

GASES GOING IN THE CONTAINMENT, AT THE TEMPERATURE T= 1832. K.
AFTER THAT THE WATER-GAS REACTION OCCURED AT THE SURFACE :

                            CO2          CO           H2O          H2
        HEAT FLUX, WATT    0.1507E+04   0.1768E+05   0.1311E+05   0.8404E+05
        MASS FLUX, KG/S    0.7428E-03   0.8371E-02   0.1907E-02   0.2973E-02
        MOL. FLUX, MOL/S   0.1688E-01   0.2988E+00   0.1059E+00   0.1479E+01
        WEIGHT FRACTION    0.5308E-01   0.5982E+00   0.1363E+00   0.2125E+00
        MOLAR FRACTION     0.8880E-02   0.1572E+00   0.5572E-01   0.7782E+00
        TOTAL MASS, KG     0.8524E-02   0.7514E-01   0.2178E-01   0.2660E-01
        TOT.MOLS, MOL      0.1937E+00   0.2683E+01   0.1210E+01   0.1323E+02

THE CAVITY SHAPE HAS BEEN CALCULATED USING  55 POINTS, COORDONATES IN CM :
  R=RADIUS  ;  Z=DEPTHNESS   ;  Z-REFERENCE: INITIAL BOTTOM OF THE CAVITY

      R        Z           R        Z           R        Z           R        Z
     0.0     -1.1         2.0     -1.1         4.0     -1.1         6.0     -1.1
     8.0     -1.1        10.0     -1.1        12.0     -1.1        14.0     -1.1
    16.0     -0.6        17.6      0.5        18.6      2.2        19.0      4.2
    19.1      6.2        19.1      8.2        19.1     10.2        19.1     12.2
    19.1     14.2        19.1     16.2        19.1     18.2        19.1     20.2
    19.1     22.2        19.1     24.2        19.1     26.2        19.1     28.2
    19.1     30.2        19.1     32.2        19.1     34.2        19.1     36.2
    19.1     38.2        19.1     40.2        19.1     42.2        19.1     44.2
    19.1     46.2        19.1     48.2        19.1     50.2        19.0     52.2
    19.0     54.2        19.0     56.2        19.0     58.8        19.0     60.2
    19.0     62.2        19.0     64.2        19.0     66.2        19.0     68.2
    19.0     70.2        19.2     72.2        19.4     74.2        19.8     76.1
    20.2     78.1        20.6     80.1        21.0     82.0        21.4     84.0
    21.9     85.9        22.3     88.0        22.7     89.8
```

```
************************
*                      *
*  TIME =   2001. SEC  *         NEXT TIME STEP= 1.00 SEC
*                      *
************************


CAVITY DIMENSIONS, M :

       VERTICAL EROSION  :  -0.437
       MAXIMAL RADIUS    :   0.243
       ZERO LEVEL RADIUS :   0.236

TEMPERATURES, K :

       POOL -      METAL      : 1676.   OXIDE     :  1620.
       SURFACES -  MET./CONC.: 1573.   OX./CONC.:  1605.
                   MET./OX.   : 1664.   OX./SURF.:  1605.
       LIQUIDUS -  METAL      : 1787.   OXIDE     :  1894.
       SOLIDUS  -  METAL      : 1777.   OXIDE     :  1533.
       GAS LEAVING THE MELT  : 1596.
       WATER GAS REACTION    : 1200.

PROPERTIES:
                                      METAL             OXIDE
       DENSITY, KG/M3              :    7280.             2650.
       HEAT CONDUCTIVITY, W/(M.K):  46.430             4.524
       HEAT CAPACITY , J/(KG.K)   :     745.              1334.
       SURFACE TENSION, KG/S2     :   1.812              4.725
       VISCOSITY , KG/(S.M)       : 0.1000E+04        0.5701E+03

  POOL-CONCRETE INTERFACE :
                                BOTTOM     METAL/WALL  OXIDE/WALL  OXIDE/SURFACE
       EROSION SPEED, CM/S :  0.2501E-02      --       0.4760E-03
       EROSION SPEED, CM/H :     9.00         --          1.71
       ENERGY FLUX,    W/M2 :  0.1098E+06  0.0000E+00  0.2090E+05  0.1624E+05
       ENERGY FLUX,   KW/M2 :     110.          0.         21.          16.

       HEAT TRANSFER FOR BOTTOM/CONCRETE FILM MODE

INTEGRATED MASS BALANCE IN THE MELT, TONS :

       INITIAL MELT MASS:    0.480    ACTUAL MASS OF MELT  :     0.819
       ERODED (CONC.+FE):    0.355    MASS OF LEAVING GASES:     0.016

       SUM OF LEFT TERMS:    0.835    SUM OF RIGHT TERMS   :     0.835
       THE ERROR BETWEEN THE 2 SUMS IS  0.361E-15 TONS, I.E   0.432E-13 %

MASSES ,VOLUMES AND HEIGHTS :
                                                    METAL       OXIDE
       MASS ,TONS                            :      0.31        0.51
       VOLUME, (INCLUDING VOID FRACTION), M3 :      0.04        0.20
       VOLUME, (WITHOUT VOID FRACTION), M3   :      0.04        0.19
       VOID FRACTION , IN PERCENT            :      0.00        2.15
       DEPTH , M                             :      0.27        1.09
       POOL HEIGHT FROM INITIAL BOTTOM, M    :           0.92
       VOLUME OF ERODED CONCRETE, M3         :           0.16
       MASS OF ERODED CONCRETE, TONS         :          0.355

WEIGHT FRACTION OF SPECIES IN EACH PHASE, % :

        METAL PHASE:(     306. KG)    OXIDE PHASE:(    513. KG)
               ZR :  0.0                        U02 :  0.0
               CR :  0.0                       ZR02 :  0.0
               FE : 94.3                        FEO :  6.7
               NI :  5.7                        CAO : 14.0
                                               SI02 : 52.9
                                              AL203 : 21.4
                                              CR203 :  5.0
```

```
CRUST THICKNESS IN EACH PHASE, CM :

        IN THE METAL PHASE:                  IN THE OXIDE PHASE:
        COMPLETELY SOLID                  OXIDE/METAL:    0.00
        HEIGHT     :   27.16              OXIDE/CONCR:    0.00
                                        OXIDE/SURFACE:    0.00

HEAT FLUX BALANCE IN EACH PHASE,  WATT :
                                                          METAL           OXIDE
        POWER DUE TO DECAY HEAT                    :   0.0000E+00      0.0000E+00
        POWER ENTERING DUE TO GAS AND OXIDES :   0.2650E+05      0.7465E+05
        POWER LEAVING DUE TO GAS AND OXIDES  :  -0.3031E+05     -0.9453E+04
        POWER DUE TO OXIDATION REACTIONS           :  -0.3767E+02      0.0000E+00
        POWER DUE TO CONCRETE DECOMPOSITION  :  -0.1966E+05     -0.3372E+05
        CONDUCTION BETWEEN PHASES                  :   0.2590E+04     -0.2590E+04
        RADIATION OR EVAPORATED AT SURFACE         :   0.0000E+00     -0.3589E+04
        SENSIBLE HEAT                              :  -0.2091E+05      0.2530E+05

INTEGRATED ENERGY BALANCE IN THE MELT, JOULE :

        INITIAL ENTHALPIE     0.1172E+10    INTEGRATED ENTHALPIE     0.1552E+10
        DECAY HEAT            0.6732E+09    CONCRETE DECOMPOSITION   0.6918E+09
        ENTERING(GAS,OX.)     0.8738E+09    LEAVING (GASES)          0.1018E+09
        OXIDAT. REACTIONS     0.5522E+08    RADIATION OR TO WATER    0.4292E+09

        SUM OF LEFT TERMS     0.2774E+10    SUM OF RIGHT TERMS       0.2774E+10
        THE ERROR BETWEEN THE 2 SUMS IS     0.9656E-04 J., I.E   0.3480E-11 %

GASES GOING IN THE CONTAINMENT, AT THE TEMPERATURE T= 1596. K.
AFTER THAT THE WATER-GAS REACTION OCCURED AT THE SURFACE :

                              CO2          CO           H2O          H2
        HEAT FLUX, WATT    0.7953E+03   0.3805E+03   0.6702E+04   0.1595E+04
        MASS FLUX, KG/S    0.4664E-03   0.2107E-03   0.1050E-02   0.6565E-04
        MOL. FLUX, MOL/S   0.1060E-01   0.7524E-02   0.5832E-01   0.3266E-01
        WEIGHT FRACTION    0.2601E+00   0.1175E+00   0.5858E+00   0.3661E-01
        MOLAR FRACTION     0.9713E-01   0.6896E-01   0.5345E+00   0.2994E+00
        TOTAL MASS, KG     0.2817E+01   0.4786E+01   0.6651E+01   0.1628E+01
        TOT.MOLS, MOL      0.6400E+02   0.1709E+03   0.3693E+03   0.8100E+03

THE CAVITY SHAPE HAS BEEN CALCULATED USING  81 POINTS, COORDONATES IN CM :
  R=RADIUS  ;  Z=DEPTHNESS   ;  Z-REFERENCE: INITIAL BOTTOM OF THE CAVITY

     R        Z          R        Z          R        Z          R        Z
    0.0     -43.7       2.0     -43.7       4.0     -43.7       6.0     -43.7
    8.0     -43.7      10.0     -43.7      12.0     -43.7      14.0     -43.6
   16.0     -43.3      17.8     -42.5      19.4     -41.3      20.7     -39.8
   21.7     -38.1      22.5     -36.2      23.0     -34.3      23.4     -32.3
   23.6     -30.3      23.7     -28.3      23.8     -26.3      23.8     -24.3
   23.9     -22.3      23.8     -20.3      23.8     -18.3      23.7     -16.6
   23.6     -14.3      24.3     -12.5      24.2     -10.5      24.1      -8.5
   24.0      -6.5      23.9      -4.5      23.8      -2.5      23.7      -0.5
   23.7       1.5      23.7       3.5      23.6       5.5      23.6       7.5
   23.5       9.5      23.5      11.5      23.4      13.5      23.4      15.5
   23.3      17.5      23.3      19.5      23.3      21.5      23.4      23.5
   23.4      25.5      23.5      27.5      23.5      29.5      23.6      31.5
   23.6      33.5      23.7      35.5      23.7      37.5      23.7      39.5
   23.7      41.5      23.7      43.5      23.7      45.5      23.7      47.5
   23.7      49.5      23.6      51.5      23.6      53.5      23.6      55.5
   23.6      57.5      23.6      59.5      23.6      61.5      23.6      63.5
   23.7      65.5      23.8      67.5      23.9      69.5      24.0      71.5
   24.1      73.5      24.3      75.5      24.5      77.5      24.8      79.5
   25.0      81.4      25.3      83.4      25.6      85.4      25.9      87.4
   26.3      89.3      26.5      92.1      26.6      93.3      26.7      95.3
   26.7      97.3
```

```
 R=RADIUS   ;  Z=DEPTHNESS    ;  Z-REFERENCE: INITIAL BOTTOM OF THE CAVITY

     R          Z            R          Z            R          Z            R          Z
    0.0      -43.7          2.0      -43.7          4.0      -43.7          6.0      -43.7
    8.0      -43.7         10.0      -43.7         12.0      -43.7         14.0      -43.6
   16.0      -43.3         17.8      -42.5         19.4      -41.3         20.7      -39.8
   21.7      -38.1         22.5      -36.2         23.0      -34.3         23.4      -32.3
   23.6      -30.3         23.7      -28.3         23.8      -26.3         23.8      -24.3
   23.9      -22.3         23.8      -20.3         23.8      -18.3         23.7      -16.6
   23.6      -14.3         24.3      -12.5         24.2      -10.5         24.1       -8.5
   24.0       -6.5         23.9       -4.5         23.8       -2.5         23.7       -0.5
   23.7        1.5         23.7        3.5         23.6        5.5         23.6        7.5
   23.5        9.5         23.5       11.5         23.4       13.5         23.4       15.5
   23.3       17.5         23.3       19.5         23.3       21.5         23.4       23.5
   23.4       25.5         23.5       27.5         23.5       29.5         23.6       31.5
   23.6       33.5         23.7       35.5         23.7       37.5         23.7       39.5
   23.7       41.5         23.7       43.5         23.7       45.5         23.7       47.5
   23.7       49.5         23.6       51.5         23.6       53.5         23.6       55.5
   23.6       57.5         23.6       59.5         23.6       61.5         23.6       63.5
   23.7       65.5         23.8       67.5         23.9       69.5         24.0       71.5
   24.1       73.5         24.3       75.5         24.5       77.5         24.8       79.5
   25.0       81.4         25.3       83.4         25.6       85.4         25.9       87.4
   26.3       89.3         26.5       92.1         26.6       93.3         26.7       95.3
   26.7       97.3         26.8       99.3         27.7      105.4         28.1      107.3
   28.9      111.2         29.3      113.2         30.0      117.2         30.8      121.0
   31.2      123.0         31.7      125.0         32.1      127.0         32.5      128.9
   33.0      130.9         33.4      132.9         33.8      134.9         34.2      136.9
   34.7      138.8         35.1      140.8         35.5      142.9         36.0      145.1
   36.5      147.7         37.1      150.1         37.6      152.6         38.1      155.0
   38.6      157.4         39.1      159.8         39.7      162.3         40.1      164.3
   40.5      166.3         40.9      168.2         41.3      170.2         41.7      172.2
   42.1      174.1         42.5      176.1         42.9      178.0         43.3      180.0
   43.7      182.0         44.0      183.9         44.4      185.9         44.8      187.8
   45.2      189.8         45.6      191.8         46.0      193.7         46.4      195.7
   46.8      197.7         47.2      199.6         47.6      201.6         48.0      203.5
   48.4      205.5         48.8      207.4         49.2      209.4         49.7      211.3
   50.1      213.3         51.1      217.6         51.5      219.6         51.9      221.6
   52.4      223.5         52.8      225.5         53.2      227.4         53.7      229.4
   54.1      231.3         54.5      233.3         55.0      235.2         55.4      237.2
   55.8      239.1         56.3      241.1         56.7      243.0         57.1      245.0
   57.6      247.0         58.0      248.9         58.4      250.9         58.9      252.8
   59.3      254.8         59.7      256.7         60.2      258.7         60.6      260.6
   61.0      262.6         61.5      264.5         61.9      266.5         62.3      268.4
   62.8      270.4         63.2      272.3         63.6      274.3         64.1      276.2
   64.5      278.2         64.9      280.1         65.4      282.1         65.8      284.1
   66.2      286.0         66.7      288.0         67.1      289.9         67.5      291.9
   68.0      293.8         68.4      295.8         68.8      297.7         69.3      299.7
   69.6      303.5
PREDEFINED STOP BECAUSE TIME=  0.2001E+04 SEC. REACHES THE TIME LIMIT TF=  0.2000E+04
GIVEN IN THE INPUT DATA.
```

```
   BETA TEST V1.8 ; WECHSL POST TEST CALCULATION.

ZEIT R_OBEN  T_OXID     CO          CO2             H2    H2O OHNE SU.  SIO2
 SEC    M       K       KG           KG             KG          KG       KG

   0.  0.190  2149.  0.2975E-03  0.7052E-04  0.1036E-03  0.1774E-03        0.
  10.  0.223  1855.  0.7514E-01  0.8524E-02  0.2660E-01  0.2178E-01        3.
  20.  0.269  1817.  0.1630E+00  0.1594E-01  0.5783E-01  0.4083E-01        7.
  30.  0.299  1813.  0.2674E+00  0.2275E-01  0.9505E-01  0.5839E-01       12.
  40.  0.389  1988.  0.3919E+00  0.3997E-01  0.1390E+00  0.1020E+00       17.
  50.  0.451  1994.  0.5335E+00  0.1019E+00  0.1872E+00  0.2543E+00       25.
  60.  0.459  1948.  0.6850E+00  0.1656E+00  0.2389E+00  0.4112E+00       33.
  70.  0.445  1915.  0.8331E+00  0.2233E+00  0.2895E+00  0.5540E+00       40.
  80.  0.424  1893.  0.9727E+00  0.2708E+00  0.3375E+00  0.6720E+00       47.
  90.  0.419  1874.  0.1103E+01  0.3155E+00  0.3824E+00  0.7831E+00       54.
 100.  0.416  1858.  0.1226E+01  0.3577E+00  0.4244E+00  0.8881E+00       60.
 110.  0.415  1844.  0.1342E+01  0.3971E+00  0.4647E+00  0.9860E+00       66.
 120.  0.415  1831.  0.1455E+01  0.4339E+00  0.5034E+00  0.1078E+01       71.
 130.  0.415  1820.  0.1563E+01  0.4686E+00  0.5408E+00  0.1164E+01       77.
 140.  0.415  1810.  0.1669E+01  0.5016E+00  0.5773E+00  0.1246E+01       82.
 150.  0.416  1801.  0.1773E+01  0.5332E+00  0.6131E+00  0.1325E+01       87.
 175.  0.430  1781.  0.2024E+01  0.6088E+00  0.6998E+00  0.1514E+01       99.
 200.  0.453  1764.  0.2268E+01  0.6847E+00  0.7840E+00  0.1703E+01      112.
 225.  0.468  1749.  0.2505E+01  0.7611E+00  0.8659E+00  0.1894E+01      123.
 250.  0.473  1734.  0.2730E+01  0.8344E+00  0.9433E+00  0.2076E+01      135.
 275.  0.467  1722.  0.2940E+01  0.9015E+00  0.1015E+01  0.2243E+01      145.
 300.  0.458  1712.  0.3135E+01  0.9620E+00  0.1083E+01  0.2394E+01      155.
 325.  0.451  1704.  0.3317E+01  0.1017E+01  0.1146E+01  0.2531E+01      164.
 350.  0.453  1700.  0.3462E+01  0.1067E+01  0.1196E+01  0.2656E+01      171.
 375.  0.378  1698.  0.3590E+01  0.1118E+01  0.1239E+01  0.2781E+01      177.
 400.  0.373  1696.  0.3711E+01  0.1167E+01  0.1281E+01  0.2903E+01      184.
 425.  0.360  1695.  0.3824E+01  0.1215E+01  0.1319E+01  0.3021E+01      190.
 450.  0.348  1695.  0.3929E+01  0.1261E+01  0.1355E+01  0.3134E+01      195.
 475.  0.339  1694.  0.4026E+01  0.1306E+01  0.1388E+01  0.3245E+01      200.
 500.  0.265  1693.  0.4085E+01  0.1346E+01  0.1408E+01  0.3340E+01      204.
 525.  0.263  1691.  0.4117E+01  0.1381E+01  0.1418E+01  0.3423E+01      206.
 550.  0.263  1689.  0.4146E+01  0.1417E+01  0.1427E+01  0.3506E+01      208.
 575.  0.262  1687.  0.4173E+01  0.1451E+01  0.1436E+01  0.3587E+01      210.
 600.  0.262  1685.  0.4199E+01  0.1486E+01  0.1444E+01  0.3667E+01      212.
 625.  0.262  1684.  0.4222E+01  0.1519E+01  0.1452E+01  0.3744E+01      214.
 650.  0.261  1682.  0.4245E+01  0.1553E+01  0.1459E+01  0.3822E+01      216.
 675.  0.261  1680.  0.4266E+01  0.1586E+01  0.1466E+01  0.3898E+01      218.
 700.  0.261  1678.  0.4287E+01  0.1619E+01  0.1473E+01  0.3974E+01      219.
 725.  0.261  1676.  0.4308E+01  0.1652E+01  0.1479E+01  0.4048E+01      221.
 750.  0.261  1675.  0.4327E+01  0.1683E+01  0.1485E+01  0.4121E+01      223.
 775.  0.261  1673.  0.4347E+01  0.1716E+01  0.1491E+01  0.4195E+01      224.
 800.  0.261  1671.  0.4366E+01  0.1747E+01  0.1497E+01  0.4266E+01      226.
 825.  0.261  1669.  0.4384E+01  0.1778E+01  0.1503E+01  0.4336E+01      228.
 850.  0.261  1667.  0.4401E+01  0.1808E+01  0.1509E+01  0.4405E+01      229.
 875.  0.261  1665.  0.4418E+01  0.1837E+01  0.1514E+01  0.4472E+01      231.
 900.  0.261  1663.  0.4436E+01  0.1866E+01  0.1519E+01  0.4539E+01      232.
 925.  0.261  1662.  0.4452E+01  0.1895E+01  0.1525E+01  0.4604E+01      233.
 950.  0.261  1660.  0.4468E+01  0.1923E+01  0.1530E+01  0.4668E+01      235.
 975.  0.261  1658.  0.4484E+01  0.1951E+01  0.1535E+01  0.4732E+01      236.
1000.  0.261  1657.  0.4500E+01  0.1978E+01  0.1540E+01  0.4794E+01      238.
1050.  0.261  1653.  0.4530E+01  0.2031E+01  0.1549E+01  0.4916E+01      240.
1100.  0.262  1651.  0.4560E+01  0.2084E+01  0.1559E+01  0.5035E+01      243.
1142.  0.260  1648.  0.4584E+01  0.2126E+01  0.1566E+01  0.5133E+01      245.
1150.  0.264  1648.  0.4586E+01  0.2135E+01  0.1567E+01  0.5151E+01      245.
1200.  0.264  1646.  0.4599E+01  0.2185E+01  0.1571E+01  0.5260E+01      247.
1250.  0.264  1644.  0.4611E+01  0.2234E+01  0.1574E+01  0.5367E+01      249.
1300.  0.265  1642.  0.4623E+01  0.2281E+01  0.1578E+01  0.5471E+01      251.
1350.  0.265  1640.  0.4635E+01  0.2327E+01  0.1582E+01  0.5572E+01      252.
1400.  0.265  1638.  0.4647E+01  0.2372E+01  0.1585E+01  0.5671E+01      254.
1450.  0.265  1636.  0.4659E+01  0.2416E+01  0.1589E+01  0.5768E+01      256.
1500.  0.265  1635.  0.4670E+01  0.2459E+01  0.1592E+01  0.5861E+01      257.
1550.  0.265  1633.  0.4681E+01  0.2501E+01  0.1596E+01  0.5953E+01      259.
1600.  0.265  1632.  0.4691E+01  0.2542E+01  0.1599E+01  0.6043E+01      260.
1650.  0.265  1630.  0.4702E+01  0.2582E+01  0.1602E+01  0.6130E+01      262.
1700.  0.266  1629.  0.4712E+01  0.2621E+01  0.1605E+01  0.6216E+01      263.
1750.  0.266  1627.  0.4723E+01  0.2659E+01  0.1608E+01  0.6300E+01      265.
1800.  0.266  1626.  0.4733E+01  0.2697E+01  0.1611E+01  0.6381E+01      266.
1850.  0.266  1625.  0.4742E+01  0.2733E+01  0.1614E+01  0.6462E+01      267.
1901.  0.266  1623.  0.4759E+01  0.2767E+01  0.1620E+01  0.6537E+01      269.
1951.  0.266  1622.  0.4775E+01  0.2793E+01  0.1624E+01  0.6596E+01      270.
2001.  0.265  1620.  0.4786E+01  0.2817E+01  0.1628E+01  0.6651E+01      271.
```

```
   BETA TEST V1.8 ; WECHSL POST TEST CALCULATION.

ZEIT |         TEMPERATUR, K                  |                   ENTHALPIESTROM, WATT
 SEC | MET_L  MET_S  OXID  O_SURF   GASE |       CO2           CO            H2O           H2        SUMME GASE

   0.  2169.   ---   2149.  2167.  2030.  0.3255E+04  0.1414E+05  0.2587E+05  0.6557E+05  0.1088E+06
  10.  1964.   ---   1855.  1843.  1832.  0.1507E+04  0.1768E+05  0.1311E+05  0.8404E+05  0.1163E+06
  20.  1922.   ---   1817.  1806.  1800.  0.1368E+04  0.1959E+05  0.1209E+05  0.9339E+05  0.1264E+06
  30.  1933.   ---   1813.  1805.  1798.  0.1356E+04  0.2415E+05  0.1201E+05  0.1154E+06  0.1529E+06
  40.  1945.   ---   1988.  1974.  1900.  0.8472E+04  0.2894E+05  0.6988E+05  0.1335E+06  0.2408E+06
  50.  1978.   ---   1994.  1979.  1882.  0.1417E+05  0.3244E+05  0.1159E+06  0.1474E+06  0.3098E+06
  60.  1984.   ---   1948.  1933.  1854.  0.1261E+05  0.3236E+05  0.1046E+06  0.1478E+06  0.2974E+06
  70.  1969.   ---   1915.  1903.  1836.  0.1069E+05  0.3065E+05  0.8972E+05  0.1407E+06  0.2718E+06
  80.  1946.   ---   1893.  1883.  1823.  0.9209E+04  0.2825E+05  0.7789E+05  0.1300E+06  0.2454E+06
  90.  1925.   ---   1874.  1865.  1808.  0.8730E+04  0.2621E+05  0.7420E+05  0.1206E+06  0.2297E+06
 100.  1910.   ---   1858.  1849.  1796.  0.8036E+04  0.2460E+05  0.6866E+05  0.1133E+06  0.2146E+06
 110.  1898.   ---   1844.  1835.  1786.  0.7413E+04  0.2345E+05  0.6367E+05  0.1081E+06  0.2027E+06
 120.  1888.   ---   1831.  1822.  1776.  0.7014E+04  0.2253E+05  0.6051E+05  0.1040E+06  0.1940E+06
 130.  1880.   ---   1820.  1811.  1768.  0.6555E+04  0.2177E+05  0.5679E+05  0.1006E+06  0.1857E+06
 140.  1873.   ---   1810.  1801.  1761.  0.6270E+04  0.2115E+05  0.5452E+05  0.9780E+05  0.1797E+06
 150.  1868.   ---   1801.  1792.  1754.  0.5891E+04  0.2058E+05  0.5142E+05  0.9530E+05  0.1732E+06
 175.  1857.   ---   1781.  1771.  1738.  0.5691E+04  0.1964E+05  0.5000E+05  0.9097E+05  0.1663E+06
 200.  1850.   ---   1764.  1753.  1722.  0.5700E+04  0.1900E+05  0.5032E+05  0.8789E+05  0.1629E+06
 225.  1840.   ---   1749.  1737.  1709.  0.5571E+04  0.1811E+05  0.4940E+05  0.8373E+05  0.1568E+06
 250.  1825.   ---   1734.  1722.  1698.  0.5199E+04  0.1681E+05  0.4631E+05  0.7773E+05  0.1461E+06
 275.  1811.   ---   1722.  1711.  1689.  0.4696E+04  0.1555E+05  0.4203E+05  0.7200E+05  0.1343E+06
 300.  1798.   ---   1712.  1701.  1682.  0.4158E+04  0.1437E+05  0.3738E+05  0.6665E+05  0.1226E+06
 325.  1789.  1780.  1704.  1693.  1676.  0.3815E+04  0.1368E+05  0.3443E+05  0.6354E+05  0.1155E+06
 350.  1790.  1778.  1700.  1689.  1673.  0.3761E+04  0.1379E+05  0.3401E+05  0.6410E+05  0.1157E+06
 375.  1791.  1778.  1698.  1687.  1665.  0.3541E+04  0.9053E+04  0.3170E+05  0.4151E+05  0.8581E+05
 400.  1790.  1777.  1696.  1685.  1663.  0.3511E+04  0.8856E+04  0.3144E+05  0.4058E+05  0.8439E+05
 425.  1790.  1777.  1695.  1684.  1662.  0.3362E+04  0.8238E+04  0.3009E+05  0.3771E+05  0.7939E+05
 450.  1790.  1776.  1695.  1683.  1661.  0.3240E+04  0.7624E+04  0.2896E+05  0.3484E+05  0.7466E+05
 475.  1790.  1775.  1694.  1683.  1659.  0.3197E+04  0.7006E+04  0.2850E+05  0.3191E+05  0.7062E+05
 500.  1787.  1769.  1693.  1675.  1644.  0.2511E+04  0.2546E+04  0.2164E+05  0.1114E+05  0.3784E+05
 525.  1787.  1759.  1691.  1672.  1641.  0.2495E+04  0.2289E+04  0.2141E+05  0.9957E+04  0.3615E+05
 550.  1787.  1752.  1689.  1670.  1638.  0.2473E+04  0.2088E+04  0.2114E+05  0.9039E+04  0.3474E+05
 575.  1787.  1746.  1687.  1667.  1636.  0.2420E+04  0.1934E+04  0.2064E+05  0.8349E+04  0.3334E+05
 600.  1787.  1741.  1685.  1665.  1634.  0.2396E+04  0.1812E+04  0.2038E+05  0.7793E+04  0.3238E+05
 625.  1787.  1737.  1684.  1663.  1632.  0.2370E+04  0.1712E+04  0.2012E+05  0.7346E+04  0.3155E+05
 650.  1787.  1734.  1682.  1661.  1631.  0.2343E+04  0.1626E+04  0.1986E+05  0.6959E+04  0.3079E+05
 675.  1787.  1712.  1680.  1659.  1630.  0.2314E+04  0.1577E+04  0.1960E+05  0.6741E+04  0.3023E+05
 700.  1787.  1714.  1678.  1657.  1628.  0.2285E+04  0.1533E+04  0.1935E+05  0.6548E+04  0.2972E+05
 725.  1787.  1714.  1676.  1656.  1627.  0.2257E+04  0.1486E+04  0.1910E+05  0.6339E+04  0.2918E+05
 750.  1786.  1714.  1675.  1654.  1626.  0.2229E+04  0.1441E+04  0.1886E+05  0.6141E+04  0.2867E+05
 775.  1786.  1714.  1673.  1652.  1625.  0.2195E+04  0.1397E+04  0.1856E+05  0.5950E+04  0.2811E+05
 800.  1786.  1714.  1671.  1650.  1624.  0.2159E+04  0.1356E+04  0.1825E+05  0.5773E+04  0.2754E+05
```

```
 BETA TEST V1.8 ; WECHSL POST TEST CALCULATION.

ZEIT |          TEMPERATUR, K               |                     ENTHALPIESTROM, WATT
 SEC | MET_L   MET_S  OXID  O_SURF   GASE |      CO2           CO             H2O            H2        SUMME GASE


 825.   1786.   1713.   1669.   1648.   1622.   0.2124E+04   0.1319E+04   0.1795E+05   0.5608E+04   0.2700E+05
 850.   1786.   1701.   1667.   1646.   1621.   0.2074E+04   0.1284E+04   0.1753E+05   0.5459E+04   0.2635E+05
 875.   1786.   1702.   1665.   1645.   1620.   0.2041E+04   0.1254E+04   0.1725E+05   0.5329E+04   0.2588E+05
 900.   1786.   1702.   1663.   1643.   1619.   0.2007E+04   0.1226E+04   0.1697E+05   0.5210E+04   0.2542E+05
 925.   1786.   1702.   1662.   1641.   1618.   0.1975E+04   0.1201E+04   0.1670E+05   0.5100E+04   0.2498E+05
 950.   1786.   1702.   1660.   1640.   1617.   0.1944E+04   0.1176E+04   0.1644E+05   0.4997E+04   0.2456E+05
 975.   1786.   1703.   1658.   1638.   1617.   0.1913E+04   0.1153E+04   0.1618E+05   0.4897E+04   0.2414E+05
1000.   1786.   1703.   1657.   1637.   1616.   0.1882E+04   0.1131E+04   0.1593E+05   0.4801E+04   0.2374E+05
1050.   1786.   1703.   1653.   1634.   1614.   0.1823E+04   0.1089E+04   0.1543E+05   0.4621E+04   0.2297E+05
1100.   1786.   1696.   1651.   1633.   1613.   0.1783E+04   0.1073E+04   0.1511E+05   0.4555E+04   0.2252E+05
1142.   1785.   1696.   1648.   1634.   1606.   0.1659E+04   0.4829E+03   0.1356E+05   0.1972E+04   0.1767E+05
1150.   1785.   1696.   1648.   1634.   1605.   0.1749E+04   0.4765E+03   0.1425E+05   0.1940E+04   0.1842E+05
1200.   1785.   1696.   1646.   1632.   1604.   0.1700E+04   0.4630E+03   0.1386E+05   0.1885E+04   0.1790E+05
1250.   1785.   1696.   1644.   1630.   1603.   0.1653E+04   0.4510E+03   0.1348E+05   0.1836E+04   0.1742E+05
1300.   1785.   1697.   1642.   1628.   1603.   0.1609E+04   0.4399E+03   0.1313E+05   0.1791E+04   0.1697E+05
1350.   1785.   1697.   1640.   1626.   1602.   0.1567E+04   0.4294E+03   0.1279E+05   0.1749E+04   0.1654E+05
1400.   1785.   1697.   1638.   1624.   1601.   0.1526E+04   0.4195E+03   0.1247E+05   0.1709E+04   0.1612E+05
1450.   1785.   1693.   1636.   1623.   1600.   0.1488E+04   0.4101E+03   0.1216E+05   0.1671E+04   0.1573E+05
1500.   1785.   1693.   1635.   1621.   1600.   0.1451E+04   0.4013E+03   0.1186E+05   0.1635E+04   0.1535E+05
1550.   1785.   1693.   1633.   1620.   1599.   0.1416E+04   0.3933E+03   0.1158E+05   0.1603E+04   0.1499E+05
1600.   1785.   1693.   1632.   1619.   1598.   0.1382E+04   0.3858E+03   0.1131E+05   0.1572E+04   0.1465E+05
1650.   1784.   1693.   1630.   1617.   1598.   0.1350E+04   0.3786E+03   0.1106E+05   0.1544E+04   0.1433E+05
1700.   1784.   1693.   1629.   1616.   1597.   0.1319E+04   0.3717E+03   0.1081E+05   0.1516E+04   0.1401E+05
1750.   1784.   1693.   1627.   1615.   1597.   0.1290E+04   0.3649E+03   0.1057E+05   0.1488E+04   0.1371E+05
1800.   1783.   1693.   1626.   1614.   1596.   0.1261E+04   0.3583E+03   0.1034E+05   0.1462E+04   0.1342E+05
1850.   1784.   1691.   1625.   1613.   1595.   0.1234E+04   0.3518E+03   0.1012E+05   0.1435E+04   0.1314E+05
1901.    ---    1686.   1623.   1611.   1600.   0.9483E+03   0.6755E+03   0.8163E+04   0.2897E+04   0.1268E+05
1951.    ---    1681.   1622.   1608.   1597.   0.8473E+03   0.4816E+03   0.7205E+04   0.2039E+04   0.1057E+05
2001.    ---    1676.   1620.   1605.   1596.   0.7953E+03   0.3805E+03   0.6702E+04   0.1595E+04   0.9473E+04
```

```
  BETA TEST V1.8 ; WECHSL POST TEST CALCULATION.

ZEIT      Q SURF        CO2          CO      H2O MIT SU.       H2     SUMPF       CO2          CO           H2O          H2        SUMPF
 SEC       WATT         KG/S         KG/S        KG/S         KG/S    KG/S        KG           KG           KG           KG          KG

   0.  -0.6500E+07  0.1410E-02  0.5951E-02  0.3549E-02  0.2071E-02 0.000  0.7052E-04  0.2975E-03  0.1774E-03  0.1036E-03        0.
  10.  -0.1954E+07  0.7428E-03  0.8371E-02  0.1907E-02  0.2973E-02 0.000  0.8524E-02  0.7514E-01  0.2178E-01  0.2660E-01        0.
  20.  -0.1923E+07  0.6898E-03  0.9463E-02  0.1776E-02  0.3369E-02 0.000  0.1594E-01  0.1630E+00  0.4083E-01  0.5783E-01        0.
  30.  -0.1741E+07  0.6843E-03  0.1168E-01  0.1765E-02  0.4168E-02 0.000  0.2275E-01  0.2674E+00  0.5839E-01  0.9505E-01        0.
  40.  -0.1809E+07  0.3988E-02  0.1314E-01  0.9957E-02  0.4537E-02 0.000  0.3997E-01  0.3919E+00  0.1020E+00  0.1390E+00        0.
  50.  -0.1730E+07  0.6755E-02  0.1489E-01  0.1660E-01  0.5062E-02 0.000  0.1019E+00  0.5335E+00  0.2543E+00  0.1872E+00        0.
  60.  -0.1571E+07  0.6122E-02  0.1511E-01  0.1512E-01  0.5162E-02 0.000  0.1656E+00  0.6850E+00  0.4112E+00  0.2389E+00        0.
  70.  -0.1438E+07  0.5256E-02  0.1448E-01  0.1303E-01  0.4967E-02 0.000  0.2233E+00  0.8331E+00  0.5540E+00  0.2895E+00        0.
  80.  -0.1338E+07  0.4569E-02  0.1345E-01  0.1136E-01  0.4627E-02 0.000  0.2708E+00  0.9727E+00  0.6720E+00  0.3375E+00        0.
  90.  -0.1265E+07  0.4377E-02  0.1260E-01  0.1087E-01  0.4329E-02 0.000  0.3155E+00  0.1103E+01  0.7831E+00  0.3824E+00        0.
 100.  -0.1204E+07  0.4062E-02  0.1192E-01  0.1010E-01  0.4097E-02 0.000  0.3577E+00  0.1226E+01  0.8881E+00  0.4244E+00        0.
 110.  -0.1157E+07  0.3774E-02  0.1143E-01  0.9393E-02  0.3935E-02 0.000  0.3971E+00  0.1342E+01  0.9860E+00  0.4647E+00        0.
 120.  -0.1118E+07  0.3595E-02  0.1105E-01  0.8953E-02  0.3806E-02 0.000  0.4339E+00  0.1455E+01  0.1078E+01  0.5034E+00        0.
 130.  -0.1091E+07  0.3378E-02  0.1073E-01  0.8423E-02  0.3701E-02 0.000  0.4686E+00  0.1563E+01  0.1164E+01  0.5408E+00        0.
 140.  -0.1068E+07  0.3250E-02  0.1048E-01  0.8106E-02  0.3615E-02 0.000  0.5016E+00  0.1669E+01  0.1246E+01  0.5773E+00        0.
 150.  -0.1054E+07  0.3067E-02  0.1024E-01  0.7660E-02  0.3537E-02 0.000  0.5332E+00  0.1773E+01  0.1325E+01  0.6131E+00        0.
 175.  -0.1037E+07  0.2999E-02  0.9880E-02  0.7487E-02  0.3412E-02 0.000  0.6088E+00  0.2024E+01  0.1514E+01  0.6998E+00        0.
 200.  -0.1035E+07  0.3037E-02  0.9649E-02  0.7571E-02  0.3328E-02 0.000  0.6847E+00  0.2268E+01  0.1703E+01  0.7840E+00        0.
 225.  -0.1009E+07  0.2996E-02  0.9278E-02  0.7463E-02  0.3197E-02 0.000  0.7611E+00  0.2505E+01  0.1894E+01  0.8659E+00        0.
 250.  -0.9247E+06  0.2820E-02  0.8679E-02  0.7023E-02  0.2990E-02 0.000  0.8344E+00  0.2730E+01  0.2076E+01  0.9433E+00        0.
 275.  -0.8033E+06  0.2564E-02  0.8079E-02  0.6392E-02  0.2785E-02 0.000  0.9015E+00  0.2940E+01  0.2243E+01  0.1015E+01        0.
 300.  -0.6852E+06  0.2282E-02  0.7502E-02  0.5697E-02  0.2590E-02 0.000  0.9620E+00  0.3135E+01  0.2394E+01  0.1083E+01        0.
 325.  -0.6030E+06  0.2104E-02  0.7169E-02  0.5257E-02  0.2478E-02 0.000  0.1017E+01  0.3317E+01  0.2531E+01  0.1146E+01        0.
 350.  -0.6016E+06  0.2078E-02  0.7240E-02  0.5197E-02  0.2505E-02 0.000  0.1067E+01  0.3462E+01  0.2656E+01  0.1196E+01        0.
 375.  -0.2376E+06  0.1969E-02  0.4779E-02  0.4859E-02  0.1631E-02 0.000  0.1118E+01  0.3590E+01  0.2781E+01  0.1239E+01        0.
 400.  -0.2221E+06  0.1955E-02  0.4680E-02  0.4820E-02  0.1596E-02 0.000  0.1167E+01  0.3711E+01  0.2903E+01  0.1281E+01        0.
 425.  -0.1822E+06  0.1874E-02  0.4357E-02  0.4614E-02  0.1485E-02 0.000  0.1215E+01  0.3824E+01  0.3021E+01  0.1319E+01        0.
 450.  -0.1469E+06  0.1807E-02  0.4036E-02  0.4443E-02  0.1373E-02 0.000  0.1261E+01  0.3929E+01  0.3134E+01  0.1355E+01        0.
 475.  -0.1160E+06  0.1786E-02  0.3713E-02  0.4376E-02  0.1259E-02 0.000  0.1306E+01  0.4026E+01  0.3245E+01  0.1388E+01        0.
 500.  -0.1193E+05  0.1419E-02  0.1364E-02  0.3340E-02  0.4441E-03 0.000  0.1346E+01  0.4085E+01  0.3340E+01  0.1408E+01        0.
 525.  -0.1152E+05  0.1413E-02  0.1228E-02  0.3307E-02  0.3976E-03 0.000  0.1381E+01  0.4117E+01  0.3423E+01  0.1418E+01        0.
 550.  -0.1115E+05  0.1403E-02  0.1123E-02  0.3268E-02  0.3615E-03 0.000  0.1417E+01  0.4146E+01  0.3506E+01  0.1427E+01        0.
 575.  -0.1082E+05  0.1375E-02  0.1041E-02  0.3192E-02  0.3344E-03 0.000  0.1451E+01  0.4173E+01  0.3587E+01  0.1436E+01        0.
 600.  -0.1052E+05  0.1363E-02  0.9767E-03  0.3154E-02  0.3125E-03 0.000  0.1486E+01  0.4199E+01  0.3667E+01  0.1444E+01        0.
 625.  -0.1023E+05  0.1351E-02  0.9242E-03  0.3116E-02  0.2949E-03 0.000  0.1519E+01  0.4222E+01  0.3744E+01  0.1452E+01        0.
 650.  -0.9967E+04  0.1337E-02  0.8786E-03  0.3077E-02  0.2797E-03 0.000  0.1553E+01  0.4245E+01  0.3822E+01  0.1459E+01        0.
 675.  -0.9736E+04  0.1322E-02  0.8527E-03  0.3038E-02  0.2712E-03 0.000  0.1586E+01  0.4266E+01  0.3898E+01  0.1466E+01        0.
 700.  -0.9516E+04  0.1306E-02  0.8296E-03  0.3000E-02  0.2636E-03 0.000  0.1619E+01  0.4287E+01  0.3974E+01  0.1473E+01        0.
 725.  -0.9299E+04  0.1291E-02  0.8047E-03  0.2963E-02  0.2554E-03 0.000  0.1652E+01  0.4308E+01  0.4048E+01  0.1479E+01        0.
 750.  -0.9089E+04  0.1277E-02  0.7810E-03  0.2926E-02  0.2476E-03 0.000  0.1683E+01  0.4327E+01  0.4121E+01  0.1485E+01        0.
 775.  -0.8858E+04  0.1258E-02  0.7581E-03  0.2881E-02  0.2401E-03 0.000  0.1716E+01  0.4347E+01  0.4195E+01  0.1491E+01        0.
 800.  -0.8621E+04  0.1239E-02  0.7367E-03  0.2834E-02  0.2331E-03 0.000  0.1747E+01  0.4366E+01  0.4266E+01  0.1497E+01        0.
```

```
   BETA TEST V1.8 ; WECHSL POST TEST CALCULATION.

ZEIT     Q SURF          CO2          CO      H2O MIT SU.        H2     SUMPF         CO2            CO           H2O           H2        SUMPF
 SEC      WATT          KG/S         KG/S        KG/S           KG/S     KG/S          KG             KG            KG            KG         KG

 825.  -0.8394E+04  0.1220E-02  0.7167E-03  0.2789E-02  0.2267E-03 0.000  0.1778E+01  0.4384E+01  0.4336E+01  0.1503E+01          0.
 850.  -0.8178E+04  0.1192E-02  0.6982E-03  0.2724E-02  0.2208E-03 0.000  0.1808E+01  0.4401E+01  0.4405E+01  0.1509E+01          0.
 875.  -0.7973E+04  0.1174E-02  0.6824E-03  0.2682E-02  0.2157E-03 0.000  0.1837E+01  0.4418E+01  0.4472E+01  0.1514E+01          0.
 900.  -0.7772E+04  0.1156E-02  0.6678E-03  0.2639E-02  0.2110E-03 0.000  0.1866E+01  0.4436E+01  0.4539E+01  0.1519E+01          0.
 925.  -0.7581E+04  0.1138E-02  0.6544E-03  0.2598E-02  0.2067E-03 0.000  0.1895E+01  0.4452E+01  0.4604E+01  0.1525E+01          0.
 950.  -0.7396E+04  0.1120E-02  0.6417E-03  0.2558E-02  0.2026E-03 0.000  0.1923E+01  0.4468E+01  0.4668E+01  0.1530E+01          0.
 975.  -0.7217E+04  0.1103E-02  0.6294E-03  0.2518E-02  0.1987E-03 0.000  0.1951E+01  0.4484E+01  0.4732E+01  0.1535E+01          0.
1000.  -0.7043E+04  0.1087E-02  0.6176E-03  0.2480E-02  0.1950E-03 0.000  0.1978E+01  0.4500E+01  0.4794E+01  0.1540E+01          0.
1050.  -0.6710E+04  0.1054E-02  0.5954E-03  0.2404E-02  0.1879E-03 0.000  0.2031E+01  0.4530E+01  0.4916E+01  0.1549E+01          0.
1100.  -0.6605E+04  0.1032E-02  0.5872E-03  0.2355E-02  0.1854E-03 0.000  0.2084E+01  0.4560E+01  0.5035E+01  0.1559E+01          0.
1142.  -0.6772E+04  0.9651E-03  0.2655E-03  0.2118E-02  0.8060E-04 0.000  0.2126E+01  0.4584E+01  0.5133E+01  0.1566E+01          0.
1150.  -0.6842E+04  0.1018E-02  0.2621E-03  0.2226E-02  0.7932E-04 0.000  0.2135E+01  0.4586E+01  0.5151E+01  0.1567E+01          0.
1200.  -0.6607E+04  0.9898E-03  0.2549E-03  0.2165E-02  0.7713E-04 0.000  0.2185E+01  0.4599E+01  0.5260E+01  0.1571E+01          0.
1250.  -0.6382E+04  0.9634E-03  0.2484E-03  0.2108E-02  0.7518E-04 0.000  0.2234E+01  0.4611E+01  0.5367E+01  0.1574E+01          0.
1300.  -0.6171E+04  0.9382E-03  0.2424E-03  0.2053E-02  0.7337E-04 0.000  0.2281E+01  0.4623E+01  0.5471E+01  0.1578E+01          0.
1350.  -0.5973E+04  0.9142E-03  0.2368E-03  0.2001E-02  0.7168E-04 0.000  0.2327E+01  0.4635E+01  0.5572E+01  0.1582E+01          0.
1400.  -0.5786E+04  0.8912E-03  0.2315E-03  0.1950E-02  0.7007E-04 0.000  0.2372E+01  0.4647E+01  0.5671E+01  0.1585E+01          0.
1450.  -0.5603E+04  0.8692E-03  0.2264E-03  0.1903E-02  0.6855E-04 0.000  0.2416E+01  0.4659E+01  0.5768E+01  0.1589E+01          0.
1500.  -0.5430E+04  0.8482E-03  0.2216E-03  0.1857E-02  0.6712E-04 0.000  0.2459E+01  0.4670E+01  0.5861E+01  0.1592E+01          0.
1550.  -0.5267E+04  0.8281E-03  0.2173E-03  0.1813E-02  0.6582E-04 0.000  0.2501E+01  0.4681E+01  0.5953E+01  0.1596E+01          0.
1600.  -0.5113E+04  0.8088E-03  0.2132E-03  0.1771E-02  0.6460E-04 0.000  0.2542E+01  0.4691E+01  0.6043E+01  0.1599E+01          0.
1650.  -0.4967E+04  0.7904E-03  0.2094E-03  0.1731E-02  0.6345E-04 0.000  0.2582E+01  0.4702E+01  0.6130E+01  0.1602E+01          0.
1700.  -0.4828E+04  0.7726E-03  0.2056E-03  0.1693E-02  0.6232E-04 0.000  0.2621E+01  0.4712E+01  0.6216E+01  0.1605E+01          0.
1750.  -0.4697E+04  0.7556E-03  0.2020E-03  0.1656E-02  0.6123E-04 0.000  0.2659E+01  0.4723E+01  0.6300E+01  0.1608E+01          0.
1800.  -0.4570E+04  0.7393E-03  0.1984E-03  0.1620E-02  0.6015E-04 0.000  0.2697E+01  0.4733E+01  0.6381E+01  0.1611E+01          0.
1850.  -0.4448E+04  0.7237E-03  0.1949E-03  0.1587E-02  0.5909E-04 0.000  0.2733E+01  0.4742E+01  0.6462E+01  0.1614E+01          0.
1901.  -0.4244E+04  0.5544E-03  0.3731E-03  0.1278E-02  0.1189E-03 0.000  0.2767E+01  0.4759E+01  0.6537E+01  0.1620E+01          0.
1951.  -0.3884E+04  0.4962E-03  0.2664E-03  0.1129E-02  0.8382E-04 0.000  0.2793E+01  0.4775E+01  0.6596E+01  0.1624E+01          0.
2001.  -0.3589E+04  0.4664E-03  0.2107E-03  0.1050E-02  0.6565E-04 0.000  0.2817E+01  0.4786E+01  0.6651E+01  0.1628E+01          0.
```

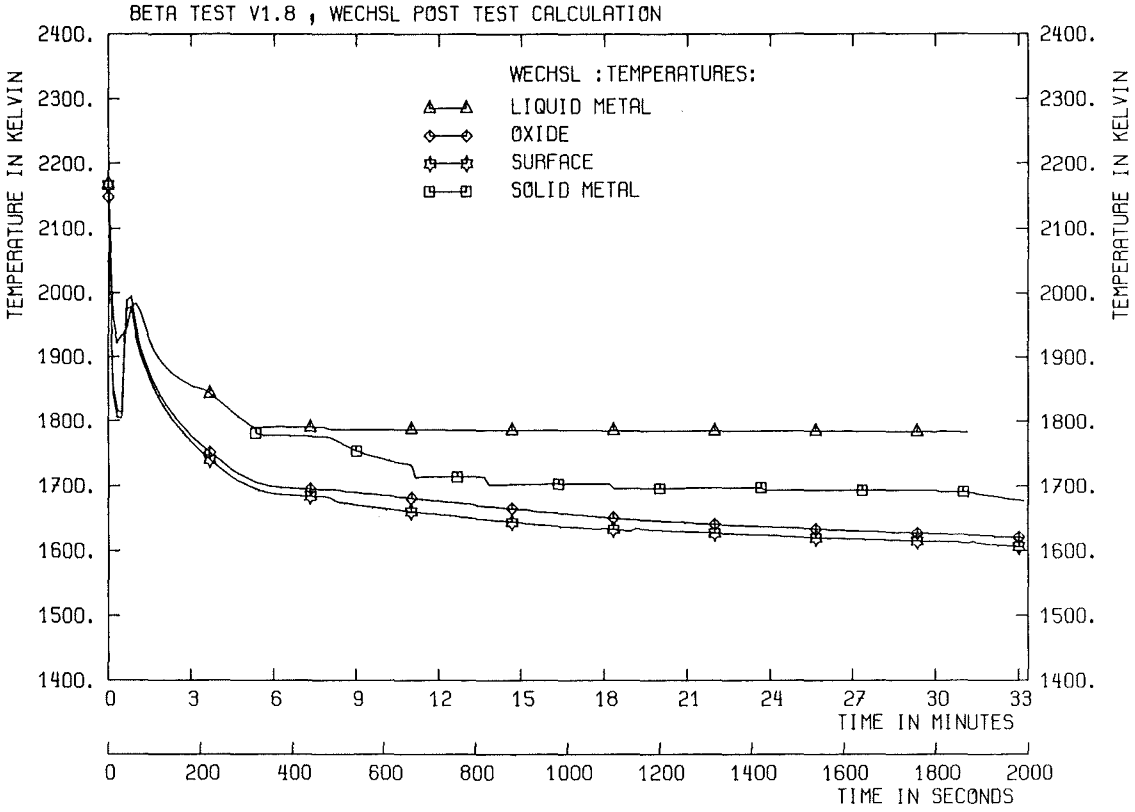
BETA TEST V1.8 , WECHSL POST TEST CALCULATION
WECHSL :TEMPERATURES:
LIQUID METAL
OXIDE
SURFACE
SOLID METAL
TEMPERATURE IN KELVIN
2400.
2300.
2200.
2100.
2000.
1900.
1800.
1700.
1600.
1500.
1400.
0
3
6
9
12
15
18
21
24
27
30
33
TIME IN MINUTES
0
200
400
600
800
1000
1200
1400
1600
1800
2000
TIME IN SECONDS

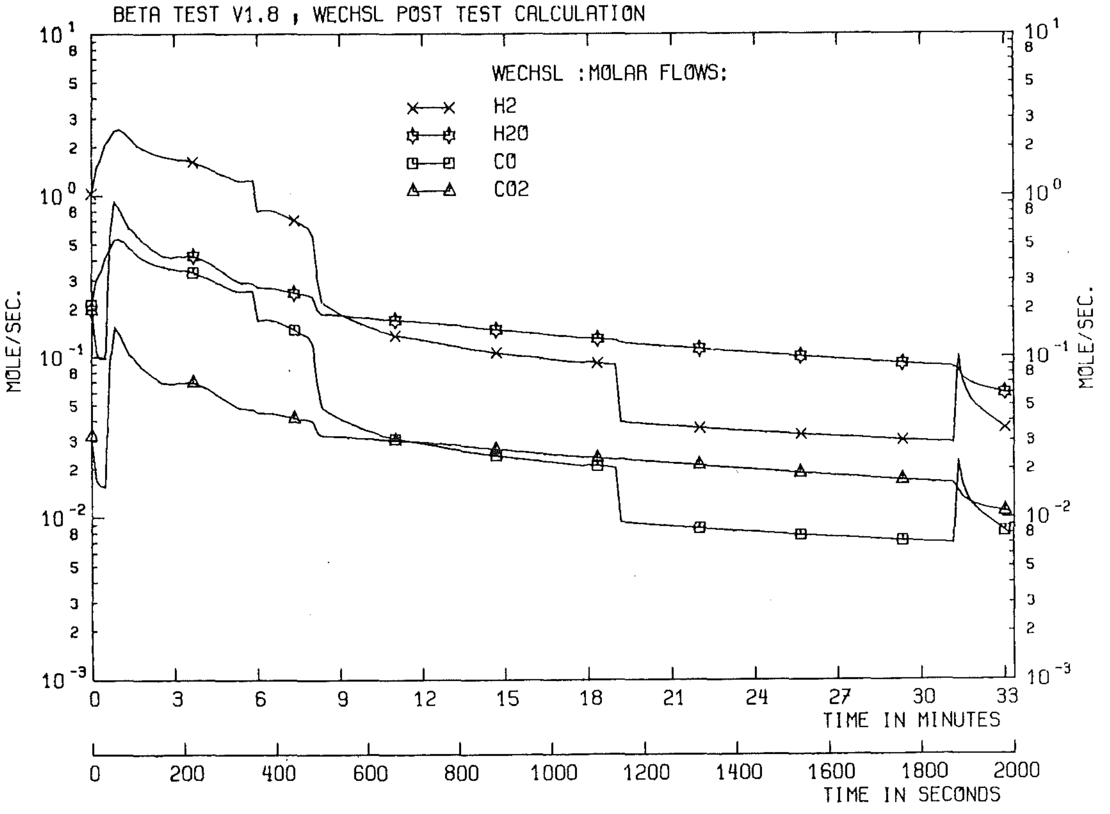
BETA TEST V1.8 , WECHSL POST TEST CALCULATION
WECHSL :MOLAR FLOWS:
H2
H2O
CO
CO2
MOLE/SEC.
10^1
10^0
10^-1
10^-2
10^-3
8
5
3
2
0
3
6
9
12
15
18
21
24
27
30
33
TIME IN MINUTES
0
200
400
600
800
1000
1200
1400
1600
1800
2000
TIME IN SECONDS

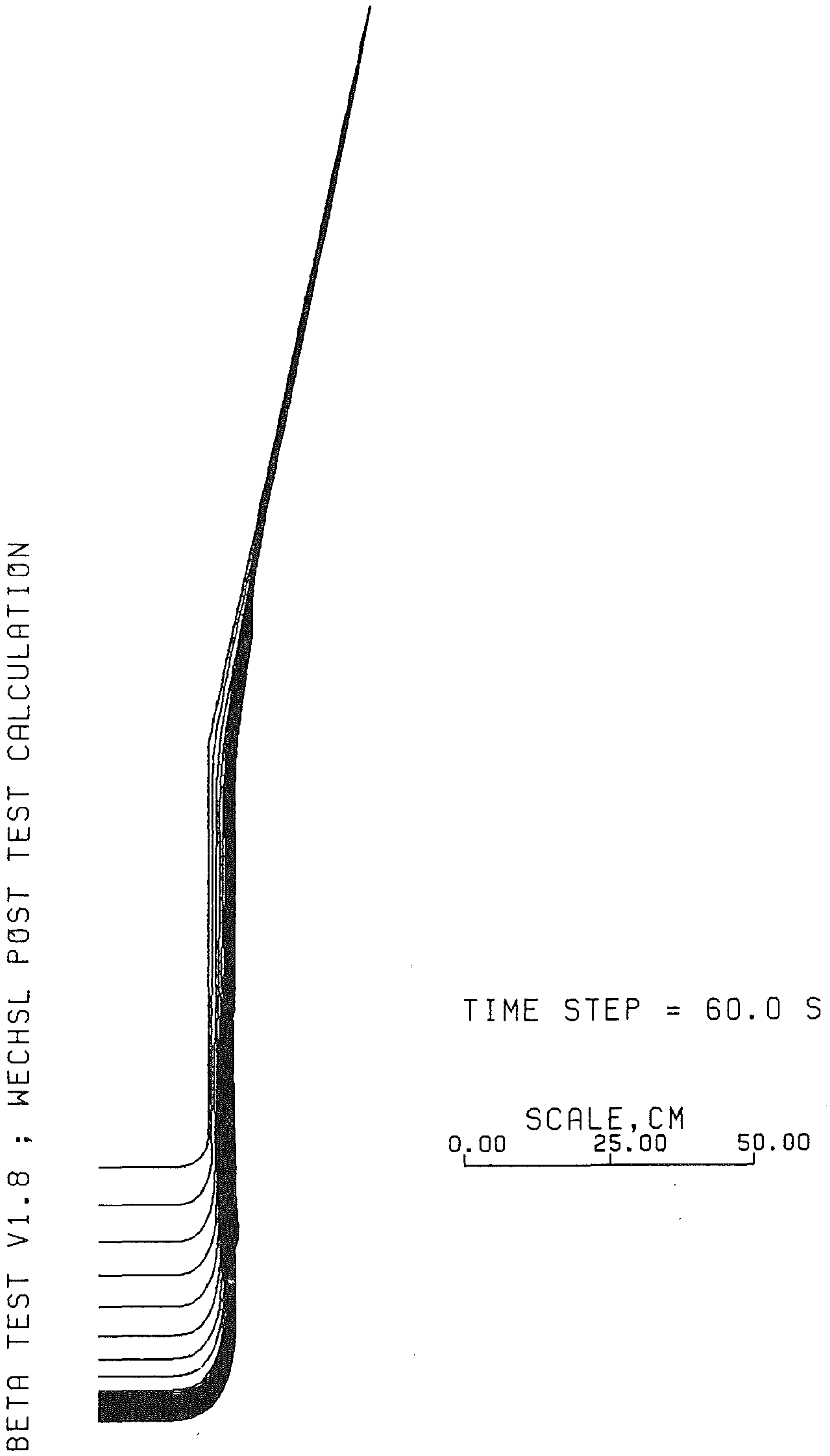
BETA TEST V1.8 ; WECHSL PØST TEST CALCULATIØN
TIME STEP = 60.0 S
SCALE,CM
0.00
25.00
50.00

APPENDIX B

Test Sample 2:
Reactor Calculation

```
 DRS-B10, 40% ZR OX.
*
*
*------  THERMITE ADDITION:  RATE AND TIME OF REACTION  ----------------
*  KG/S  |  SEC.   |
        0.        0.
*
*------  ADDITION OF OTHER MATERIALS  ----------------------------------
*
*  NUMBER OF ADDITIONS :
        0
*
*
*------  CHARACTERISTICS OF CONCRETE WITHOUT STEEL  --------------------
*
*WEIGHT FRACTION OF THE COMPONENTS : (AL203 IS THE COMPLEMENT)
*  CAC03 | CA(OH)2 |    SI02 | FREE H20|
      .0663    .0728     .7655     .0422
*   STEEL; MELT TEMP.; DECOMP. ENTH. ; DENSITY (ALL WITHOUT STEEL)
*KG/KGCON|  KELVIN |    J/KG |   KG/M3 |
       .065     1573.  2.075E6     2.3E3
*
*
*------ CHARACTERISTICS OF THE LIQUIDUS/SOLIDUS CURVE OF THE OXIDE PHASE
*       TABLE INPUT; NUMBER OF TABLE POINTS IMAT
*MAT|
   11
*
*    LOW TEMPERATURE GROUP :
*NUMBER OF SPECIES; SPECIES:1=U02; 2=ZR02; 3=FEO; 4=CAO; 5=SI02; 6=AL203
*---|----|----|----|----|----|----|----|
    4    3    4    5    6
*LIQUIDUS: CCL,TLL (3 COUPLES PER CARD)
*      CCL|       TLL|       CCL|       TLL|       CCL|       TLL|
         .0     1573.         .1     1773.         .2     1893.
         .3     2073.         .4     2193.         .5     2293.
         .6     2373.         .7     2453.         .8     2523.
         .9     2583.         1.     2673.
*
*    HIGHT TEMPERATURE GROUP :
*NUMBER OF SPECIES; SPECIES:1=U02; 2=ZR02; 3=FEO; 4=CAO; 5=SI02; 6=AL203
*---|----|----|----|----|----|----|----|
    2    1    2
*SOLIDUS: CCL,TLL (3 COUPLES PER CARD)
*      CCS|       TSS|       CCS|       TSS|       CCS|       TSS|
         .0     1423.         .1     1483.         .2     1543.
         .3     1615.         .4     1715.         .5     1815.
         .6     1930.         .7     2073.         .8     2201.
         .9     2313.         1.     2423.
*
*
*------  CHARACTERISTICS OF THE OXIDE PHASE  --------------------------
*
* INITIAL MASS OF OXIDES IN KG :
*    U02 |    ZR02 |     FE0 |     CAO |    SI02 |   AL203 |   CR203 |
   103000.   16486.        0.        0.        0.        0.        0.
* INITIAL TEMPERATURE OF OXIDE :
* KELVIN |
    2673.
```

```
* POWER IN THE OXIDE PHASE :
* NUMBER OF COUPLES : (TIME IN SEC. ; INTERNAL POWER IN WATT )
*---| IF THIS NUMBER IS 0,GOTO METAL PHASE(NO CARDS FOR SHIFT AND POWER)
   23
* SHIFT TIME FOR INTERNAL HEAT GENERATION.
*  SEC.  |
    25200.
*COUPLES (TIME IN SEC. ; INTERNAL POWER IN WATT ) ( 3 COUPLES/CARD )
*   TIME |   POWER |    TIME |   POWER |    TIME |   POWER |
        0.  13.177E7       60.  6.9754E7      360.  5.1946E7
      600.  4.6950E7     1080.   4.069E7     2700.  3.1046E7
     3600.  2.8560E7     7800.  2.3744E7    10800.  2.2232E7
    14400.  2.0944E7    15000.  2.0754E7    15600.  2.0586E7
    16200.  2.0418E7    18000.  1.9947E7    25200.  1.8458E7
    36000.  1.6912E7    72000.  1.4146E7    86400.  1.3496E7
   172800.  1.1200E7   259800.  9.9792E6   432000.  8.5456E6
   864000.  6.7872E6  1730000.  5.1856E6
*
*
*------  CHARACTERISTICS OF THE METAL PHASE  ---------------------------
*
* INITIAL MASS OF METALS IN KG :
*     FE |      ZR |      CR |      NI |
    53000.    18000.    11000.     6400.
*
* INITIAL TEMPERATURE OF METAL :
* KELVIN |
     2673.
*
* POWER IN THE METAL PHASE :
* NUMBER OF COUPLES : (TIME IN SEC. ; INTERNAL POWER IN WATT )
*---| IF THIS NUMBER IS 0,GOTO THE CARD : TIME STEP AND FINAL TIME.
   23
*COUPLES (TIME IN SEC. ; INTERNAL POWER IN WATT ) ( 3 COUPLES/CARD )
*   TIME |   POWER |    TIME |   POWER |    TIME |   POWER |
        0.  17.965E6       60.  9.5088E6      360.  7.0784E6
      600.  6.4064E6     1080.  5.5440E6     2700.  4.2336E6
     3600.  3.8976E6     7800.  3.2368E6    10800.  3.0240E6
    14400.  2.8560E6    15000.  2.8336E6    15600.  2.8000E6
    16200.  2.7776E6    18000.  2.7104E6    25200.  2.5200E6
    36000.  2.3072E6    72000.  1.9264E6    86400.  1.8368E6
   172800.  1.5232E6   259800.  1.3552E6   432000.  1.1648E6
   864000.  0.9184E6  1730000.  0.7056E6
*
*
*------  TIME CHARACTERISTICS  -----------------------------------------
*
*TIME STEP, FINAL TIME, MIN  /  MAX TIME STEP:
*  SEC.  |   SEC.  |   SEC.  |   SEC.  |
       1.0  1000000.       0.4       15.
*
* PRINTOUT :
* NUMBER OF PRINTOUT COUPLES :
    2
*COUPLES ( START PRINTOUT TIME,S ; PRINTOUT INTERVAL,S ; 3 COUPLES/CARD)
*   TIME |    STEP |    TIME |    STEP |    TIME |    STEP |
        0.    10000.   150000.     5000.
*
*
```

```
*------  AMBIENT ATMOSPHERIC PRESSURE  ---------------------------------
*
*NUMBER OF COUPLES ( TIME, S ; PRESSURE,BAR )
*---|
    2
*COUPLES (TIME IN SEC. ; PRESSURE, BAR ) ( 3 COUPLES/CARD )
*   TIME | PRESSURE|    TIME | PRESSURE|---------|---------|
        0.        4.      1.E7        4.
*
*
*------  AMBIENT TEMPERATURE FOR RADIATION ON THE TOP OF CORIUM  -------
*
* NUMBER OF COUPLES ( TIME, S ; TEMPERATURE, K )
*---|
    4
*COUPLES (TIME IN SEC. ; TEMPERATURE, K ) ( 3 COUPLES/CARD )
*   TIME | TEMPERA.|    TIME | TEMPERA.|---------|---------|
        0.     1700.     1000.     1500.   345600.     1000.
      1.E7     1000.
*
*
*------  CAVITY CHARACTERISTICS  ---------------------------------------
*
* OPTION FOR INITIAL SHAPE : 1000<NB<1499 : CYLINDER WITH ROUNDED CORNER
*---|
 1032
* NUMBER OF POINTS ON FLOOR AND CORNER, RADIUS OF CYLINDER AND CORNER,
* INTERVAL BETWEEN POINTS ON CYLINDER, CYLINDER HEIGHT.
*FLO| COR|RADIUS,M |CORNER,M |INTERV.,M| HEIGHT,M|
   40    10       3.2         .2      .075       11.
* INTERVAL BETWEEN CAVITY POINTS DURING PROGRAM RUN.
*  METER |
      .070
* RADIUS SUMP WATER INGRESSION ; BASEMAT THICKNESS ; TIME SUMP WATER
*  METER |   METER |   SEC   |
       4.1          6.      1.E7
*
*
*------  PRINTOUT OPTIONS: ( 0 = NO   ,  1 = YES )  ---------------------
*
*TEMP.   / PROPERT./ INTERFA./ MASS BAL/
         1         1         1         1
*ENER.BAL/ GAS REL./  CAVITY /DIAGNOST./
         1         1         1         1
*
*------  PLOT FILE OPTIONS: ( 0 = NO   ,  1 = YES )  --------------------
*
*DO YOU WANT PLOTS (CAVITY NOT INCLU.)? ; DO YOU WANT THE CAVITY SHAPE ?
* PLOTS  /  CAVITY /
         1         1
*START TIME AND INTERVAL TO WRITE PLOT FILE, SEC (THIS CARD MUST STAY)
* WARNING ! FOR KFK PLOT PROGRAM, NO MORE THAN 500 TIMES CAN BE WRITTEN!
* START  | INTERVAL|    ( FOR THE FIRST 3600 S, THEN SET TO 3600 )
        0.      100.
*START TIME AND INTERVAL TO WRITE CAVITY PLOT, SEC (THIS CARD MUST STAY)
* START  | INTERVAL|
        0.     3600.
*
*------  END OF WECHSL INPUT DATA  -------------------------------------
```

```
    DRS-B10, 40% ZR OX., SIEHE B9

NO ADDITIONS MADE

COMPOSITION OF CONCRETE ( INCLUDING STEEL CONTENT )
 CACO3     CA(OH)2  SIO2     H2O      AL2O3
 0.062     0.068    0.719    0.040    0.050
WEIGHT FRACTION, IN MASS UNIT OF CONCRETE, OF:
  CAO      SIO2     AL2O3    H2O      CO2
  0.087    0.719    0.050    0.056    0.027

TSB=1573. K  HB= 0.2075E+07 J/KG  RHO=2300. KG/M3 ( ALL WITHOUT STEEL )
 0.065 KG FE PER KG CONCRETE ( WITHOUT STEEL )

 HB  FOR CONC.+FE =  0.2038E+07 J/KG
 RHO FOR CONC.+FE = 2.4037 T/M3

INITIAL MASS OF OXIDES, KG
 UO2        ZRO2       FEO         CAO         SIO2        AL2O3       CR2O3
 103000.    16486.          0.          0.          0.          0.          0.
INITIAL OXIDE TEMPERATURE T= 2673. K

INTERNAL HEAT GENERATION IN OXIDE PHASE
 TIME,S       POWER,W
 0.0000E+00  0.1318E+09
 0.6000E+02  0.6975E+08
 0.3600E+03  0.5195E+08
 0.6000E+03  0.4695E+08
 0.1080E+04  0.4069E+08
 0.2700E+04  0.3105E+08
 0.3600E+04  0.2856E+08
 0.7800E+04  0.2374E+08
 0.1080E+05  0.2223E+08
 0.1440E+05  0.2094E+08
 0.1500E+05  0.2075E+08
 0.1560E+05  0.2059E+08
 0.1620E+05  0.2042E+08
 0.1800E+05  0.1995E+08
 0.2520E+05  0.1846E+08
 0.3600E+05  0.1691E+08
 0.7200E+05  0.1415E+08
 0.8640E+05  0.1350E+08
 0.1728E+06  0.1120E+08
 0.2598E+06  0.9979E+07
 0.4320E+06  0.8546E+07
 0.8640E+06  0.6787E+07
 0.1730E+07  0.5186E+07

INITIAL MASS OF METAL, KG
 FE          ZR          CR          NI
   53000.     18000.     11000.      6400.
  INITIAL METAL TEMPERATURE T= 2673. K
```

```
 INTERNAL HEAT GENERATION IN METAL PHASE
 TIME,S         POWER,W
 0.0000E+00   0.1797E+08
 0.6000E+02   0.9509E+07
 0.3600E+03   0.7078E+07
 0.6000E+03   0.6406E+07
 0.1080E+04   0.5544E+07
 0.2700E+04   0.4234E+07
 0.3600E+04   0.3898E+07
 0.7800E+04   0.3237E+07
 0.1080E+05   0.3024E+07
 0.1440E+05   0.2856E+07
 0.1500E+05   0.2834E+07
 0.1560E+05   0.2800E+07
 0.1620E+05   0.2778E+07
 0.1800E+05   0.2710E+07
 0.2520E+05   0.2520E+07
 0.3600E+05   0.2307E+07
 0.7200E+05   0.1926E+07
 0.8640E+05   0.1837E+07
 0.1728E+06   0.1523E+07
 0.2598E+06   0.1355E+07
 0.4320E+06   0.1165E+07
 0.8640E+06   0.9184E+06
 0.1730E+07   0.7056E+06

  COMPUTATIONS MADE EVERY  1.00 SECONDS UNTIL 200000.0 SEC.
  MINIMUM TIME STEP IS =  0.400 SEC.
  MAXIMUM TIME STEP IS = 15.000 SEC.
  PRINTOUT EVERY  500.SEC., BEGINNING AT    0. SEC.
  PRINTOUT EVERY 1000.SEC., BEGINNING AT 2000. SEC.
  PRINTOUT EVERY 2000.SEC., BEGINNING AT30000. SEC.
  PRINTOUT EVERY 5000.SEC., BEGINNING AT****** SEC.

 FEO   CAO   SIO2  ALOX

 UO2   ZRO2

LIQUIDUS TEMPERATURE OF THE OXIDE PHASE:
MOL. FRACT. H.T.GROUP  TEMPERATURE, K
 0.000                   1573.
 0.100                   1773.
 0.200                   1893.
 0.300                   2073.
 0.400                   2193.
 0.500                   2293.
 0.600                   2373.
 0.700                   2453.
 0.800                   2523.
 0.900                   2583.
 1.000                   2673.

SOLIDUS TEMPERATURE OF THE OXIDE PHASE:
MOL. FRACT. H.T.GROUP  TEMPERATURE, K
 0.000                   1423.
 0.100                   1483.
 0.200                   1543.
 0.300                   1615.
 0.400                   1715.
 0.500                   1815.
 0.600                   1930.
 0.700                   2073.
 0.800                   2201.
 0.900                   2313.
 1.000                   2423.
```

```
PRESSURE HISTORY
 TIME,S       PRESSURE,BAR
 0.0000E+00  0.4000E+01
 0.1000E+08  0.4000E+01

AMBIENT TEMPERATURE HISTORY
 TIME,S       TEMPERATURE,K
 0.0000E+00  0.1700E+04
 0.1000E+04  0.1500E+04
 0.3456E+06  0.1000E+04
 0.1000E+08  0.1000E+04

============================================================
                 AT TIME =     1. SEC.
            BEGINNING OF THE OXIDATION OF ZR
              ZR + 2H2O <=====> ZRO2 + 2H2
              ZR + 2CO2 <=====> ZRO2 + 2CO

============================================================
============================================================


 ============================================================
                     TIME =     1. SEC.
  THE HEAT TRANSFER MODEL BETWEEN BOTTOM METAL AND CONCRETE
  IS ,FROM NOW, THE MIXED MODEL (OR TRANSITION MODEL)
  THE REYNOLD NUMBER OF THIS GAS FLOW IS :     0.6532E+01
  THERE IS NO METAL CRUST..

 ============================================================
 ============================================================
```

```
************************
*                      *
*  TIME =      1. SEC  *         NEXT TIME STEP= 0.80 SEC
*                      *
************************


CAVITY DIMENSIONS, M :

       VERTICAL EROSION  :  -0.002
       MAXIMAL RADIUS    :   3.202
       ZERO LEVEL RADIUS :   3.137

TEMPERATURES, K :

       POOL -      LIQ. METAL: 2662.   OXIDE    :  2659.
       SURFACES -  MET./CONC.: 2609.   OX./CONC.:  2423.
                   MET./OX.  : 2673.   OX./SURF.:  2663.
       LIQUIDUS -  METAL     : 1755.   OXIDE    :  2660.
       SOLIDUS  -  METAL     : 1744.   OXIDE    :  2407.
       GAS LEAVING THE MELT  : 2310.
       WATER GAS REACTION    : 1200.

PROPERTIES:
                                      METAL             OXIDE
       DENSITY, KG/M3            :    6595.             8763.
       HEAT CONDUCTIVITY, W/(M.K):  58.828              3.000
       HEAT CAPACITY , J/(KG.K)  :     666.              517.
       SURFACE TENSION, KG/S2    :   1.536              0.445
       VISCOSITY , KG/(S.M)      : 0.1979E-02        0.5716E-02

POOL-CONCRETE INTERFACE :
                               BOTTOM      METAL/WALL  OXIDE/WALL  OXIDE/SURFACE
       EROSION SPEED, CM/S :  0.2238E+00  0.1680E+00  0.1616E+00
       EROSION SPEED, CM/H :   805.83      604.72      581.67
       ENERGY FLUX,    W/M2 :  0.1097E+08  0.8229E+07  0.7915E+07  0.1308E+07
       ENERGY FLUX,   KW/M2 :   10966.      8229.       7915.       1308.

       HEAT TRANSFER FOR BOTTOM/CONCRETE MIXED MODE

INTEGRATED MASS BALANCE IN THE MELT, TONS :

       INITIAL MELT MASS:  207.886    ACTUAL MASS OF MELT   :  208.411
       ERODED (CONC.+FE):    0.550    MASS OF LEAVING GASES:     0.026

       SUM OF LEFT TERMS:  208.436    SUM OF RIGHT TERMS    :  208.436
       THE ERROR BETWEEN THE 2 SUMS IS  0.711E-14 TONS, I.E   0.341E-14 %

MASSES ,VOLUMES AND HEIGHTS :
                                                   METAL       OXIDE
       MASS ,TONS                           :      88.38      120.04
       VOLUME, (INCLUDING VOID FRACTION), M3 :      89.33       92.39
       VOLUME, (WITHOUT VOID FRACTION), M3   :      13.40       13.86
       VOID FRACTION , IN PERCENT            :      85.00       85.00
       DEPTH, M                              :       2.78        2.83
       POOL HEIGHT FROM INITIAL BOTTOM, M    :            5.61
       VOLUME OF ERODED CONCRETE, M3         :            0.23
       MASS OF ERODED CONCRETE, TONS         :           0.550

WEIGHT FRACTION OF SPECIES IN EACH PHASE, % :

       METAL PHASE:(    88375. KG)    OXIDE PHASE:( 120036. KG)
              ZR : 20.3                         UO2 : 85.8
              CR : 12.4                        ZRO2 : 13.8
              FE : 60.0                         FEO :  0.0
              NI :  7.2                         CAO :  0.0
                                               SIO2 :  0.3
                                              AL2O3 :  0.0
```

```
HEAT FLUX BALANCE IN EACH PHASE,  WATT :
                                                      METAL           OXIDE
        POWER DUE TO DECAY HEAT                  :   0.2520E+07      0.1846E+08
        POWER ENTERING DUE TO GAS AND OXIDES     :   0.8647E+09      0.1758E+10
        POWER LEAVING DUE TO GAS AND OXIDES      :  -0.1282E+10     -0.2094E+09
        POWER DUE TO OXIDATION REACTIONS         :   0.4728E+09      0.0000E+00
        POWER DUE TO CONCRETE DECOMPOSITION      :  -0.6964E+09     -0.4254E+09
        CONDUCTION BETWEEN PHASES                :   0.0000E+00      0.0000E+00
        RADIATION OR EVAPORATED AT SURFACE       :   0.0000E+00     -0.6891E+08
        SENSIBLE HEAT                            :  -0.6388E+09      0.1073E+10

INTEGRATED ENERGY BALANCE IN THE MELT, JOULE :

        INITIAL ENTHALPIE     0.3855E+12    INTEGRATED ENTHALPIE       0.3859E+12
        DECAY HEAT            0.2098E+08    CONCRETE DECOMPOSITION     0.1122E+10
        ENTERING(GAS,OX.)     0.1340E+10    LEAVING (GASES)            0.2094E+09
        OXIDAT. REACTIONS     0.4728E+09    RADIATION OR TO WATER      0.6891E+08

        SUM OF LEFT TERMS     0.3873E+12    SUM OF RIGHT TERMS         0.3873E+12
        THE ERROR BETWEEN THE 2 SUMS IS     0.1967E-05 J., I.E    0.5078E-15 %

GASES GOING IN THE CONTAINMENT, AT THE TEMPERATURE T= 2310. K.
AFTER THAT THE WATER-GAS REACTION OCCURED AT THE SURFACE :

                            CO2          CO           H2O          H2
        HEAT FLUX, WATT    0.1366E+08   0.1766E+08   0.9423E+08   0.7732E+08
        MASS FLUX, KG/S    0.5027E+01   0.6390E+01   0.1202E+02   0.2114E+01
        MOL. FLUX, MOL/S   0.1142E+03   0.2281E+03   0.6674E+03   0.1052E+04
        WEIGHT FRACTION    0.1967E+00   0.2501E+00   0.4704E+00   0.8272E-01
        MOLAR FRACTION     0.5541E-01   0.1107E+00   0.3238E+00   0.5101E+00
        TOTAL MASS, KG     0.5027E+01   0.6390E+01   0.1202E+02   0.2114E+01
        TOT.MOLS, MOL      0.1142E+03   0.2281E+03   0.6674E+03   0.1052E+04
```

```
THE CAVITY SHAPE HAS BEEN CALCULATED USING 160 POINTS, COORDONATES IN CM :
  R=RADIUS   ;  Z=DEPTHNESS    ;  Z-REFERENCE: INITIAL BOTTOM OF THE CAVITY

     R          Z          R          Z          R          Z          R          Z
    0.0       -0.2        7.0       -0.2       14.0       -0.2       21.0       -0.2
   28.0       -0.2       35.0       -0.2       42.0       -0.2       49.0       -0.2
   56.0       -0.2       63.0       -0.2       70.0       -0.2       77.0       -0.2
   84.0       -0.2       91.0       -0.2       98.0       -0.2      105.0       -0.2
  112.0       -0.2      119.0       -0.2      126.0       -0.2      133.0       -0.2
  140.0       -0.2      147.0       -0.2      154.0       -0.2      161.0       -0.2
  168.0       -0.2      175.0       -0.2      182.0       -0.2      189.0       -0.2
  196.0       -0.2      203.0       -0.2      210.0       -0.2      217.0       -0.2
  224.0       -0.2      231.0       -0.2      238.0       -0.2      245.0       -0.2
  252.0       -0.2      259.0       -0.2      266.0       -0.2      273.0       -0.2
  280.0       -0.2      287.0       -0.2      294.0       -0.2      301.0       -0.1
  307.9        1.4      313.7        5.3      318.0       10.9      319.9       17.6
  320.1       24.6      320.1       31.6      320.1       38.6      320.1       45.6
  320.1       52.6      320.1       59.6      320.1       66.6      320.1       73.6
  320.1       80.6      320.1       87.6      320.1       94.6      320.1      101.6
  320.1      108.6      320.1      115.6      320.1      122.6      320.1      129.6
  320.1      136.6      320.1      143.6      320.1      150.6      320.1      157.6
  320.1      164.6      320.1      171.6      320.1      178.6      320.1      185.6
  320.1      192.6      320.2      199.6      320.2      206.6      320.2      213.6
  320.2      220.6      320.2      227.6      320.2      234.6      320.2      241.6
  320.2      248.6      320.2      255.6      320.2      262.6      320.2      269.6
  320.2      278.4      320.2      283.6      320.2      290.6      320.2      297.6
  320.1      304.6      320.1      311.6      320.1      318.6      320.1      325.6
  320.1      332.6      320.1      339.6      320.1      346.6      320.1      353.6
  320.1      360.6      320.1      367.6      320.1      374.6      320.1      381.6
  320.1      388.6      320.1      395.6      320.1      402.6      320.1      409.6
  320.1      416.6      320.1      423.6      320.2      430.6      320.2      437.6
  320.2      444.6      320.2      451.6      320.2      458.6      320.2      465.6
  320.2      472.6      320.2      479.6      320.2      486.6      320.2      493.6
  320.2      500.6      320.2      507.6      320.2      514.6      320.2      521.6
  320.2      528.6      320.2      535.6      320.2      542.6      320.2      549.6
  320.2      556.6      320.2      560.9      320.0      570.6      320.0      577.6
  320.0      584.6      320.0      591.6      320.0      598.6      320.0      605.6
  320.0      612.6      320.0      619.6      320.0      626.6      320.0      633.6
  320.0      640.6      320.0      647.6      320.0      654.6      320.0      661.6
  320.0      668.6      320.0      675.6      320.0      682.6      320.0      689.6
  320.0      696.6      320.0      703.6      320.0      710.6      320.0      717.6
  320.0      724.6      320.0      731.6      320.0      738.6      320.0      745.6
  320.0      752.6      320.0      759.6      320.0      766.6      320.0      773.6
  320.0      780.6      320.0      787.6      320.0      794.6      320.0      807.0
```

```
***********************
*                     *
*  TIME =    500. SEC *         NEXT TIME STEP= 0.42 SEC
*                     *
***********************


CAVITY DIMENSIONS, M :

       VERTICAL EROSION  :  -0.705
       MAXIMAL RADIUS    :   3.315
       ZERO LEVEL RADIUS :   3.315

TEMPERATURES, K :

       POOL -      LIQ. METAL: 1821.   OXIDE     :  1873.
       SURFACES -  MET./CONC.: 1814.   OX./CONC.:  1782.
                   MET./OX.  : 1824.   OX./SURF.:  1863.
       LIQUIDUS -  METAL     : 1758.   OXIDE     :  2144.
       SOLIDUS  -  METAL     : 1748.   OXIDE     :  1674.
       GAS LEAVING THE MELT  : 1841.
       WATER GAS REACTION    : 1200.

PROPERTIES:
                                       METAL             OXIDE
       DENSITY, KG/M3              :    6921.             4428.
       HEAT CONDUCTIVITY, W/(M.K):  53.142             2.986
       HEAT CAPACITY , J/(KG.K)    :     716.               821.
       SURFACE TENSION, KG/S2      :   1.789              3.451
       VISCOSITY , KG/(S.M)        : 0.5171E-02        0.3259E+01

POOL-CONCRETE INTERFACE :
                                 BOTTOM     METAL/WALL  OXIDE/WALL  OXIDE/SURFACE
       EROSION SPEED, CM/S :  0.8796E-01  0.1387E-01  0.5061E-02
       EROSION SPEED, CM/H :   316.67       49.95       18.22
       ENERGY FLUX,    W/M2 :  0.4309E+07  0.6797E+06  0.2479E+06  0.1713E+06
       ENERGY FLUX,   KW/M2 :    4309.        680.        248.         171.

       HEAT TRANSFER FOR BOTTOM/CONCRETE MIXED MODE

INTEGRATED MASS BALANCE IN THE MELT, TONS :

       INITIAL MELT MASS:  207.886    ACTUAL MASS OF MELT  :  286.221
       ERODED (CONC.+FE):   81.230    MASS OF LEAVING GASES:    2.896

       SUM OF LEFT TERMS:  289.116    SUM OF RIGHT TERMS   :  289.116
       THE ERROR BETWEEN THE 2 SUMS IS -0.284E-12 TONS, I.E  -0.983E-13 %

MASSES ,VOLUMES AND HEIGHTS :
                                                    METAL      OXIDE
       MASS ,TONS                                :    82.25      203.97
       VOLUME, (INCLUDING VOID FRACTION), M3 :    17.59      102.27
       VOLUME, (WITHOUT VOID FRACTION), M3   :    11.88       46.07
       VOID FRACTION , IN PERCENT                :    32.46       54.95
       DEPTH, M                                  :     0.53        3.00
       POOL HEIGHT FROM INITIAL BOTTOM, M        :          2.83
       VOLUME OF ERODED CONCRETE, M3             :         33.79
       MASS OF ERODED CONCRETE, TONS             :        81.230

WEIGHT FRACTION OF SPECIES IN EACH PHASE, % :

        METAL PHASE:(   82251. KG)    OXIDE PHASE:( 203969. KG)
              ZR :  8.4                      UO2 : 50.5
              CR : 13.4                     ZRO2 : 15.4
              FE : 70.5                      FEO :  0.0
              NI :  7.8                      CAO :  3.4
                                            SIO2 : 28.6
                                           AL2O3 :  2.0
                                           CR2O3 :  0.0
```

```
HEAT FLUX BALANCE IN EACH PHASE,  WATT :
                                                     METAL          OXIDE
        POWER DUE TO DECAY HEAT                 :   0.2510E+07     0.1839E+08
        POWER ENTERING DUE TO GAS AND OXIDES :   0.1750E+09     0.2300E+09
        POWER LEAVING DUE TO GAS AND OXIDES   :  -0.2137E+09    -0.1957E+08
        POWER DUE TO OXIDATION REACTIONS      :   0.9402E+08     0.0000E+00
        POWER DUE TO CONCRETE DECOMPOSITION   :  -0.1540E+09    -0.1459E+08
        CONDUCTION BETWEEN PHASES             :   0.6871E+08    -0.6871E+08
        RADIATION OR EVAPORATED AT SURFACE    :   0.0000E+00    -0.7460E+07
        SENSIBLE HEAT                         :  -0.2754E+08     0.1381E+09

INTEGRATED ENERGY BALANCE IN THE MELT, JOULE :

        INITIAL ENTHALPIE      0.3855E+12    INTEGRATED ENTHALPIE       0.4736E+12
        DECAY HEAT             0.1047E+11    CONCRETE DECOMPOSITION     0.1655E+12
        ENTERING(GAS,OX.)      0.1927E+12    LEAVING (GASES)            0.2383E+11
        OXIDAT. REACTIONS      0.8423E+11    RADIATION OR TO WATER      0.9941E+10

        SUM OF LEFT TERMS      0.6729E+12    SUM OF RIGHT TERMS         0.6729E+12
        THE ERROR BETWEEN THE 2 SUMS IS      0.5554E-02 J., I.E    0.8254E-12 %

GASES GOING IN THE CONTAINMENT, AT THE TEMPERATURE T= 1841. K.
AFTER THAT THE WATER-GAS REACTION OCCURED AT THE SURFACE :

                              CO2          CO           H2O          H2
        HEAT FLUX, WATT    0.3322E+06   0.2840E+07   0.2853E+07   0.1343E+08
        MASS FLUX, KG/S    0.1628E+00   0.1338E+01   0.4161E+00   0.4728E+00
        MOL. FLUX, MOL/S   0.3700E+01   0.4775E+02   0.2310E+02   0.2352E+03
        WEIGHT FRACTION    0.6815E-01   0.5598E+00   0.1741E+00   0.1979E+00
        MOLAR FRACTION     0.1194E-01   0.1542E+00   0.7458E-01   0.7593E+00
        TOTAL MASS, KG     0.3782E+03   0.1174E+04   0.9380E+03   0.4052E+03
        TOT.MOLS, MOL      0.8594E+04   0.4193E+05   0.5208E+05   0.2016E+06

THE CAVITY SHAPE HAS BEEN CALCULATED USING 144 POINTS, COORDONATES IN CM :
  R=RADIUS  ;  Z=DEPTHNESS   ;  Z-REFERENCE: INITIAL BOTTOM OF THE CAVITY

      R          Z           R          Z           R          Z           R          Z
     0.0       -70.5        7.0       -70.5       14.0       -70.5       21.0       -70.5
    28.0       -70.5       35.0       -70.5       42.0       -70.5       49.0       -70.5
    56.0       -70.5       63.0       -70.5       70.0       -70.5       77.0       -70.5
    84.0       -70.5       91.0       -70.5       98.0       -70.5      105.0       -70.5
   112.0       -70.5      119.0       -70.5      126.0       -70.5      133.0       -70.5
   140.0       -70.5      147.0       -70.5      154.0       -70.5      161.0       -70.5
   168.0       -70.5      175.0       -70.5      182.0       -70.5      189.0       -70.5
   196.0       -70.5      203.0       -70.5      210.0       -70.5      217.0       -70.5
   224.0       -70.5      231.0       -70.5      238.0       -70.5      245.0       -70.5
   252.0       -70.5      259.0       -70.5      266.0       -70.5      273.0       -70.5
   280.0       -70.5      287.0       -70.5      294.0       -70.5      301.0       -70.2
   307.9       -69.1      314.3       -66.3      319.2       -61.3      323.0       -55.3
   325.8       -48.9      328.0       -42.3      329.6       -35.5      330.8       -28.6
   331.4       -21.6      331.4       -17.5      331.4        -7.6      331.5        -0.6
   331.5         6.4      331.4        13.4      331.4        20.4      331.3        27.4
   331.2        34.4      331.0        41.4      330.8        48.4      330.6        55.4
   330.3        62.4      330.0        69.4      329.8        76.4      329.5        83.4
   329.3        90.4      329.1        97.4      328.9       104.4      328.8       111.4
   328.6       118.4      328.6       125.4      328.5       132.4      328.4       139.4
   328.4       146.4      328.3       153.4      328.3       160.4      328.3       167.4
   328.3       174.4      328.3       181.4      328.3       188.4      328.3       195.4
   328.3       202.4      328.3       209.4      328.3       216.4      328.3       223.4
   328.3       230.4      328.3       237.4      328.3       244.4      328.2       251.4
   328.2       258.4      328.2       265.4      328.1       272.4      328.0       279.4
   328.0       283.0      327.8       293.4      327.7       300.4      327.6       307.4
   327.5       314.4      327.4       322.7      327.3       331.1      327.3       339.2
   327.2       347.4      327.2       355.4      327.2       363.4      327.1       371.4
   327.1       379.5      327.0       387.4      327.0       395.4      327.0       403.3
   326.9       411.2      326.9       419.0      326.9       426.9      326.9       434.7
   326.8       442.5      326.8       450.1      326.8       457.7      326.8       465.1
   326.8       472.6      326.7       480.1      326.7       487.5      326.7       494.9
   326.6       502.3      326.5       509.7      326.4       517.1      326.2       524.5
   325.9       531.9      325.6       539.2      325.3       546.6      324.9       553.9
   324.3       561.3      323.8       568.6      323.2       576.0      322.6       583.2
   322.1       590.8      321.6       598.1      321.1       605.5      320.8       612.9
   320.5       620.4      320.2       628.0      320.1       635.6      320.0       643.2
```

```
************************
*                      *
*  TIME =  26004. SEC  *        NEXT TIME STEP=10.03 SEC
*                      *
************************


CAVITY DIMENSIONS, M :

       VERTICAL EROSION  :  -1.559
       MAXIMAL RADIUS    :   4.108
       ZERO LEVEL RADIUS :   4.090

TEMPERATURES, K :

       POOL -       LIQ. METAL: 1771.   OXIDE     :  1801.
                    SOL. METAL: 1680.
       SURFACES -   MET./CONC.: 1600.   OX./CONC.:   1719.
                    MET./OX.  : 1772.   OX./SURF.:    424.
       LIQUIDUS -   METAL     : 1767.   OXIDE     :  1861.
       SOLIDUS  -   METAL     : 1757.   OXIDE     :  1527.
       GAS LEAVING THE MELT   :  417.
       WATER GAS REACTION     : 1200.

PROPERTIES:
                                           METAL              OXIDE
       DENSITY, KG/M3                :     7144.              3309.
       HEAT CONDUCTIVITY, W/(M.K):   48.231                   3.097
       HEAT CAPACITY , J/(KG.K)   :       748.                1038.
       SURFACE TENSION, KG/S2     :    1.793                  5.359
       VISCOSITY , KG/(S.M)       :  0.5633E-02           0.2546E+02

POOL-CONCRETE INTERFACE :
                                 BOTTOM      METAL/WALL   OXIDE/WALL   OXIDE/SURFACE
       EROSION SPEED, CM/S :   0.1639E-02   0.1021E-02   0.2499E-02
       EROSION SPEED, CM/H :      5.90         3.67         9.00
       ENERGY FLUX,    W/M2 :  0.8027E+05   0.5000E+05   0.1224E+06   0.3867E+06
       ENERGY FLUX,   KW/M2 :      80.          50.          122.          387.

       HEAT TRANSFER FOR BOTTOM/CONCRETE FILM MODE

INTEGRATED MASS BALANCE IN THE MELT, TONS :

       INITIAL MELT MASS:  207.886     ACTUAL MASS OF MELT  :   438.207
       ERODED (CONC.+FE):  242.318     MASS OF LEAVING GASES:    11.997

       SUM OF LEFT TERMS:  450.204     SUM OF RIGHT TERMS   :   450.204
       THE ERROR BETWEEN THE 2 SUMS IS  0.136E-11 TONS, I.E    0.303E-12 %

MASSES ,VOLUMES AND HEIGHTS :
                                                         METAL       OXIDE
       MASS ,TONS                                :       80.97       357.24
       VOLUME, (INCLUDING VOID FRACTION), M3 :           11.41       108.49
       VOLUME, (WITHOUT VOID FRACTION), M3     :         11.33       107.96
       VOID FRACTION , IN PERCENT                :        0.72         0.49
       DEPTH, M                                  :        0.34         2.14
       POOL HEIGHT FROM INITIAL BOTTOM, M        :             0.92
       VOLUME OF ERODED CONCRETE, M3             :           100.81
       MASS OF ERODED CONCRETE, TONS             :           242.318

WEIGHT FRACTION OF SPECIES IN EACH PHASE, % :

        METAL PHASE:(    80965. KG)     OXIDE PHASE:( 357242. KG)
               ZR :  0.0                        UO2 : 28.8
               CR :  8.4                       ZRO2 : 11.4
               FE : 83.7                        FEO :  0.0
               NI :  7.9                        CAO :  5.9
                                               SIO2 : 48.8
                                              AL2O3 :  3.4
                                              CR2O3 :  1.7
```

```
CRUST THICKNESS IN EACH PHASE, CM :

        IN THE METAL PHASE:            IN THE OXIDE PHASE:
        METAL/OXIDE:     0.00          OXIDE/METAL:    0.00
        METAL/CONCR:    13.01          OXIDE/CONCR:    0.00
                                     OXIDE/SURFACE:    0.85

HEAT FLUX BALANCE IN EACH PHASE,  WATT :
                                                   METAL           OXIDE
        POWER DUE TO DECAY HEAT                :  0.2146E+07      0.1574E+08
        POWER ENTERING DUE TO GAS AND OXIDES   :  0.3792E+07      0.1321E+08
        POWER LEAVING DUE TO GAS AND OXIDES    : -0.4215E+07     -0.1838E+07
        POWER DUE TO OXIDATION REACTIONS       :  0.5217E+06      0.0000E+00
        POWER DUE TO CONCRETE DECOMPOSITION    : -0.2872E+07     -0.7597E+07
        CONDUCTION BETWEEN PHASES              :  0.3621E+06     -0.3621E+06
        RADIATION OR EVAPORATED AT SURFACE     :  0.0000E+00     -0.1814E+08
        SENSIBLE HEAT                          : -0.2653E+06      0.1020E+07

INTEGRATED ENERGY BALANCE IN THE MELT, JOULE :

        INITIAL ENTHALPIE     0.3855E+12     INTEGRATED ENTHALPIE      0.8829E+12
        DECAY HEAT            0.4992E+12     CONCRETE DECOMPOSITION    0.4938E+12
        ENTERING(GAS,OX.)     0.5796E+12     LEAVING (GASES)           0.7587E+11
        OXIDAT. REACTIONS     0.1463E+12     RADIATION OR TO WATER     0.1579E+12

        SUM OF LEFT TERMS     0.1611E+13     SUM OF RIGHT TERMS        0.1611E+13
        THE ERROR BETWEEN THE 2 SUMS IS      0.1260E+00 J., I.E    0.7823E-11 %

GASES GOING IN THE CONTAINMENT, AT THE SATURATION TEMPERATURE TSAT=  417. K.
OF THE SUMP WATER FLOODING THE SURFACE OF THE CORIUM :

                            CO2          CO           H2O          H2
        HEAT FLUX, WATT    0.3347E+05   0.1205E+05   0.3564E+08   0.5090E+05
        MASS FLUX, KG/S    0.9631E-01   0.2819E-01   0.9147E+01   0.8584E-02
        MOL. FLUX, MOL/S   0.2188E+01   0.1006E+01   0.5079E+03   0.4270E+01
        WEIGHT FRACTION    0.1038E-01   0.3038E-02   0.9857E+00   0.9249E-03
        MOLAR FRACTION     0.4246E-02   0.1953E-02   0.9855E+00   0.8286E-02
        TOTAL MASS, KG     0.2605E+04   0.2563E+04   0.5974E+04   0.8542E+03
        TOT.MOLS, MOL      0.5920E+05   0.9151E+05   0.3317E+06   0.4250E+06

THE SUMP WATER FLOODS THE CORIUM SURFACE AND IS EVAPORATED.
THIS WATER EVAPORATES AT TSAT= 417. K WITH A MASS FLOW OF   8.935 KG/S.
THE EVAPORATION ENTHALPIE OF THIS WATER IS 2737.2 KJ/KG
THE TOTAL MASS OF THE EVAPORATED WATER IS NOW:     2578. KG.

THE CAVITY SHAPE HAS BEEN CALCULATED USING  92 POINTS, COORDONATES IN CM :
  R=RADIUS   ;  Z=DEPTHNESS    ;  Z-REFERENCE: INITIAL BOTTOM OF THE CAVITY

    R          Z            R          Z            R          Z            R          Z
   0.0      -155.9         7.0      -155.9        14.0      -155.9        21.0      -155.9
  28.0      -155.9        35.0      -155.9        42.0      -155.9        49.0      -155.9
  56.0      -155.9        63.0      -155.9        70.0      -155.9        77.0      -155.9
  84.0      -155.9        91.0      -155.9        98.0      -155.9       105.0      -155.9
 112.0      -155.9       119.0      -155.9       126.0      -155.9       133.0      -155.9
 140.0      -155.9       147.0      -155.9       154.0      -155.9       161.0      -155.9
 168.0      -155.9       175.0      -155.9       182.0      -155.9       189.0      -155.9
 196.0      -155.9       203.0      -155.9       210.0      -155.9       217.0      -155.9
 224.0      -155.9       231.0      -155.9       238.0      -155.9       245.0      -155.9
 252.0      -155.9       259.0      -155.9       266.0      -155.9       273.0      -155.9
 280.0      -155.9       287.0      -155.9       294.0      -155.8       300.9      -154.9
 307.6      -152.7       313.7      -149.3       319.2      -145.0       324.2      -140.1
 328.7      -134.7       333.0      -129.2       337.5      -123.8       339.4      -121.5
 342.2      -118.1       348.1      -114.3       354.3      -111.1       361.0      -109.0
 367.8      -107.4       374.6      -105.8       381.4      -104.2       388.2      -102.6
 394.8      -100.2       399.2       -94.7       402.3       -88.4       404.6       -81.8
 406.4       -75.1       407.9       -68.2       409.0       -61.3       409.8       -54.3
 410.3       -47.4       410.7       -40.4       410.8       -33.4       410.8       -26.4
 410.6       -19.4       410.3       -12.4       409.9        -5.4       409.5         1.6
 409.0         8.6       408.5        15.6       407.9        22.5       407.3        29.5
 406.7        36.5       406.1        43.5       405.4        50.4       404.6        57.4
 403.5        64.3       402.1        71.2       400.2        77.9       397.2        84.2
 392.7        89.6       386.4        92.4       379.4        93.6       372.6        95.3
```

```
***********************
*                     *
*  TIME = 405569. SEC *        NEXT TIME STEP=10.03 SEC
*                     *
***********************


CAVITY DIMENSIONS, M :

       VERTICAL EROSION  :  -6.000
       MAXIMAL RADIUS    :   6.622
       ZERO LEVEL RADIUS :   6.517

TEMPERATURES, K :

       POOL -      METAL      : 1746.   OXIDE     :  1610.
       SURFACES -  MET./CONC.: 1573.   OX./CONC.:  1592.
                   MET./OX.   : 1656.   OX./SURF.:   419.
       LIQUIDUS -  METAL      : 1794.   OXIDE     :  1626.
       SOLIDUS  -  METAL      : 1784.   OXIDE     :  1439.
       GAS LEAVING THE MELT   :  417.
       WATER GAS REACTION     : 1200.

PROPERTIES:
                                          METAL              OXIDE
       DENSITY, KG/M3                :    7258.              2540.
       HEAT CONDUCTIVITY, W/(M.K):  46.118              3.006
       HEAT CAPACITY , J/(KG.K)   :     746.              1310.
       SURFACE TENSION, KG/S2     :   1.787              6.965
       VISCOSITY , KG/(S.M)       : 0.1000E+04        0.2552E+04

  POOL-CONCRETE INTERFACE :
                                BOTTOM     METAL/WALL  OXIDE/WALL  OXIDE/SURFACE
       EROSION SPEED, CM/S :  0.7969E-03      --       0.3100E-03
       EROSION SPEED, CM/H :     2.87         --          1.12
       ENERGY FLUX,   W/M2 :  0.3904E+05  0.3904E+05  0.1519E+05  0.2130E+05
       ENERGY FLUX,  KW/M2 :      39.         39.         15.         21.

       HEAT TRANSFER FOR BOTTOM/CONCRETE FILM MODE

INTEGRATED MASS BALANCE IN THE MELT, TONS :

       INITIAL MELT MASS:  207.886    ACTUAL MASS OF MELT  : 1905.646
       ERODED (CONC.+FE): 1831.457    MASS OF LEAVING GASES:  133.698

       SUM OF LEFT TERMS: 2039.343    SUM OF RIGHT TERMS   : 2039.343
       THE ERROR BETWEEN THE 2 SUMS IS -0.210E-11 TONS, I.E  -0.103E-12 %

MASSES ,VOLUMES AND HEIGHTS :
                                                    METAL      OXIDE
       MASS ,TONS                             :    143.09     1762.55
       VOLUME, (INCLUDING VOID FRACTION), M3 :     19.71      694.98
       VOLUME, (WITHOUT VOID FRACTION), M3   :     19.71      694.01
       VOID FRACTION , IN PERCENT             :      0.00        0.14
       TOTAL DEPTH, M                         :           6.39
       POOL HEIGHT FROM INITIAL BOTTOM, M     :           0.39
       VOLUME OF ERODED CONCRETE, M3          :         770.18
       MASS OF ERODED CONCRETE, TONS          :        1831.457

WEIGHT FRACTION OF SPECIES IN EACH PHASE, % :

        METAL PHASE:(  143093. KG)    OXIDE PHASE:(1762553. KG)
               ZR :  0.0                       UO2 :  5.8
               CR :  0.0                      ZRO2 :  2.3
               FE : 95.5                       FEO :  2.0
               NI :  4.5                       CAO :  9.0
                                              SIO2 : 74.7
                                             AL2O3 :  5.2
                                             CR2O3 :  0.9
```

```
CRUST THICKNESS IN EACH PHASE, CM :

        IN THE METAL PHASE:                 IN THE OXIDE PHASE:
        COMPLETELY SOLID                 OXIDE/METAL:     0.00
        HEIGHT     :    34.39            OXIDE/CONCR:     0.00
                                       OXIDE/SURFACE:    17.78

HEAT FLUX BALANCE IN EACH PHASE,  WATT :
                                                      METAL            OXIDE
        POWER DUE TO DECAY HEAT                  :   0.1166E+07      0.8556E+07
        POWER ENTERING DUE TO GAS AND OXIDES :   0.1060E+07      0.9591E+07
        POWER LEAVING DUE TO GAS AND OXIDES    :  -0.8606E+06     -0.1428E+07
        POWER DUE TO OXIDATION REACTIONS        :  -0.9762E+03      0.0000E+00
        POWER DUE TO CONCRETE DECOMPOSITION    :  -0.5775E+06     -0.6980E+07
        CONDUCTION BETWEEN PHASES                :  -0.5821E+06      0.5821E+06
        RADIATION OR EVAPORATED AT SURFACE     :   0.0000E+00     -0.2632E+07
        SENSIBLE HEAT                            :   0.2047E+06      0.7688E+07

INTEGRATED ENERGY BALANCE IN THE MELT, JOULE :

        INITIAL ENTHALPIE      0.3855E+12    INTEGRATED ENTHALPIE       0.4374E+13
        DECAY HEAT             0.5137E+13    CONCRETE DECOMPOSITION    0.3733E+13
        ENTERING(GAS,OX.)      0.4703E+13    LEAVING (GASES)            0.6785E+12
        OXIDAT. REACTIONS      0.1649E+12    RADIATION OR TO WATER     0.1605E+13

        SUM OF LEFT TERMS      0.1039E+14    SUM OF RIGHT TERMS         0.1039E+14
        THE ERROR BETWEEN THE 2 SUMS IS     0.3912E+01 J.,  I.E   0.3765E-10 %

GASES GOING IN THE CONTAINMENT, AT THE SATURATION TEMPERATURE TSAT=  417. K.
OF THE SUMP WATER FLOODING THE SURFACE OF THE CORIUM :

                               CO2           CO           H2O           H2
        HEAT FLUX, WATT    0.3206E+05  0.2522E+04  0.6721E+07  0.1014E+05
        MASS FLUX, KG/S    0.9224E-01  0.5899E-02  0.1725E+01  0.1710E-02
        MOL. FLUX, MOL/S   0.2096E+01  0.2106E+00  0.9576E+02  0.8506E+00
        WEIGHT FRACTION    0.5056E-01  0.3233E-02  0.9453E+00  0.9371E-03
        MOLAR FRACTION     0.2119E-01  0.2129E-02  0.9681E+00  0.8599E-02
        TOTAL MASS, KG     0.4008E+05  0.6398E+04  0.8524E+05  0.1983E+04
        TOT.MOLS, MOL      0.9107E+06  0.2284E+06  0.4733E+07  0.9864E+06

THE SUMP WATER FLOODS THE CORIUM SURFACE AND IS EVAPORATED.
THIS WATER EVAPORATES AT TSAT= 417. K WITH A MASS FLOW OF  1.531 KG/S.
THE EVAPORATION ENTHALPIE OF THIS WATER IS 2737.2 KJ/KG
THE TOTAL MASS OF THE EVAPORATED WATER IS NOW:  809344. KG.
```

```
THE CAVITY SHAPE HAS BEEN CALCULATED USING 190 POINTS, COORDONATES IN CM :
  R=RADIUS   ;  Z=DEPTHNESS    ;  Z-REFERENCE: INITIAL BOTTOM OF THE CAVITY

     R         Z            R         Z            R         Z            R         Z
    0.0    -506.6          7.0    -506.6         14.0    -506.6         21.0    -506.6
   28.0    -506.6         35.0    -506.6         42.0    -506.6         49.0    -506.6
   56.0    -506.6         63.0    -506.6         70.0    -506.6         77.0    -506.6
   84.0    -506.6         91.0    -506.6         98.0    -506.6        105.0    -506.6
  112.0    -506.6        119.0    -506.6        126.0    -506.6        133.0    -506.6
  140.0    -506.6        147.0    -506.6        154.0    -506.6        161.0    -506.6
  168.0    -506.6        175.0    -506.6        182.0    -506.6        189.0    -506.6
  196.0    -506.6        203.0    -506.6        210.0    -506.6        217.0    -506.6
  224.0    -506.6        231.0    -506.6        238.0    -506.6        245.0    -506.6
  252.0    -506.6        259.0    -506.6        266.0    -506.6        273.0    -506.6
  280.0    -506.6        287.0    -506.6        294.0    -506.5        300.9    -505.6
  307.6    -503.4        313.7    -500.1        319.2    -495.7        324.2    -490.8
  328.7    -485.5        333.0    -479.9        337.5    -474.5        339.4    -472.2
  222.0    -506.6        224.9    -513.0        229.4    -518.4        234.2    -523.4
  239.1    -528.4        244.1    -533.4        249.1    -538.3        254.1    -543.1
  259.2    -548.0        264.3    -552.8        269.4    -557.6        274.5    -562.3
  279.7    -567.0        284.9    -571.7        290.2    -576.3        295.6    -580.7
  301.1    -585.1        306.5    -589.5        311.9    -594.0        317.3    -598.4
  324.2    -599.8        331.2    -600.0        338.1    -598.8        343.5    -594.4
  349.2    -590.3        354.9    -586.3        360.7    -582.3        366.5    -578.5
  372.4    -574.7        378.4    -571.0        384.3    -567.3        390.2    -563.6
  396.2    -559.8        402.1    -556.0        407.9    -552.2        413.8    -548.4
  419.6    -544.5        425.4    -540.6        431.2    -536.7        437.0    -532.7
  442.8    -528.8        448.6    -524.9        454.4    -521.0        460.2    -517.1
  466.1    -513.2        471.9    -509.4        477.7    -505.5        483.5    -501.6
  489.4    -497.7        495.2    -493.8        500.9    -489.8        506.7    -485.9
  512.4    -481.8        518.1    -477.8        523.8    -473.7        529.4    -469.5
  535.0    -465.2        540.4    -460.9        545.9    -456.4        551.2    -451.9
  556.5    -447.3        561.7    -442.6        566.8    -437.8        571.7    -432.9
  576.6    -427.9        581.4    -422.7        586.0    -417.5        590.6    -412.2
  595.0    -406.7        599.2    -401.2        603.4    -395.5        607.4    -389.8
  611.3    -384.0        615.0    -378.0        618.6    -372.0        622.0    -365.9
  625.3    -359.7        628.4    -353.5        631.4    -347.1        634.2    -340.7
  636.9    -334.3        639.4    -327.7        641.8    -321.2        644.0    -314.5
  646.1    -307.8        648.0    -301.1        649.8    -294.3        651.4    -287.5
  652.9    -280.7        654.2    -273.8        655.5    -266.9        656.6    -260.0
  657.5    -253.1        658.4    -246.1        659.1    -239.2        659.8    -232.2
  660.3    -225.2        660.8    -218.2        661.2    -211.2        661.5    -204.2
  661.7    -197.3        661.9    -190.3        662.0    -183.3        662.1    -176.3
  662.1    -169.3        662.2    -162.3        662.2    -155.3        662.2    -148.3
  662.1    -141.3        662.1    -134.3        662.0    -127.3        662.0    -120.3
  661.9    -113.3        661.7    -106.3        661.6     -99.3        661.4     -92.3
  661.2     -85.3        660.9     -78.3        660.6     -71.3        660.2     -64.3
  659.8     -57.3        659.3     -50.3        658.7     -43.3        658.1     -36.4
  657.4     -29.4        656.5     -22.5        655.6     -15.5        654.5      -8.6
  653.2      -1.7        651.7       5.1        649.9      11.9        647.7      18.5
  644.9      24.9        641.2      30.9        636.1      35.7        627.1      38.7
  622.8      40.1        616.1      42.1
```

```
R=RADIUS  ;  Z=DEPTHNESS   ;  Z-REFERENCE: INITIAL BOTTOM OF THE CAVITY

     R         Z          R         Z          R         Z          R         Z
    0.0    -506.6        7.0    -506.6       14.0    -506.6       21.0    -506.6
   28.0    -506.6       35.0    -506.6       42.0    -506.6       49.0    -506.6
   56.0    -506.6       63.0    -506.6       70.0    -506.6       77.0    -506.6
   84.0    -506.6       91.0    -506.6       98.0    -506.6      105.0    -506.6
  112.0    -506.6      119.0    -506.6      126.0    -506.6      133.0    -506.6
  140.0    -506.6      147.0    -506.6      154.0    -506.6      161.0    -506.6
  168.0    -506.6      175.0    -506.6      182.0    -506.6      189.0    -506.6
  196.0    -506.6      203.0    -506.6      210.0    -506.6      217.0    -506.6
  224.0    -506.6      231.0    -506.6      238.0    -506.6      245.0    -506.6
  252.0    -506.6      259.0    -506.6      266.0    -506.6      273.0    -506.6
  280.0    -506.6      287.0    -506.6      294.0    -506.5      300.9    -505.6
  307.6    -503.4      313.7    -500.1      319.2    -495.7      324.2    -490.8
  328.7    -485.5      333.0    -479.9      337.5    -474.5      339.4    -472.2
  222.0    -506.6      224.9    -513.0      229.4    -518.4      234.2    -523.4
  239.1    -528.4      244.1    -533.4      249.1    -538.3      254.1    -543.1
  259.2    -548.0      264.3    -552.8      269.4    -557.6      274.5    -562.3
  279.7    -567.0      284.9    -571.7      290.2    -576.3      295.6    -580.7
  301.1    -585.1      306.5    -589.5      311.9    -594.0      317.3    -598.4
  324.2    -599.8      331.2    -600.0      338.1    -598.8      343.5    -594.4
  349.2    -590.3      354.9    -586.3      360.7    -582.3      366.5    -578.5
  372.4    -574.7      378.4    -571.0      384.3    -567.3      390.2    -563.6
  396.2    -559.8      402.1    -556.0      407.9    -552.2      413.8    -548.4
  419.6    -544.5      425.4    -540.6      431.2    -536.7      437.0    -532.7
  442.8    -528.8      448.6    -524.9      454.4    -521.0      460.2    -517.1
  466.1    -513.2      471.9    -509.4      477.7    -505.5      483.5    -501.6
  489.4    -497.7      495.2    -493.8      500.9    -489.8      506.7    -485.9
  512.4    -481.8      518.1    -477.8      523.8    -473.7      529.4    -469.5
  535.0    -465.2      540.4    -460.9      545.9    -456.4      551.2    -451.9
  556.5    -447.3      561.7    -442.6      566.8    -437.8      571.7    -432.9
  576.6    -427.9      581.4    -422.7      586.0    -417.5      590.6    -412.2
  595.0    -406.7      599.2    -401.2      603.4    -395.5      607.4    -389.8
  611.3    -384.0      615.0    -378.0      618.6    -372.0      622.0    -365.9
  625.3    -359.7      628.4    -353.5      631.4    -347.1      634.2    -340.7
  636.9    -334.3      639.4    -327.7      641.8    -321.2      644.0    -314.5
  646.1    -307.8      648.0    -301.1      649.8    -294.3      651.4    -287.5
  652.9    -280.7      654.2    -273.8      655.5    -266.9      656.6    -260.0
  657.5    -253.1      658.4    -246.1      659.1    -239.2      659.8    -232.2
  660.3    -225.2      660.8    -218.2      661.2    -211.2      661.5    -204.2
  661.7    -197.3      661.9    -190.3      662.0    -183.3      662.1    -176.3
  662.1    -169.3      662.2    -162.3      662.2    -155.3      662.2    -148.3
  662.1    -141.3      662.1    -134.3      662.0    -127.3      662.0    -120.3
  661.9    -113.3      661.7    -106.3      661.6     -99.3      661.4     -92.3
  661.2     -85.3      660.9     -78.3      660.6     -71.3      660.2     -64.3
  659.8     -57.3      659.3     -50.3      658.7     -43.3      658.1     -36.4
  657.4     -29.4      656.5     -22.5      655.6     -15.5      654.5      -8.6
  653.2      -1.7      651.7       5.1      649.9      11.9      647.7      18.5
  644.9      24.9      641.2      30.9      636.1      35.7      627.1      38.7
  622.8      40.1      616.1      42.1      609.4      44.0      602.6      45.9
  587.3      50.2      379.7     102.1      373.1     105.4      366.8     108.6
  356.9     115.9      351.5     120.3      346.0     124.8      340.6     129.2
  335.2     133.6      329.8     143.9      329.2     154.4      329.2     161.5
  329.2     168.6      329.2     175.7      329.2     182.7      329.2     189.7
  329.1     196.7      329.1     203.7      329.0     210.7      328.9     217.7
  328.8     224.7      328.7     231.7      328.7     238.7      328.5     248.7
  328.3     263.6      328.2     272.2      328.0     280.5      327.9     289.1
  327.7     297.4      327.6     305.8      327.5     314.3      327.4     322.7
  327.3     331.1      327.3     339.2      327.2     347.4      327.2     355.4
  327.2     363.4      327.1     371.4      327.1     379.5      327.0     387.4
  327.0     395.4      327.0     403.3      326.9     411.2      326.9     419.0
  326.9     426.9      326.9     434.7      326.8     442.5      326.8     450.1
  326.8     457.7      326.8     465.1      326.8     472.6      326.7     480.1
  326.7     487.5      326.7     494.9      326.6     502.3      326.5     509.7
  326.4     517.1      326.2     524.5      325.9     531.9      325.6     539.2
  325.3     546.6      324.9     553.9      324.3     561.3      323.8     568.6
  323.2     576.0      322.6     583.2      322.1     590.8      321.6     598.1
  321.1     605.5      320.8     612.9      320.5     620.4      320.2     628.0
  320.1     635.6      320.0     643.2      320.0     650.7      320.0     658.3
  320.0     665.9      320.0     675.6      320.0     682.6      320.0     689.6
  320.0     696.6      320.0     703.6      320.0     710.6      320.0     717.6
  320.0     724.6      320.0     731.6      320.0     738.6      320.0     745.6
  320.0     752.6      320.0     759.6      320.0     766.6      320.0     773.6
  320.0     780.6      320.0     787.6      320.0     794.6      320.0     807.0
STOP BECAUSE OF BASEMAT PENETRATION AT TIME =  0.4056E+06 SEC
```

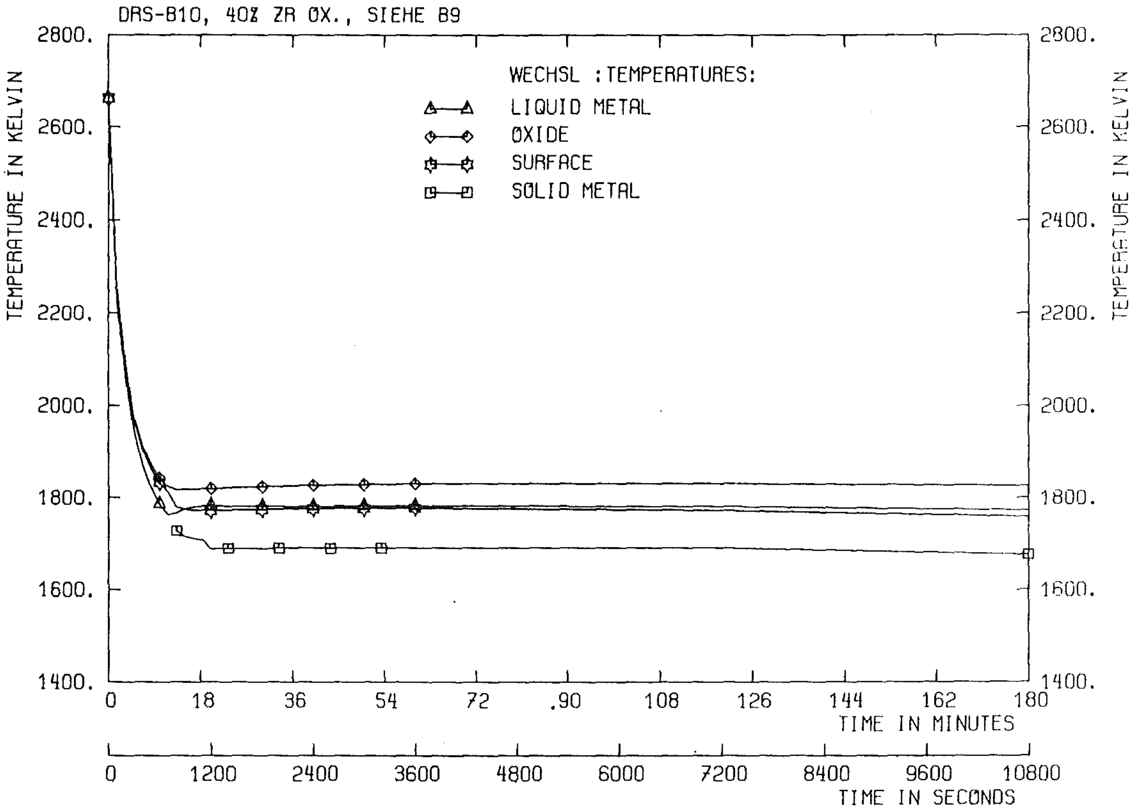
DRS-B10, 40% ZR OX., SIEHE B9
WECHSL :TEMPERATURES:
LIQUID METAL
OXIDE
SURFACE
SOLID METAL
TEMPERATURE IN KELVIN
2800.
2600.
2400.
2200.
2000.
1800.
1600.
1400.
0
18
36
54
72
90
108
126
144
162
180
TIME IN MINUTES
0
1200
2400
3600
4800
6000
7200
8400
9600
10800
TIME IN SECONDS

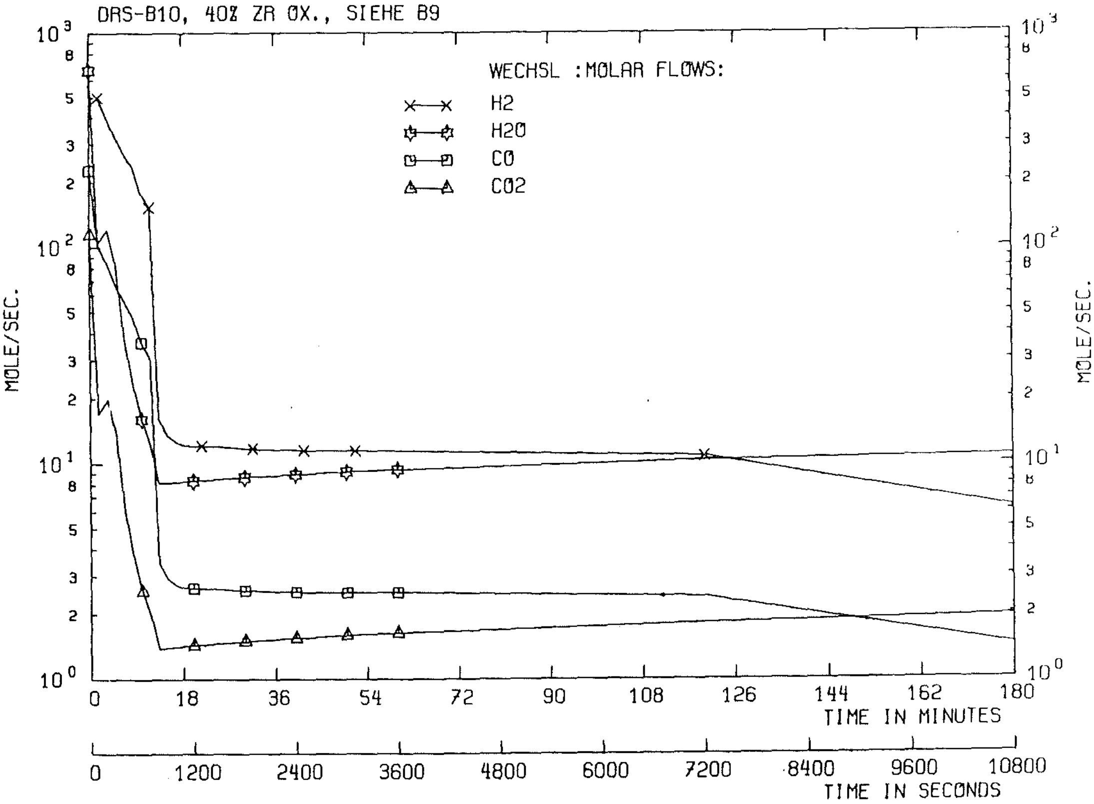
DRS-B10, 40% ZR OX., SIEHE B9
WECHSL :MOLAR FLOWS:
H2
H2O
CO
CO2
MOLE/SEC.
10^3
10^2
10^1
10^0
8
5
3
2
0
18
36
54
72
90
108
126
144
162
180
TIME IN MINUTES
0
1200
2400
3600
4800
6000
7200
8400
9600
10800
TIME IN SECONDS

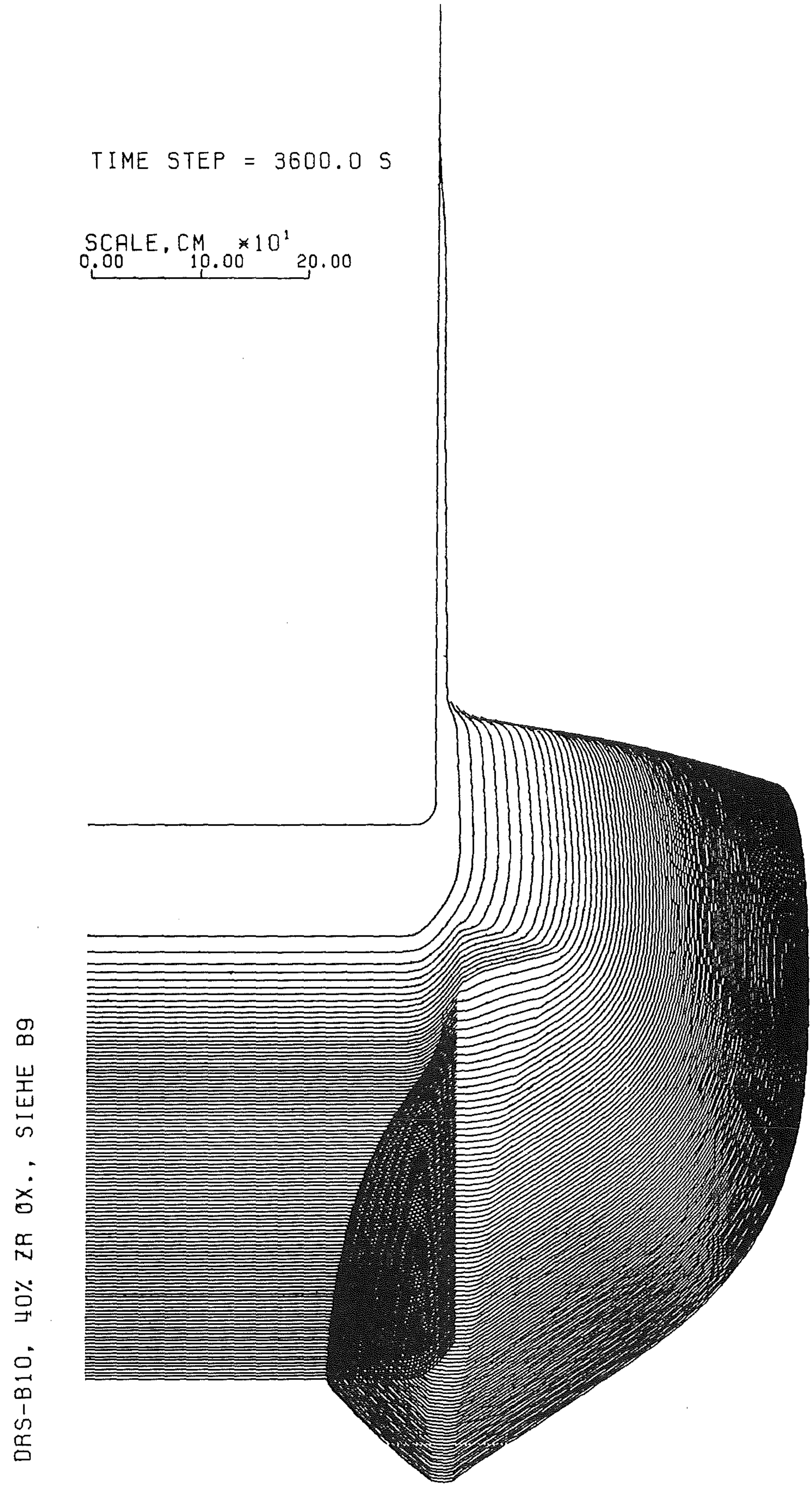
TIME STEP = 3600.0 S
SCALE, CM $\ast 10^1$
0.00
10.00
20.00
DRS-B10, 40% ZR OX., SIEHE B9